IOWA STATE UNIVERSITY
Digital Repository

2009

Experimental investigation of bio inspired flapping wings for MAV and NAV applications

Anand Gopa Kumar
Iowa State University

Follow this and additional works at: https://lib.dr.iastate.edu/etd

Part of the Aerospace Engineering Commons

Experimental investigation of bio inspired flapping wings for MAV and NAV applications

by

Anand Gopa Kumar

A thesis submitted to the graduate faculty

in partial fulfillment of the requirements for the degree of

MASTER OF SCIENCE

Major: Aerospace Engineering

Program of Study Committee:
Hui Hu, Major Professor
Tom I-P. Shih
Zhi Jian Wang

Iowa State University

Ames, Iowa

2009

TABLE OF CONTENTS

LIST OF FIGURES

LIST OF TABLES

ACKNOWLEDGEMENTS

ABSTRACT

The current investigation focuses on achieving a greater understanding on the aerodynamic phenomena that takes place during flapping flight and its application in the development of Micro Air Vehicles (MAVs) and Nano Air Vehicles (NAVs). Quantitative force measurements were made on the MAV model to understand its aerodynamic performance of flapping wings at different operational flight conditions. A comparative analysis was also made to understand the effects of wing membrane flexibility on the aerodynamic performance of an MAV. The results obtained from this study would help design a membrane based flapping wings which would have an optimum aerodynamic performance

Dragonflies are considered to be some of the most agile and maneuverable insects known to man due to which they taken as an inspiration for the study of flapping wing NAVs. Piezoelectric fans were used to simulate the flapping motion of insect wings due to their ability to generate a high wing beat frequency. Flow measurement studies on the fans placed in a tandem wing configuration were carried out with the help of Digital Particle Image Velocimetry (DPIV) by which quantitative flow field measurements were made. The PIV results provide a greater understanding of the vortex structures which were generated due to high frequency flapping motion of the wings.

CHAPTER 1. INTRODUCTION

In the latter half of the 20th century has witnessed events which have changed the face of warfare. Conventional warfare which has been in the realm of full scale war between nations has now diminished into what is known as Low Intensity Conflicts (LIC). This new form of warfare involves restricted use of conventional military assets mostly for political reasons which would involve solving short term objectives in foreign policy of a country without the risk of all out war.

Wars over the recent years including the NATO intervention in the Balkans and the current operations in Iraq and Afghanistan have seen an increasing role played by uninhabited areal systems which are acting as the "eyes in the sky" for military commander. This capability gives them up-to-date intelligence thereby increasing the situational awareness of all arms of a fighting force. As the years progress more UAVs are pushed into a quasi multi role capability with new onboard systems being added on to existing platforms. Apart from the traditional photo-reconnaissance and targeting capabilities, UAVs now also carry various SIGINT (Signals Intelligence) systems which can also intercept enemy communications and also delivery of Precision Guided Munitions (PGM) on specific targets.

With the ever-growing need for greater intelligence on enemy forces especially in the case of such low intensity irregular warfare would require the use of a new breed of UAVs which are cheaper and capable of extended missions within enemy territory. The next generation of such unmanned systems would include the use of miniature UAV. They would satisfy primary goal of being a squad based device which can be used by a small group of soldiers and also making the entire system man portable. These systems would operate within

the realm of bird and insect flight. The possibility of developing such a system is due to recent advancements in miniaturization of sensors and other electronics which are light weight and can be mounted on such micro air vehicles. Wide arrays of these sensors are now available off the shelf, which include cameras which are capable of thermal imaging and other low light infra red night vision applications. These systems can also be fitted with sophisticated listening devices which would be used as a means of intelligence gathering or can also be used in the area of disaster relief. Highly sensitive listening devices can also be used to locate people who are trapped beneath the rubble of a collapsed building or other structure. Another application where MAVs can be used is for detecting contamination by Nuclear Biological or Chemical (NBC) agents. In this scenario it is safer to deploy an unmanned system in such a situation for reasons of safety.

Though the development of such a system may sound very straight forward, there are several challenges which lie in the path to developing a complete working model of a bio inspired flapping wing miniature uninhabited air vehicle. The primary goal of this investigation is to study the aerodynamic characteristics of both micro and nano scale UAVs and to understand the underlying aerodynamic phenomenon which would later prove useful while developing such a system in the future.

1.1. Oscillating Airfoil

In order to study the aerodynamics of flapping flight, the first step would be to understand the aerodynamic phenomenon behind oscillating airfoil. When compared to flapping flight, oscillating airfoils can be represented as a two dimensional cross sectional region of the entire wing which is in motion. Several researchers have extensively studied the

effects of flapping flight results of which have shed light on the aerodynamic phenomenon which takes place with motion similar to that of flapping wings. Apart from studying the effects of flapping flight, such a study can shed greater light into the hydrodynamic performance of aquatic animals by which a more efficient underwater propulsion method can be developed [1]. Extensive research both in computational and experimental fronts have been conducted by various research groups to understand vortex sheets generated by the wings as they oscillate. Some studies have also been conducted to calculate force measurements in order to understand the aerodynamic forces produced by oscillating wings and some of the research is directed towards assessing their possible applications in unmanned air systems and submarines by which a more efficient means of propulsion can be developed.

Initial studies in oscillating bluff bodies at low Reynolds numbers were conducted by von Karman and Burgers where these vortex structures on the wake were first observed [2]. The wake region of oscillating airfoils was found to produce two discreet rows of vortices. On having a repetitive oscillatory motion of the wing over a period of time, a continuous trend can be observed in the wake of the airfoil which is called a vortex street. The term Karman Vortex Street has been coined with from these early studies figure 1.1 shows an illustration of the Karman Vortex Sheet.
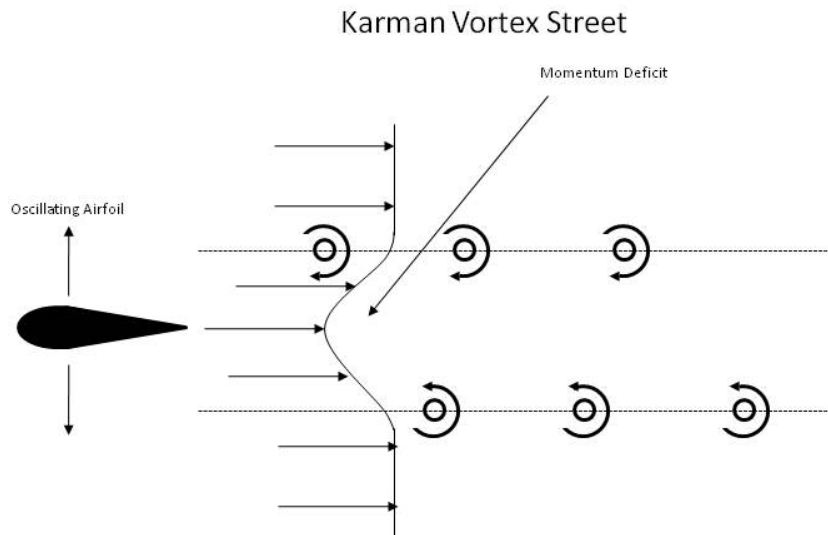
Figure 1.1. Karman Vortex Street

This vortex structure consists of dual rows of vortices which have been generated due to oscillatory motion of the airfoil. In this wake structure, it can be found that the vortices in the upper row of the sheet have a clockwise orientation and the ones on the lower row have an orientation in the counter-clockwise direction. On calculating the time averaged velocity profile of this flow, a slight decrease in the velocity profile can be observed in the wake region of the airfoil. This decrease in the velocity indicates a momentum deficit and is associated with drag being produced by the airfoil. A similar velocity profile in the wake structure can be observed in the trailing edges of stationary bluff bodies as they produce drag under such conditions. The resultant wake structure in this particular case can also be called a Drag Producing Wake.

Figure 1.2 shows a different wake structure which would be observed in the wake of oscillating airfoils.
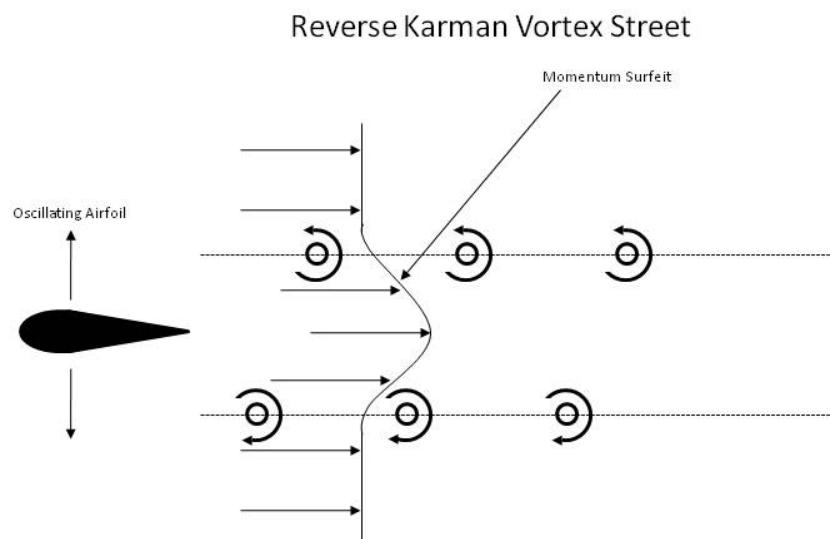
Figure 1.2. Reverse Karman Vortex Street

In this particular configuration, the vortices are oriented opposite to each other with the upper row having a counter clockwise direction and the lower row with a clockwise direction. The time averaged velocity profile of the wake shows a momentum surfeit can be observed with an increase in the velocity in the wake region of the airfoil. This increase in the velocity in the wake region can be attributed to the thrust being produced by the wake. This vortex structure is known as a Reverse Karman Vortex Street or a Thrust Producing Wake.

A third case which is observed in oscillating airfoils is what can be described as a neutral wake Figure 1.3 shows a neutral wake configuration in the wake of an oscillating airfoil.
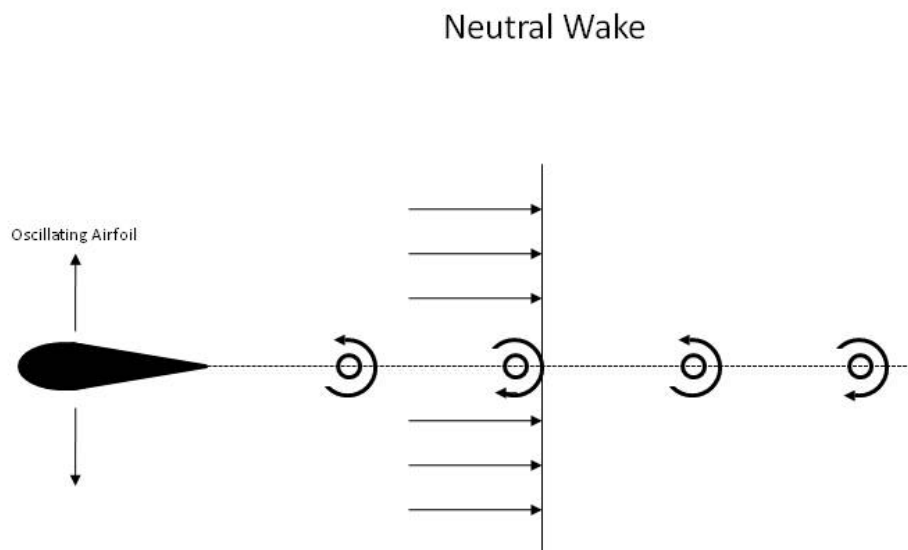
Neutral Wake

Figure 1.3. Neutral Wake

In this vortex structure, a single row of vortices can be observed with each of the vortex having an alternating orientation. In this case, the resultant velocity profile would produce net drag and net thrust which would cancel each other out thereby giving a uniform flow in the wake region. This case is referred to as a Neutral Wake as there is no net resultant force being observed in the wake region.

1.2. Propulsive Efficiency

Vortex structures similar to the ones mentioned above were observed in experiments conducted by Lai and Platzer [4]. A 10mm NACA 0012 airfoil following a sinusoidal wave pattern was used to study the wake structures. The parameters which were varied during the experiments include a non-dimensional term called Reduced Frequency (k)

$$k = \frac{\pi f c}{U_\infty}$$

Where f is the oscillation frequency c is the chord length of the airfoil and U_∞ is the free stream velocity in the test section. The other non-dimensional term which is varied during the experiment is the plunge amplitude (h)

$$h = \frac{a}{c}$$

Where 'a' is the plunge amplitude of the airfoil. During these experiments, a drag producing wake was found at an instance when kh = 0.29 but as the kh value was increased to a higher value of 0.6 the same airfoil was found generate a thrust producing wake.

Similar experiments were conducted by Koochesfahani[5], where the wake structures of airfoils oscillating with a pitching motion in both sinusoidal and non-sinusoidal wave forms were studied. Apart from flow visualization, qualitative flow measurements were also conducted using Laser Doppler Velocimetry (LDV). A special case has also been noted during these experiments where two vortices of the same orientation are shed during each half cycle of the oscillation. A time averaged results of this particular case shows, a dual double vortex structure were observed on both the upper and lower planes of flapping. It was observed that a similar stable configuration could not be maintained when the airfoil is oscillating at lower amplitude. This specific case where vortex pairs are being shed into the wake can only be observed when the ratio of amplitude to chord length of the wing is high. These vortex structures which are deviant from the traditional Karman Vortex Street will be observed in future experiments involving Piezoelectric Tandem Wings. It was also mentioned that the

critical reduced frequency for thrust generation would depend on the oscillating amplitude of the wing.

Further experiments conducted by Anderson et al. [6] involved oscillating airfoils placed in a water tunnel. These studies were oriented more towards studying the propulsive efficiency of these oscillating airfoils. It was mentioned earlier that an optimal jet in the wake structure depends on a larger distance between the vortex sheets. An understanding of such efficiency would be of great advantage when it comes to finding a suitable means to increase the endurance of micro air vehicles to make optimum use of onboard power sources. Once an optimal set of flapping parameters can be obtained for the micro air vehicle, the use of such a flight profile can increase its effectiveness during extended missions.

A non dimensional term that can be used while calculating the power generated by the system would be the power coefficient or C_{power} which is

$$C_{Power} = \frac{Power}{\frac{1}{2}\rho\,S\,U^3}$$

Another term which is to be calculated would be the thrust coefficient generated by the oscillating wing which is given by the equation

$$C_T = \frac{T}{\frac{1}{2}\rho\,S\,U^2}$$

The power consumed by the oscillating airfoil calculated by multiplying the voltage (V) and the current flow (I) through the circuit, S is the planform area of the wing, ρ is the fluid density and

U is the free stream velocity. The propulsive efficiency of the system can be calculated using the equation

$$\eta_P = \frac{C_T}{C_{Power}}$$

The above equation can also be written as

$$\eta_P = \frac{TU}{Power}$$

In the current study will focus more on looking at the propulsive efficiency of the flapping mechanism as a function of the advance ratio in which the vehicle would be traveling. This is also useful as a term by which the aerodynamic flight regime can be determined where the vehicle can operate allowing the onboard propulsion system to operate with maximum efficiency thereby increasing the endurance of the vehicle.

1.3. Leading Edge Vortex

Leading Edge Vortex (LEV) is a relatively new concept as early studies on insect and bird flight have ignored the possibility of the existence of a leading edge vortex. When studies were conducted to explain the aerodynamic of flapping flight, the comparative results which were obtained were found to have severe inconsistencies between theoretical and experimental results. For a period of time it was considered that insects and birds cannot fly according to conventional laws of aerodynamics. Ellington et al. [7] have conducted flow visualization studies on insects and mechanical flapping devices and have detected the presence of a large leading edge vortex structure during the down stroke of the flapping wing. The vortex structure which is created by dynamic stalling of the wing was found to have sufficient strength and also

explains the high lift forces being generated at these conditions. The flow separation at the leading edge was found to re-attach itself on to the surface of the wing thereby creating the vortex structure. Span wise flow also plays a major part in understanding leading edge vortices as the size of the vortex is found to increase towards the wing tip [7-9].

The leading edge vortex essentially creates a low pressure region around the leading edge of the wing causing a larger suction in the upper surface of the wing by which the extra lift is generated. An enhanced circulation due to the low pressure is the reason for the presence of this extra lift during flapping motion. The dynamic stalling which is responsible for the creation of these leading edge vortices allows the wing to travel at high angles of attack for brief amounts of time before it stalls. Flapping motion will thereby allow the flyer to continue flying at higher angles of attack with much larger lift being produced during flight. From their initial observation Ellington et al. [7] were able to determine that the circulation at the leading edge of the wing increases in the first half of the down stroke. As the wing reaches towards the end of the down stroke, the leading edge vortex detaches itself from the surface of the wing and is shed into the wake. The presence of a leading edge vortex is relatively less prominent in the case of oscillating airfoils as leading edge flow separation over them is delayed due to their shape. Insect wings on the other hand have a cross sectional profile similar to that of a flat plate which would promote the formation of leading edge separation.

The stability of the leading edge vortex has also been a primary area of investigation, Viieru et al. [8] have conducted various numerical simulations to study the aerodynamics of low Reynolds number flight vehicles where the stability of leading edge vortices have been discussed. In 2D flow studies, the leading edge vortices are generally found to remain stable for

only short periods of time. In reality this is not the case as leading edge vortices are much stable in 3D conditions. The stability of the leading edge vortex is maintained by removing the vorticity through span wise axial flow along the vortex core. The flow structure of the leading edge vortex has been found to have a cylindrical structure from these studies. Another observation was that the size of the vortex varies with size and the operating Reynolds number of the flyer. This prominence of the span wise flow has also been understood during the early studies by Ellington et al. [7] which have been mentioned earlier. Through the mathematical modeling of the leading edge vortex and its effect, Viieru et al [8]. have concluded that the stability of the vortex can be explained from the momentum equation where the pressure gradient, the centrifugal force and the Coriolis force tend to keep the vortex stable. The stability of the vortex allows the flyer to operate at very low velocities without the wings stalling during flight.

Further studies have also been conducted by Lu and Shen [10] where stereoscopic digital particle image velocimetry data was gathered in the span-wise direction of a wing to study the evolution of the leading edge vortex in three dimensional spaces. With their observations, it was concluded that the LEV is a collection of four different vortices comprising of a primary vortex and three other minor vortex. This finding has made it possible to imagine that the LEV is much more complex in a 3D plane than what is usually observed in studies involving 2D flows. Earlier studies have shed light on the complexity of the LEV structure by Lu et al. [9]. The presence of a dual leading edge vortex has been noted during their experiments on the 2D plane of the wing where the presence of a much more complex vortex structure on the leading edge of the wing has been suspected initially.

1.4. Membrane Wings and their Application

Micro air vehicles, owing to their smaller size are generally expected to carry out their desired operations in regions where conventional UAVs are unable to operate. The decreased size of the vehicle is one of the main factors which make a micro air vehicle more deploy-able and portable than conventional UAVs which have a much larger wing span. Due to these factors, the vehicle also operates in lower Reynolds numbers than their UAV counterparts. A basic outline of the flight speeds at which micro air vehicles operate are within the range of around 10 m/s with the operating chord Reynolds number in the range of 10^3 to 10^5. At these operating speeds, the conventional airfoils which could be used in micro air vehicle wings will be subjected high levels of viscosity effects due to the low Reynolds numbers which would cause the aerodynamic performance to degrade by a large factor. This decrease in aerodynamic performance can be attributed to the effects of boundary layer separation and their growth. Studies involving the use of Digital Particle Image Velocimetry (DPIV) and surface pressure measurements have been used by Yang et al.[11], where the effects of boundary layer separation were studied in the case of a NACA GA(W)-1 airfoil operating at low speeds. Their efforts were focused on studying the process of the transition of a laminar boundary layer, where separation of the laminar boundary layer begins to take place with increase in the angle of attack and its transition to turbulent flow with the presence of unsteady vortex structures which were formed due to Kelvin-Helmholtz instabilities. The studies also focused on the phenomena of flow re-attachment on the upper surface of the airfoil by the turbulent boundary layer. This particular study has illustrated some of the conditions to which micro air vehicles of both fixed and flapping wing category could be

subjected while they operate at lower speeds and higher angles of attack. Particularly in situations where the vehicle would be subjected to operating in confined spaces such as inside buildings, where it would be expected to fly at much lower speeds. The performance of such airfoils at low Reynolds numbers can cause critical restrictions to the operability of micro air vehicles.

To overcome such an obstacle, one could look at nature for inspiration as in most cases. There are many natural fliers which operate at much lower speeds and higher angles of attack with relative ease and with higher aerodynamic performance. The interesting fact about this breed of fliers is that they do not have a rigid wing structures. An exceptionally interesting case would be that of the flying mammals namely the Bat and the Flying Squirrel. The flexible membrane wings used by these mammals were found to increase their performance in terms of maneuverability and agility though they fly under conditions identical to micro air vehicles. Such wings also allow bats to have a higher degree of control over the surface of the wing whose shape can be altered with the help of their elbows, wrist and fingers thereby making them much more maneuverable. Due to these factors, these bio-inspired wings have a growing interest among researchers and their properties and applied with a great amount of success.

Figure 1.4. Townsend's Big-Eared Bat (*Corynorhinus townsendii)*[14]

Figure 1.5. Northern Flying Squirrel (*Glaucomys sabrinus*) in gliding flight [15]

A study conducted by Hu et al.[12] involved a comparison of varying membrane flexibility and their advantages over a rigid wing of the same profile. The study involved using rigid spars on the surface of the wing to control the flexibility of the membrane. An optimum design was selected based on the lift-to-drag ratios calculated on flexible wings made with different spar numbers. Aerodynamic testing on these wings showed a similar amount of lift being produced by all the wings alike irrespective of their flexibility levels however, the drag generated by these wings were found to vary significantly. From this finding, it was concluded that the flexibility of the membrane on the

wing could severely affect their aerodynamic performance and it was very much essential to find a wing with the optimum flexibility. It was also learned from this comparative study that the wings with a higher degree of flexibility can have a much lower lift-to-drag ratio than a rigid wing; this was later found to be due to the presence of fluttering of the membrane in the trailing edge of the wing even at lower angles of attack. Due to this reason, a wing with a moderate amount of flexibility was selected which proved to have the highest lift-to-drag ratio among the group of wings tested. As part of the next phase in understanding the flexible wing was subjected to flow field analysis with a Digital Particle Image Velocimetry (DPIV) method in a wind tunnel.

When the rigid wing was subjected to high angles of attack, it was found that a significantly large turbulent wake was visible in the trailing edge of the wing. The boundary layer was found to be separated from the upper surface of the airfoil and thus resulting in the presence of a large unsteady wake in the trailing edge thereby causing a separation bubble.
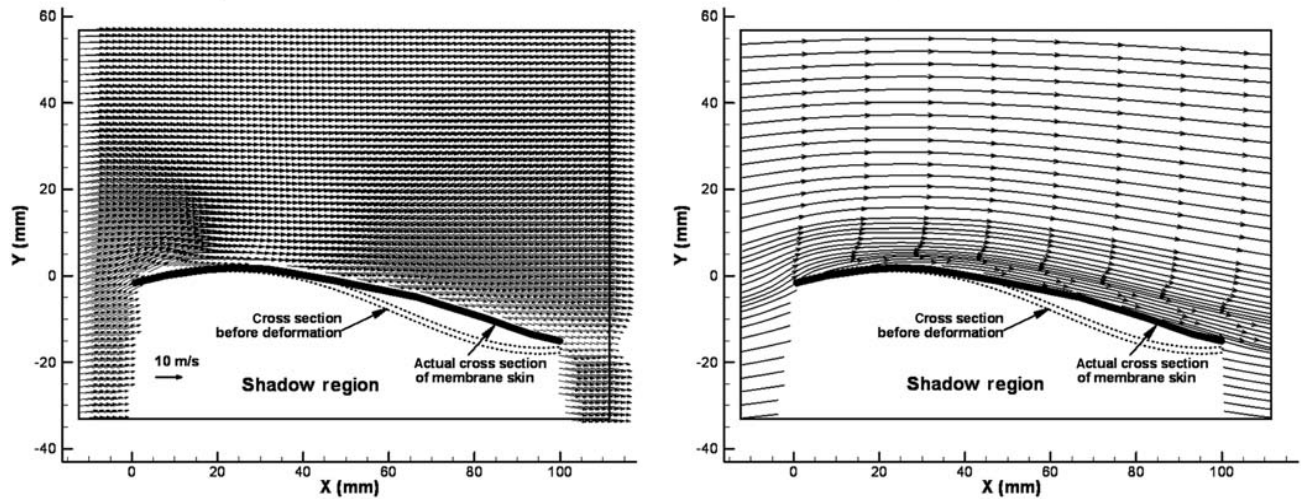
Figure 1.6. Results from Aerodynamic testing of membrane wing at AoA = 14° using
DPIV(Digital Particle Image Velocimetry) [12]

When the flexible wing was subjected to similar flow conditions with the same angle
of attack, a totally different set of results were obtained than compared to the rigid wing. It
was found that due to the severe pressure difference between the upper and lower surfaces of
the wing, the wing membrane was found to experience a large trailing edge deformation from
its initial position of the membrane. This particular phenomenon of having a deformation in
the trailing edge of the wing allows the boundary layer to stay attached to the surface of the
wing which considerably decreases the effective angle of attack of the wing. The wake
region of the wing showed a minimal amount of turbulence thereby indicating the presence
of a reduced amount of drag than compared to its rigid counterpart. Deformation of the
membrane wing surface thus allows it to operate at higher geometric angles of attack without
any significant loss of aerodynamic performance. A decrease in the effective angle of attack
also delays the stall of the wing allowing it to operate at much lower speeds and at higher

angles of attack than conventional rigid wings. From these findings, it can be very well concluded that wings with flexible membrane are ideally suited for vehicles which operate within the general flight envelope of a micro air vehicle.

One of the areas where the flexible membrane wings were effectively employed was in the case of the University of Florida MAV research group. As part of their studies into the area of micro air vehicles, the MAV research group has adopted a membrane wing configuration. The design of their vehicle involved the use of carbon fiber battens which are later covered with a flexible membrane thereby providing shape to the wings. Levels of flexibility of the wing surface were varied in this case by changing the number of fiber glass battens which were used on the surface of the wings. Extensive computational and experimental studies were conducted on these designs [13] which were inclined towards studying the process of flow separation over the body of the MAV.

Findings from the study concluded that the wing surface is capable of what is known as 'passive shape adaptation' which thereby acts as a means to delay stall. It was also concluded that the membrane decreased the effective angle of attack of the vehicle thereby allowing it to fly at much lower speeds with an increased geometric angle of attack than its conventional rigid counterparts. High frequency fluttering was also detected in the membrane of these wings during flight. Another aspect which is discussed with regard to this particular system is its ability to absorb instantaneous turbulent flows in the free-stream air during its flight. This phenomenon is called 'gust suppression' by which the MAV is able to fly in a much more stable condition than MAVs of similar design and a rigid wing.
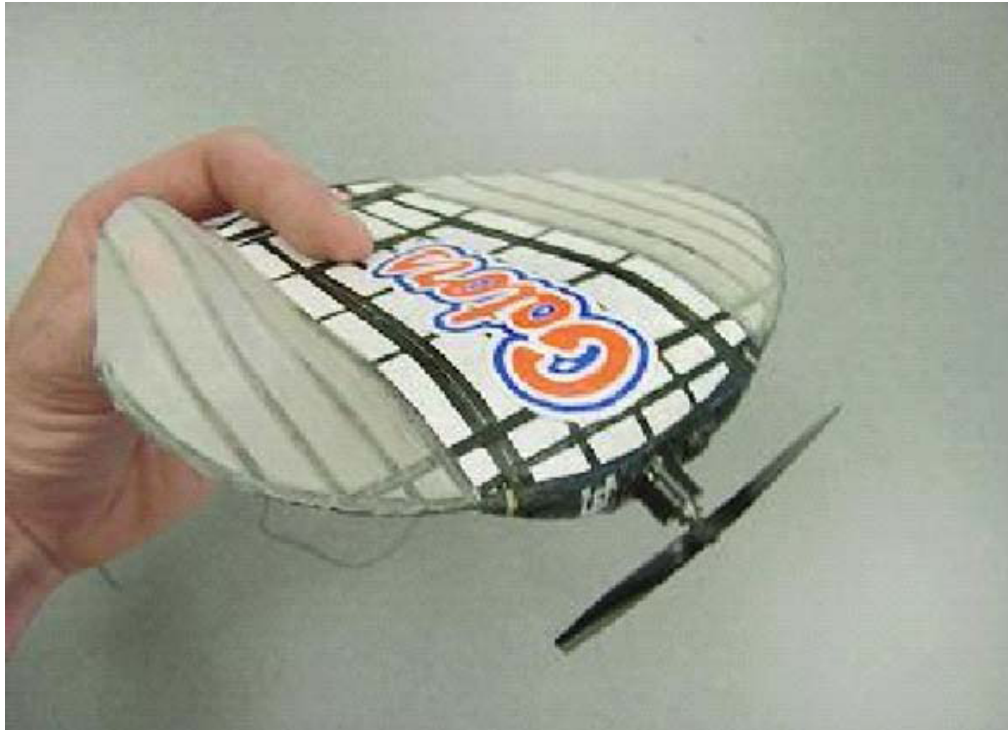
Figure 1.7. University of Florida 15cm Membrane Wing Micro Air Vehicle Exhibiting
Menbrane Flexibility [13]

Prevalence of such gusts in air can be seen very commonly outdoors especially between buildings where the wind velocity can suddenly vary at certain instances and the use of membrane wings does not allow the vehicle to be blown away from its original flight path due to these gusts of air.

CHAPTER 2. FLAPPING WING MICRO AIR VEHICLES WITH MEMBRANE WINGS

2.1. Experimental Setup and Micro Air Vehicle Mechanism

To simulate bird flight many different methods have been used by researchers with the use of various mechanical systems. But for this study, an off the shelf product was used to test the flight characteristics of flapping wing MAVs. Cybird P1 is a commercially available ornithopter model which is popular among many model remote control airplane and ornithopter enthusiasts. The flapping mechanism consists of two main cranks which are connected together with the help of a main gear which in-turn is connected to a 370 series brush-less DC motor which is very commonly used in remote controlled aircraft and toys due to its high rpm. Before the motor is connected to the crank, the initial motor RPM is first reduced using of a set of gears for reasons of structural integrity. Figure 2.1 shows the mechanism used by the Cybird P1 to generate flapping motion during flight.

The wings of the ornithopter are clipped on to the holding posts which are shown in figure 2.1 which generate the flapping motion. The Cybird mechanism is used by other researchers for their studies on flapping wing micro air vehicles some of whom include Hong and Hong and Altman [16] and Kim et al.[17] allowing them to obtain a crucial understanding of the aerodynamics of flapping wing flight and its potential for application in micro air vehicles.
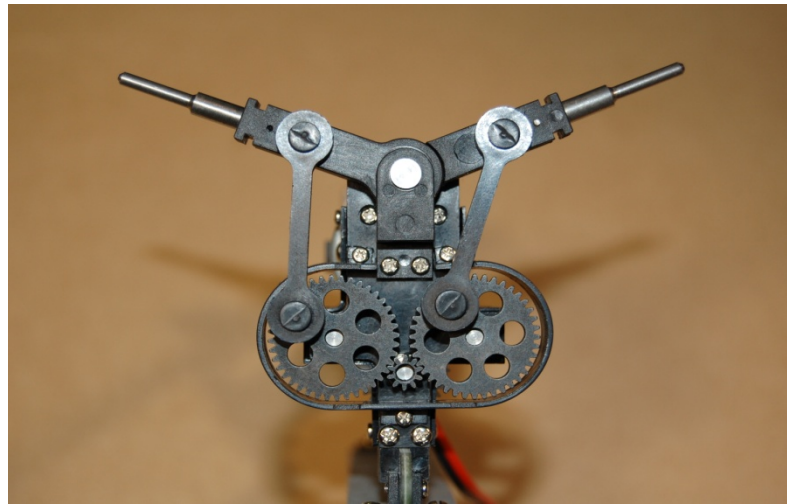
Figure 2.1. Gear Mechanism for Cybird Ornithopter

Figure 2.2. BK Precision 1760A Power Source [21]

During the course of the experiment, the motor of the flapping mechanism was subjected to a voltage range within the safe application limit of the motor. The voltage range during the experiment was varied from 1V to 7V with increments of 1V during each step to vary the wing beat frequency of the flapping mechanism. The DC power supply which was used during this experiment was the BK Precision 1760A, 4 digit triple output power supply.

With this particular power source, the output given to the system which is used is very precise with an accuracy of 0.01VDC. It is also capable of performing both constant current and constant voltage applications but for the following experiment; the voltage was varied leaving a constant flow of current into the circuit. Another feature of the power source was that of parallel connection and combined tracking of the two power outputs. Setting the output terminals in parallel connection allowed the power sources to reach voltages in excess of 7 volts and also allowing the simultaneous tracking of the current variation in the circuit. The reading of the current flowing through the circuit is visible in the secondary display panel of the power source though the current flow through the circuit was measured with the help of a multi-meter for better accuracy. This data of the current flow would later be used to calculate the efficiency of the motor at different flight conditions of the Cybird by which an assessment could be made on whether the vehicle is producing enough thrust to remain airborne with respect to the amount of power it consumes.

Figure 2.3. Flapping mechanism mount

The flapping mechanism is screwed into place on top of a mount which will then be connected to a load cell. Owing to the fact that the aerodynamics of the mount would come

into picture, the cross sectional profile of the mount is that of a symmetrical airfoil. This particular profile does not allow the creation of any excessive additional aerodynamic forces during the experimental process. A provision to change the angle of attack of the flapping mechanism is also provided on the mount and the bottom of the mount has a threaded rod which allows the mount to be bolted on to a force sensor.

Force measurements for this experiment are to be carried out in all the three axes in space using a JR3 force measurement module model number 30E12A-I40. The force sensor is capable of gathering data on the forces and moments in all three axes with a very high degree of accuracy and a very high data acquisition rate. Design accuracy of the force sensor is within the level of $\pm 0.05\%$ thereby allowing it to measure very low amounts of force.
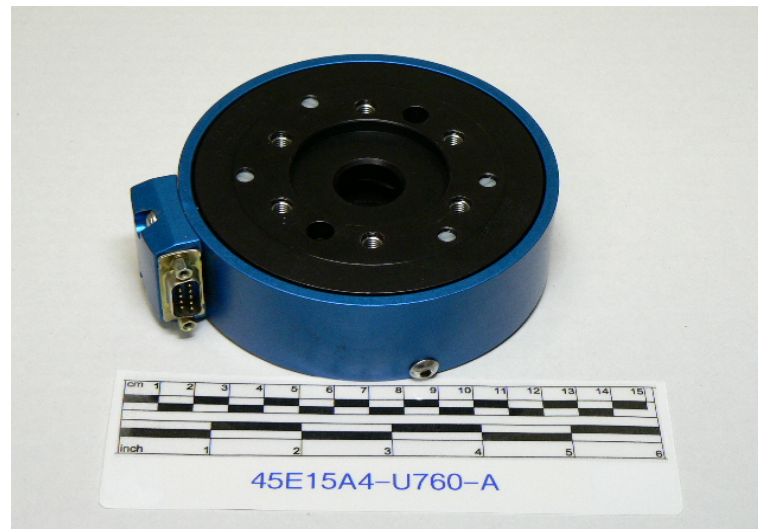
Figure 2.4. JR3 force sensor [18]

For acquiring the data provided by the force measurement sensor, a LabVIEW program allows the measurement of forces being applied on the sensor. The sensor uses the principle of Wheatstone's bridge to calculate the forces acting on it. Voltages from each of the directions are received by the data acquisition device in six separate channels in the order of forces F_x, F_y, F_z and moments M_x, M_y and M_z. Each of the voltages from the channels are then multiplied with a preset calibration matrix which is obtained for individual force measurement units. On multiplying the output voltages from the load cell with the calibration matrix, the output in terms of SI units would be obtained and can be saved into data files. During the experiment, data acquisition rate of the JR3 was 1 KHz for the time period of 30 seconds thereby gathering a total of 30,000 data points. Gathering a large number of data points ensures that enough data is gathered with a good resolution and for a sustained period of time there by allowing the average of the output to reduce the effects any of the noise or inertial conditions which would be encountered by the load cell.

Figure 2.5. Bill James Wind Tunnel

Wind tunnel testing for this study was conducted in the Wind Simulation and Testing Laboratory's Bill James wind tunnel at Iowa State University. The test section of the wind tunnel has a cross sectional measurements of 3ft x 2.5ft and can reach speeds of up to 80m/s [19]. A high power motor is used to propel the air through the wind tunnel and the motor is controlled by a programmable heavy duty power source which ensures a steady rpm of the motor thereby ensuring a constant flow velocity in the test section of the airfoil.

Being an open circuit wind tunnel, air is sucked into the test section from ambient atmosphere and ejected through the exit of the wind tunnel compared to a closed circuit wind tunnel which re-circulates air which is already inside the wind tunnel into a closed loop. During the current round of tests conducted on the flapping wing mechanism, the shutters which are generally left open during operation at higher speeds were closed. This was done because of the current operating speeds of the wind tunnel which would never exceed a flow velocity of 10m/s for these experiments. Despite the presence of a lot of added advantages and disadvantages of the application of both open circuit and closed circuit wind tunnels however for the tests in question, there are no serious issues which would interfere with the results obtained during testing.

Another sensor which was used during the testing phase was a pressure sensor called the DSA (Digital Sensor Array). The DSA is a temperature sensitive piezoresistive pressure sensor which can measure pressures at the rate of 500Hz with an accuracy scale of within $\pm0.05\%$. These sensors come in a variety or ranges and the sensor which was used for the current set of experiment has a pressure range of 750psid. The sensor also has a 16 channel input which can be connected to small diameter rubber tubing which carry the small variation in pressure into the sensor. Data acquisition from the sensor is carried out through a local area network (LAN) where the DSA has a designated IP address through which a computer can remotely control the sensor and acquire data with preset parameters. The calibration of the Bill James wind tunnel was conducted by measuring the test section pressure using the DSA pressure sensor with the help of a pitot static probe.

Figure 2.6. Scanivalve DSA 3217 pressure sensor array [20]

In previously mentioned studies, varying the flexibility of the membrane over a wing was done by changing the number of batons on the wing structure. In this particular set of experiments, it would not be easy to add new spars owing to the complex structure of the original Cybird wing frame. Hence, a much simpler approach was take by which the material of the wing membrane would be varied causing the flexibility of the membrane also to change. This is particularly easier as the original nylon membrane which is glued to the wing of the Cybird can be removed and a new membrane can be glued on to the surface of the wing. The wing structure of the original Cybird wing was made with carbon fiber rods giving it a characteristic shape similar to bat wings. For the initial set of experiments, the original wing shape was used and the membrane material was changed simulating different flexibility levels. However a second round of experiments was conducted with a wing plan form which is similar to that of an elliptical wing.

The flexibility study of the wing was carried out by varying the membrane present on the wing surface. Test carried out with this aspect are conducted with the addition of a latex membrane over one of the wings and also a rigid plywood plate which is placed on the other

wing. The skin flexibility is varied from the most flexible; in this case latex to moderately flexible being the nylon wing and finally the least flexible being the rigid wood wing. While replacing the wing membrane on the latex wing, special care has to be taken so that the membrane structure is not wrinkled in any way. This could result in the loss of rigidity of the wing membrane by which the flexibility characteristics of the wing would vary. A latex membrane was first stretched and then taped on to a wooden board. Superglue was applied on the carbon fiber spars and the wing frame was placed on the stretched membrane. The glue is allowed to cure for a few hours after which the membrane is removed from the wooden board. Finally the wing profile of the original Cybird wing is cut out from the latex membrane the structure is then reinforced with scotch tape. For the rigid wooden wing, the wing profile of the Cybird wing was cut out from a wooden plate and then glued to the original Cybird wing by which the nylon membrane would provide additional support to the relatively heavy wooden plates.

Table 1. Parameters of Membrane Wings

Wing	Mass [g]	Planform Area of Wing [m^2]	Wingspan [m]	Chord Length [m]	Amplitude [deg.]
Elliptical	8.8	0.045107	0.425	0.106	47.1
Rigid	59.7	0.09502	0.736	0.165	47.4
Nylon	15.1	0.09502	0.736	0.165	47.4
Latex	30	0.09502	0.736	0.165	47.4

Figure 2.7. Elleptical Wing

Figure 2.8. Nylon Wing
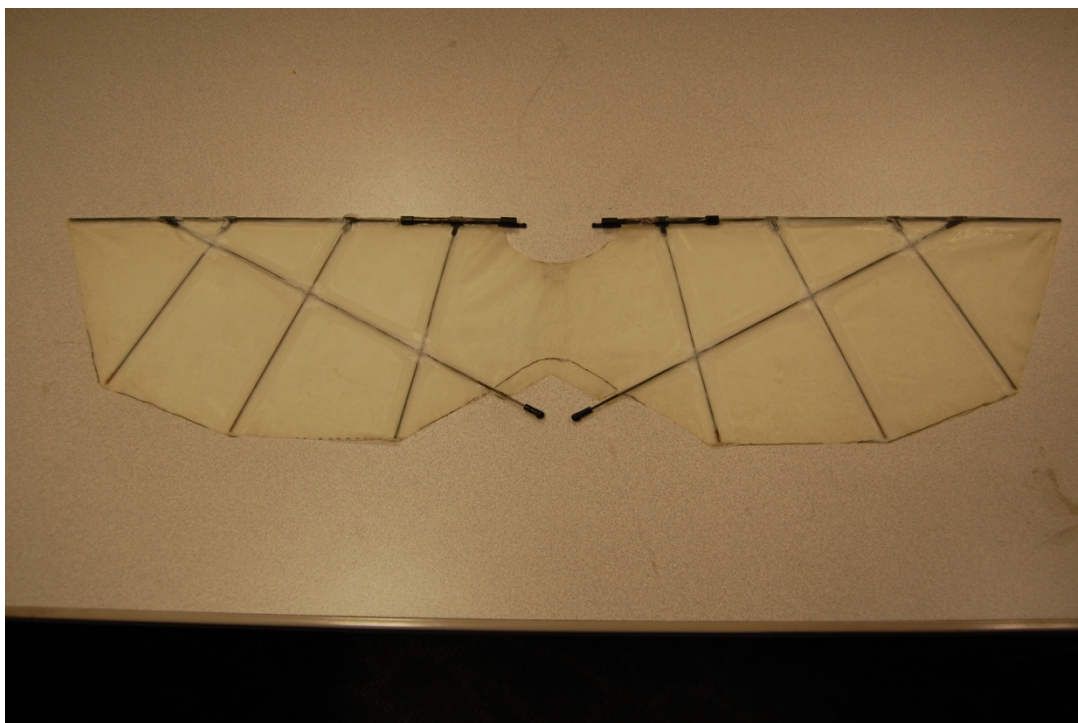
Figure 2.9. Latex Wing
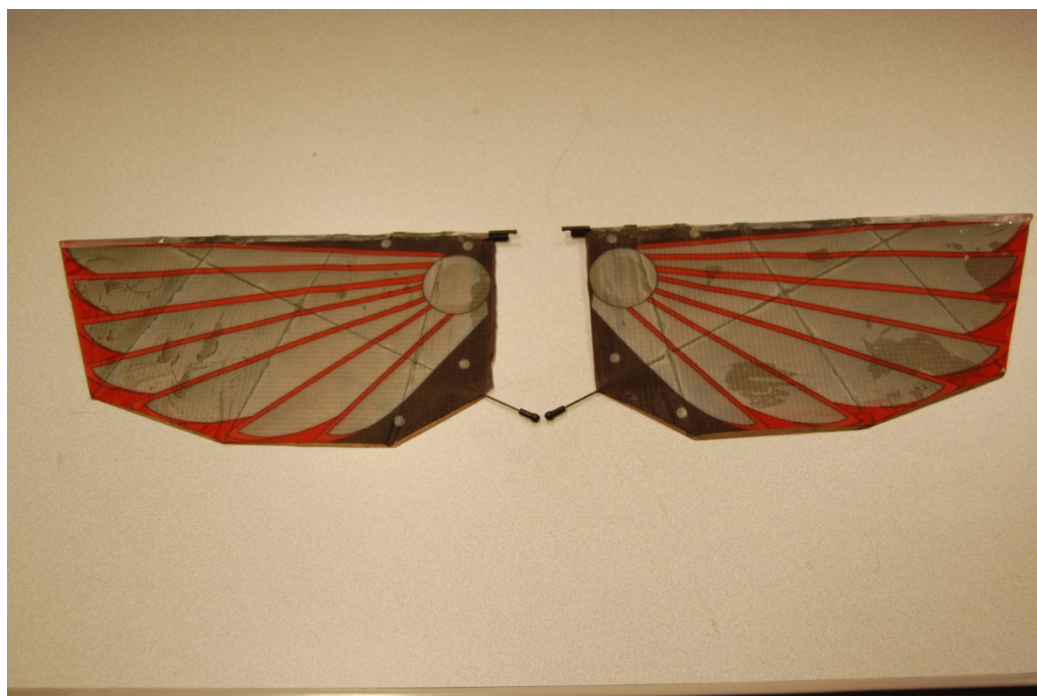
Figure 2.10. Rigid Wing

On measuring the thicknesses of the wing membrane, the latex wing was found to have a thickness of 120µm, the original nylon membrane of the wing was found to have a thickness of 70µm and the wood plate of the rigid wing is 200µm. Table – 1 shows the parameters of the wings which are being tested in the current set of experiments with additional data gathered from Hu et al. [22].

In-order to build a new wing which is compatible with the existing Cybird mechanism, various other options were considered but later but modifying an existing wing was later found to be a more feasible option. The reason for making a new wing was primarily due to test section dimensions of the Bill James wind tunnel. The original wing of the Cybird has a span of 36.8 cm the on the other hand the Bill James wind tunnel which was used for testing has a test section dimensions of 3ft x 2.5ft which would mean that the wing-tips would be moving close to the walls of the test section. This close interaction with the wall of the wind tunnel and the wingtip would cause a distortion in the vortex structures generated by the wing resulting in data which is obtained during testing to be significantly different from free-flight conditions. Due to these reasons, a new wing was adopted for testing with geometry different from the original Cybird wing. An elliptical was traced on the body of original wing and the region around it was cut out of the original wing. The reinforcing spar on the surface of the wing, which is also acts as a connection to a ball and socket joint on the rear end of the Cybird mount. Having a connection to the rear of the mount allows the wing to have only a one degree of freedom motion which is also known as plunging motion and also firmly fixes the wing on the mount. If the rearward fixture was not present, during the flapping of the wing a rotational or pitching motion which is commonly

seen in bird flight could be observed. Though this is an important factor which is to be studied in detail when it comes to flapping wing flight however adding a rotational component to the wing motion would cause the fixture to the wing post to wear considerably over a period of time and leading to permanent damage to the wing after extensive use. Also the current study is restricted to only plunging motion of the wing and the rotational component is ignored. The original Nylon wing membrane was used for these tests as well, the only change made was the shape of the wing and the size. An elliptical wing profile was chosen with an aspect ratio of 0.61, the total wing span of the wing was reduced to 425.4mm and with a smaller root chord length of 105mm compared to the original wing. These parameters make the modified wing a lot smaller than the original wing and thereby giving a much larger wingtip clearance of approximately 247.65mm thereby effectively reducing the possibility of the test section wall interfering with the wing tip vortices which are generated by the flapping wing.

2.2. Aerodynamic Testing

The aerodynamic testing of the modified Cybird wing was carried out by varying parameters such as the orientation angle, the voltage input into the system and the incoming flow velocity. These different parameters were selected so as to study the effects of the angle of orientation which could decide on what direction the aerodynamic forces would be acting, the input voltage which would show the effect of the increase or decrease of wing beat frequency during flight and also the incoming flow velocity.

Though there is a calibration curve which specifies the relation between the wind tunnel motor frequency of the Bill James wind tunnel and the flow velocity which is

generated by the motor. It was found that such a calibration was not focused on some of the lower velocities which would be used in the current experiments. A new calibration curve was generated with the help of pressure measurements in the test section of the wind tunnel for a corresponding motor frequency input into the wind tunnel. A Scanivalve DSA 3217 pressure sensor was used to gather the data in terms of static and total pressures. The pressure sensor was attached to a pitot-static probe which is mounted in test section of the airfoil. Before the test was conducted, it was ensured that the pitot-static probe is placed in the middle of the test section and the head is placed parallel to the flow. A data acquisition rate of 400Hz was used with a total of 12,000 samples being gathered during the experiment with each case lasting 30 seconds. The resulting pressure values are an average of all the instantaneous pressure readings that were taken during the experiment. During the experiment, the motor frequency of the wind tunnel was increased in increments of 0.5Hz giving a higher amount of resolution while making the curve fit. Figure 2.11 shows the curve fit between the motor frequency of the wind tunnel as a function of the free stream velocity inside the test section of the wind tunnel. Combining the two values, a linear fit was made so as to predict the velocity for a given motor frequency.
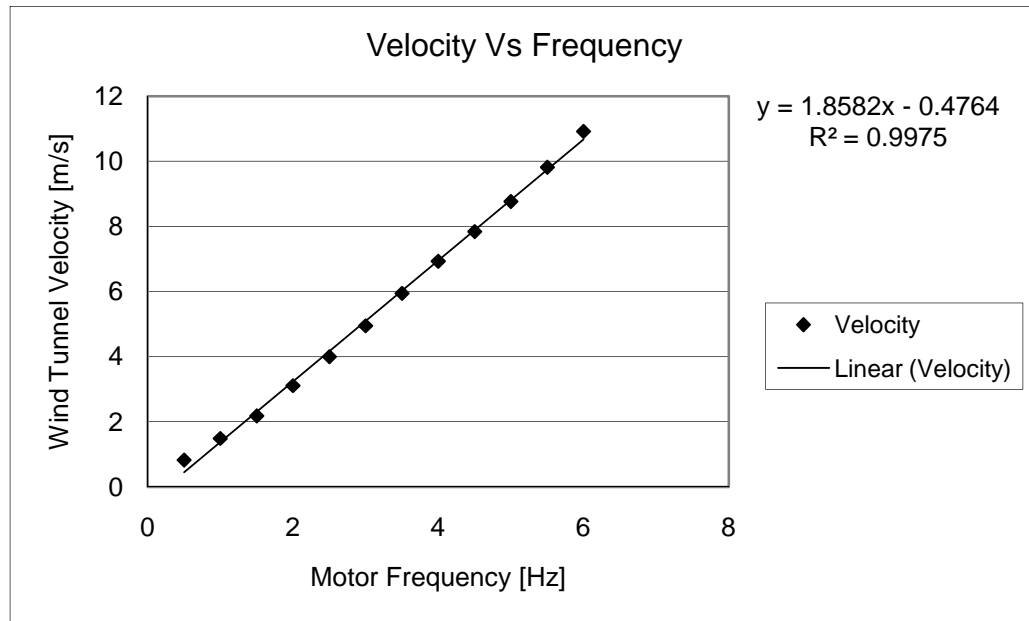
Figure 2.11. Motor Frequency Vs Free Stream Velocity

A slight amount of curved nature can be traced in the velocity profile however a linear fit was placed on it making no significant variation in the values which were obtained during the calculation of velocity and a residual of close to 1 was also obtained in the fit.

2.2.1. Soaring Flight

The first round of testing involved the study of the aerodynamic characteristics of the wing during soaring flight. During this phase, the wing's aerodynamic loads are calculated while it is not flapping so that a comparison can be made with the augmentation of the thrust and the lift with the wing flapping in comparison with while the wing do not undergo motion. To test the aerodynamic characteristics of the wing during soaring flight, the wing was placed in the test section of the wind tunnel and is subjected to flow velocities from 1m/s to 10m/s with increments of 1m/s each. The orientation angle of the wing is also varied from -10° to +20° with increments of 5° in each case. With this study, the stall condition of the

wing is assessed the orientation angle was variation was carried out for a the entire range of velocities for which the experiment was conducted. Figures 2.12 to 2.14 show the results obtained from these tests thereby showing the aerodynamic performance of the wing during flight.
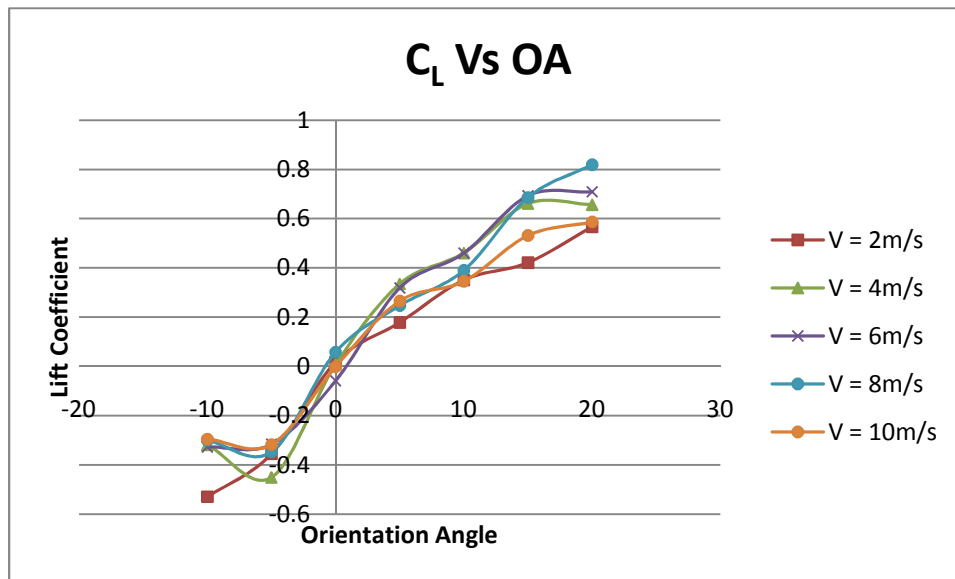
Figure 2.12. Lift Coefficient Vs Orientation Angle for Soaring Flight
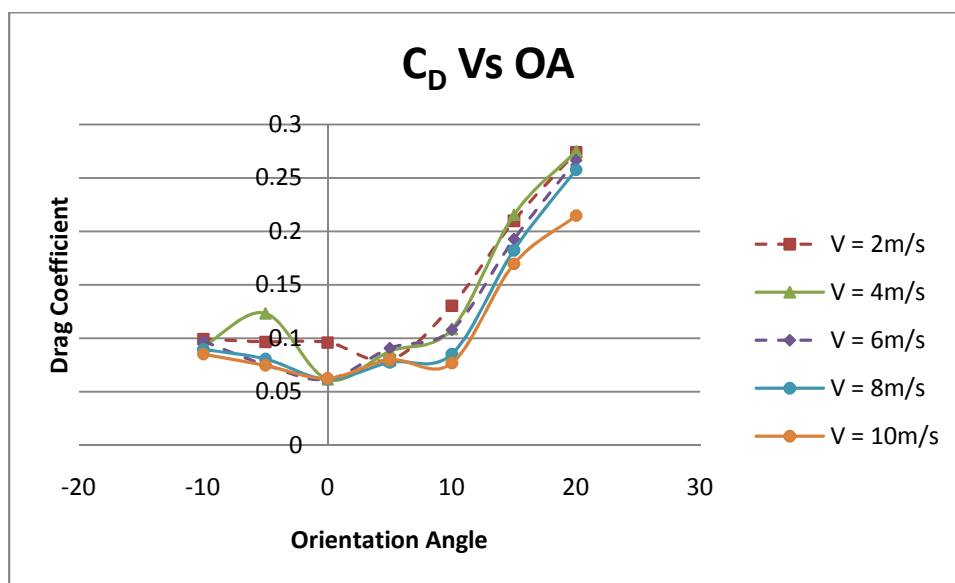
Figure 2.13. Drag Coefficient Vs Orientation Angle for Soaring Flight
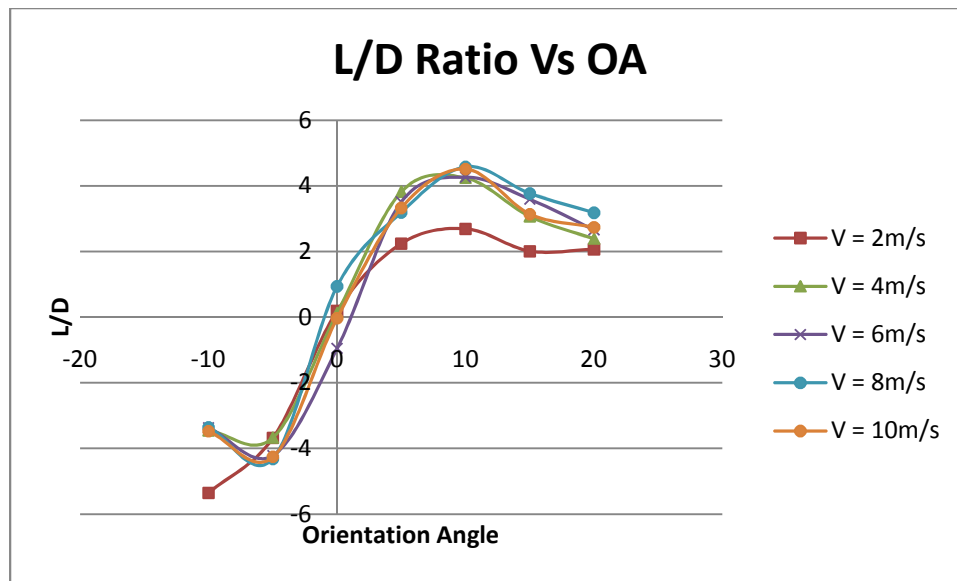
Figure 2.14. L/D Ratio Vs Orientation Angle for Soaring Flight

The figure 2.12 shows the distribution of lift coefficient with respect to the increase in orientation angle of the wing. As it is seen in the figures, the lift coefficient is found to increase in all the cases with increase in orientation angle. However the lift coefficient curves show only a constant increase in their values thereby indicating an absence of stall. The values of lift coefficient at different velocities do not exhibit any increasing or decreasing trend between each other, though they exist within a certain range of values though the results are highly scattered. This scattering can be attributed to the measurement uncertainty of the sensor. When we consider the case of drag coefficient shown in figure 2.13, it was found that the drag coefficient values first decreases with increase an increase in orientation angle at negative orientation angle. This is followed by an increase in of the drag coefficient with an increase in orientation angle. The lift values obtained in this region do not exhibit any pattern either however all the plots follow the same trend of the drag coefficient values decreasing with increase in flow velocity. This steady trend can be seen in all cases up to an

orientation angle of 20°. When we try to understand the effects of these forces acting on the wing, we have to divide the values of lift over that of drag so that the predominant force comes forward. It is visible that the L/D ratio as shown in figure 2.14, increases with an increase in the orientation angle of the wing showing that lift forces generated by the wing is predominant over the drag being generated by the wing. As the angle further increases beyond the OA $= 10^o$, it was found that the L/D ratio begins to decrease with increase in the orientation angle. This proves that the amount of drag produced by the wing increases at higher orientation angles. This decrease L/D ratio shows a decrease in aerodynamic performance of the wing at higher orientation angles where drag begins to play a significant role. This assumption is reached as it was previously observed that airfoils tend to have an increase in drag due to momentum deficit which is produced due to an increase in wake region in the trailing edge of the airfoil. Gradual increase in drag is observed as an initial phase to the stall of an airfoil though in this particular case, the stall angle of the wing is not found out as tests were not carried out at higher angles of attack. In almost all cases where the aerodynamic performance of the wing were matching up with varying velocities in which they were tested. A small anomaly can however be observed in the case where $V_\infty = 2m/s$. Lower L/D values are observed at lower flow velocities but the values gradually tend to increase in the flow velocity. The decrease in the aerodynamic force coefficients can be attributed to the low velocity at which the test was conducted thereby causing the sensor to operate in regions within its design uncertainty parameter. At higher flow velocities, this issue begins to disappear as the forces acting on the wing are larger now and within the operating range of the load cell.

2.2.2 Flapping Flight Force Measurements

The next phase in the testing of the membrane wings using the Cybird flapping mechanism would be to test the aerodynamic characteristics of the wing during flapping flight. The mechanism is powered by the BK Precision 1760A 4 digit triple output power supply the specifications of both of these are mentioned in section 2.1 dealing with the experimental setup. During the aerodynamic testing, the first step would be to remove the initial weight applied by the testing rig and the mechanism when the system does not experience any external loads upon them which in this case would be the aerodynamic forces. This essentially is the instance where the weight of the test subject is removed from the load cell so that the forces acting on it during the testing phase can be distinguished from the forces acting on the load cell during static conditions. Due to the presence of a zero drift in the load cell, the load cell is recalibrated before the experiment begins is repeated regularly before each individual case as the values were found to shift by a small amount as the experiment progresses, possibly due to the fact that the load cell begins to show signs of heating with time. During the initial phase of testing of each case where the velocity is varied, the load cell is zeroed before the experiment begins.

Another factor which also requires consideration is the aerodynamic forces acting on the body of the mount on which the wings are attached. Though the forces acting on the mount are not of a large magnitude, they are still taken in to consideration for the sake of accuracy of the measurements. During the testing process of each case, the aerodynamic forces acting on the mount is measured by removing the wings on them during the testing process. The measurements are taken in conditions similar to flapping flight where the

change in orientation simulates varying geometric angle of attack of the wing at different flow velocities and wing beat frequencies. Though the wings are removed by opening the door of the test section while the wind tunnel is operational, a reasonable amount of time is given before the data acquisition is initialized again so as to allow a sufficient amount of time allowing the flow conditions to become steady after the apparent disturbance caused by opening the test section door dies down.

While conducting the force measurements on the flapping wing, the mount is placed at a specific angle of attack measured by a digital angle gauge and the wind tunnel is set to a specific flow velocity as per the calibration curve which was generated earlier. As a first step in the experiment the measurement of aerodynamic forces of soaring flight condition of the wing is carried out. This is done in-order to calculate the lift and thrust augmentation generated by the wings due to flapping flight. The explanation of these terms would be done later in the chapter. Before each test case for the flapping flight, the force measurements are carried out on the wings in the soaring condition first so that the data gathered would be under the same ambient conditions. Voltage in the power supply is varied with increments of 1 Volt and the force data is gathered by the load cell for each of the cases. The Voltage limit for the experiment was restricted to 7 volts as it would prevent the motor from overloading and also to prevent the case of excessive vibration of the mount which was observed when tests were conducted simulating hovering flight. The load cell gathers a total of 30,000 data points over a period of 30 seconds with an acquisition frequency of 1 kHz. Upon further analysis of the data gathered during the experiment, it was also found that the application of

up to 7 volts would lead to the system reaching a wing beat frequency slightly in excess of 10Hz.

The wing beat frequency was measured with the help of instantaneous time series data. During the data acquisition of the aerodynamic forces by the load cell, the time history of the force measurements are gathered by the wing are also registered during the experiment. By applying an FFT (Fast Fourier Transform) algorithm to the time series of the force measurement, the frequency of the variation in the forces due to flapping flight can be determined thereby the wing beat frequency of the test subject is determined. To apply an FFT algorithm on the data gathered during the experiment, a MATLAB code was used to generate the FFT power spectrum. The x-axis value of the highest peak which will be visible after the analysis would represent the frequency of the system. Figure 2.15 shows a sample power spectrum and its corresponding frequency for one of the cases of the current experiment.
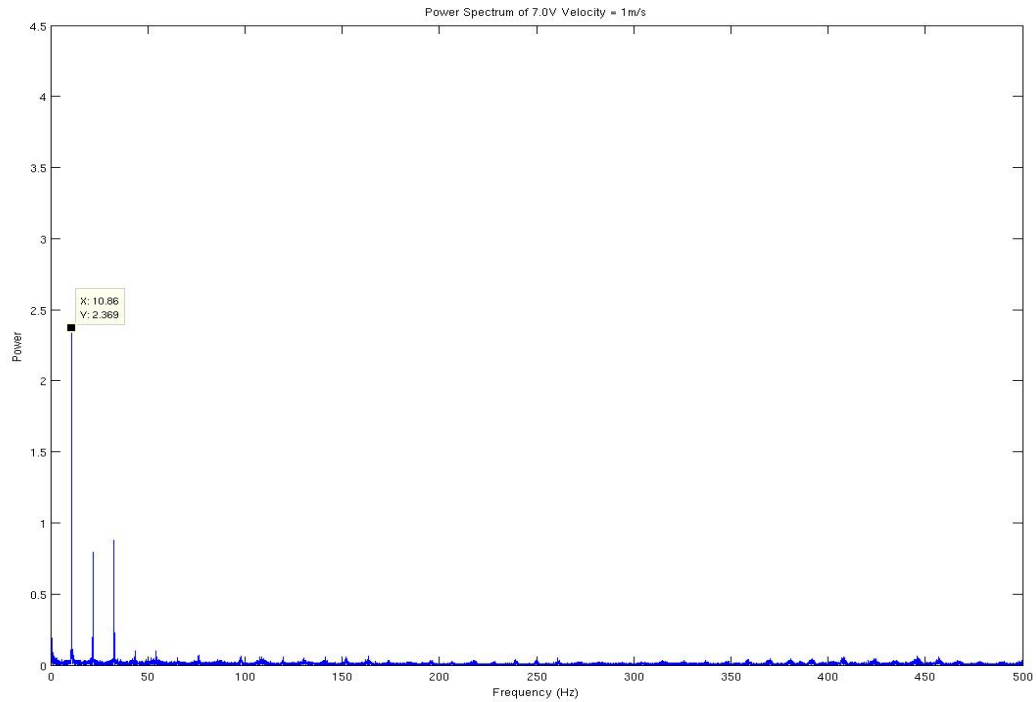
Figure 2.15. Power Spectrum and Frequency for a sample case

During the analysis of the data, the forces generated by the flapping motion of the wing is measured proportional to the wing beat frequency of the system. The results from the experiments conducted on the Cybird mechanism is shown from figures 2.16 – 2.22. These results will provide an outlook into the performance of a flapping wing while it is subjected to varying flight speeds and angles of attack with increasing wing beat frequency is increased in each of the cases. These results obtained are from conditions which simulate flight parameters and characteristics to which MAVs would be subjected to during its operation.
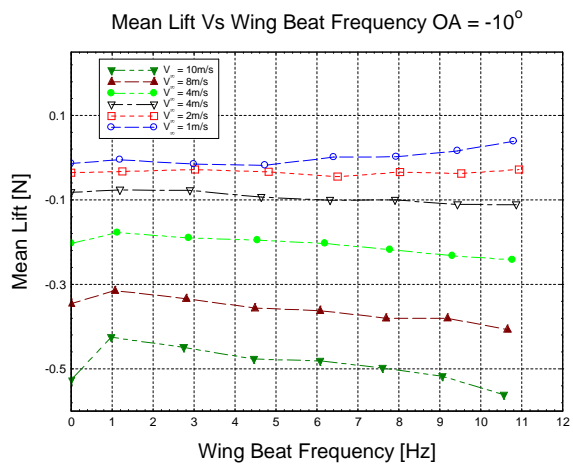
(a)Mean Lift
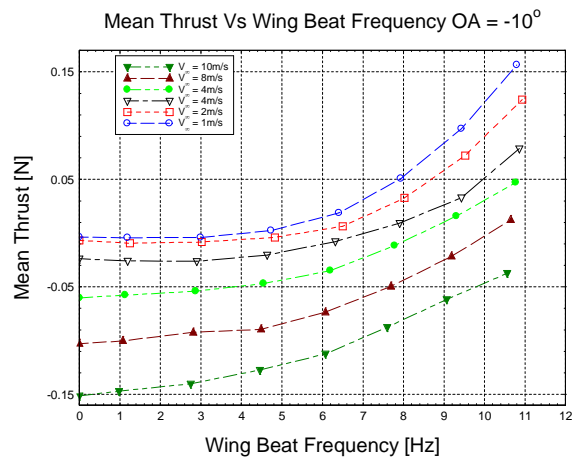
(b) Mean Thrust

Figure 2.16. Time averaged Lift and Thrust values at OA = -10°
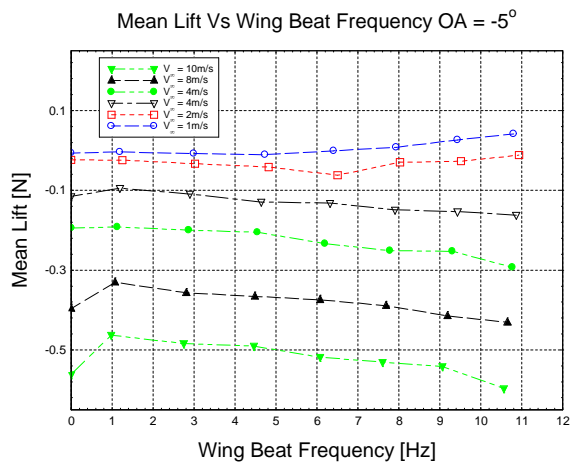
(a) Mean Lift

(b) Mean Thrust

Figure 2.17. Time averaged Lift and Thrust values at OA = -5°
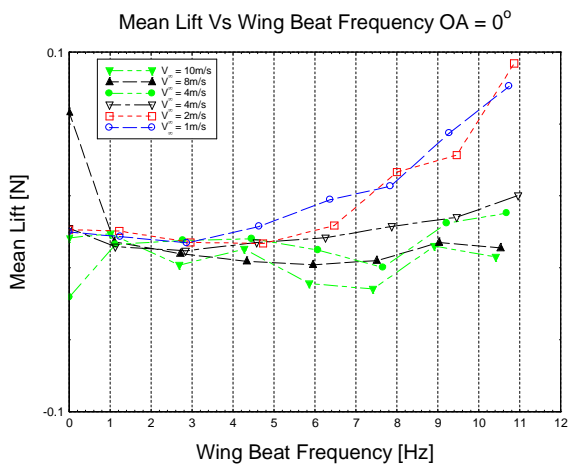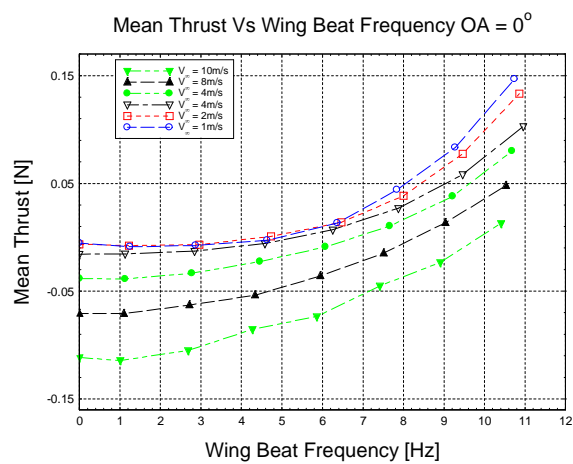
(a) Mean Lift

(b) Mean Thrust

Figure 2.18. Time averaged Lift and Thrust values at OA = 0°
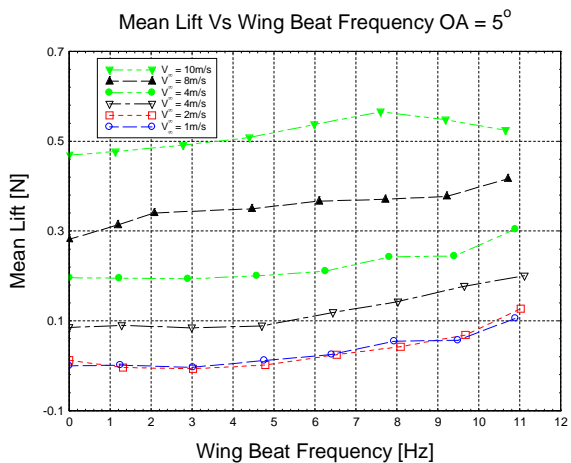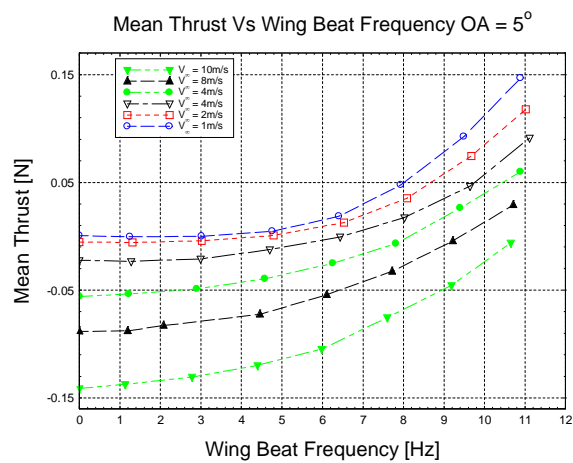
(a) Mean Lift

(b) Mean Thrust

Figure 2.19. Time averaged Lift and Thrust values at OA = 5°
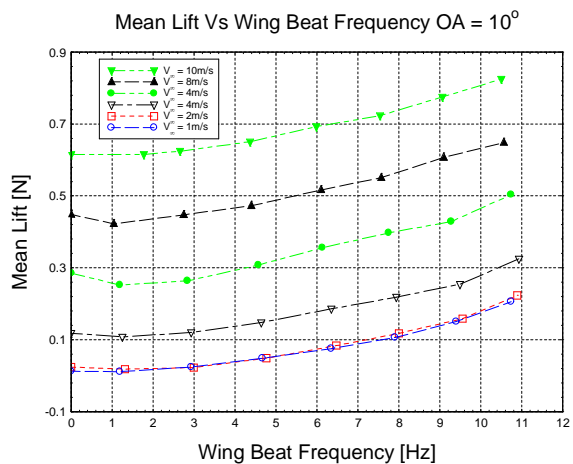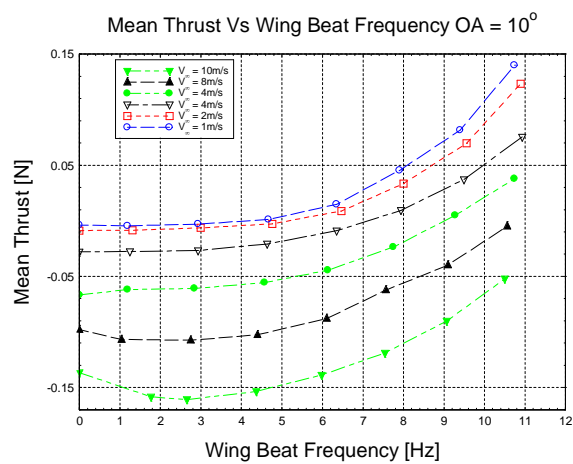
(a) Mean Lift

(b) Mean Thrust

Figure 2.20. Time averaged Lift and Thrust values at OA = 10°
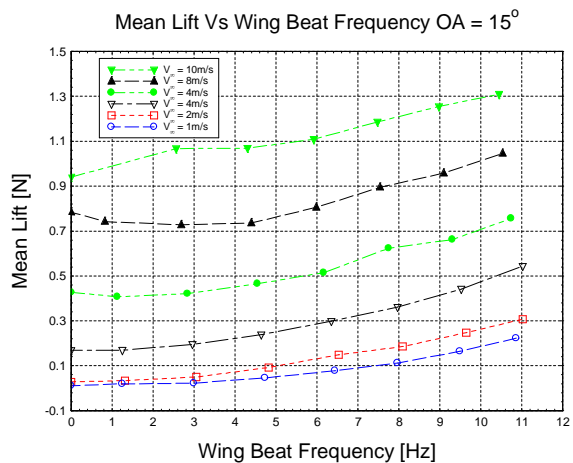
(a) Mean Lift
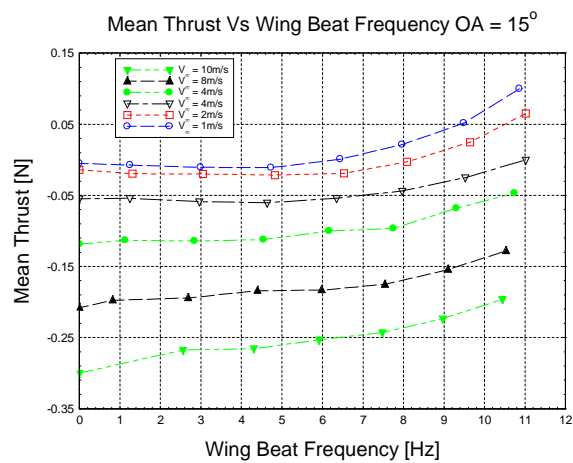
(b) Mean Thrust

Figure 2.21. Time averaged Lift and Thrust values at OA = 15°

Mean Lift Vs Wing Beat Frequency OA = 20°

Mean Thrust Vs Wing Beat Frequency OA = 20°

(a) Mean Lift

(b) Mean Thrust
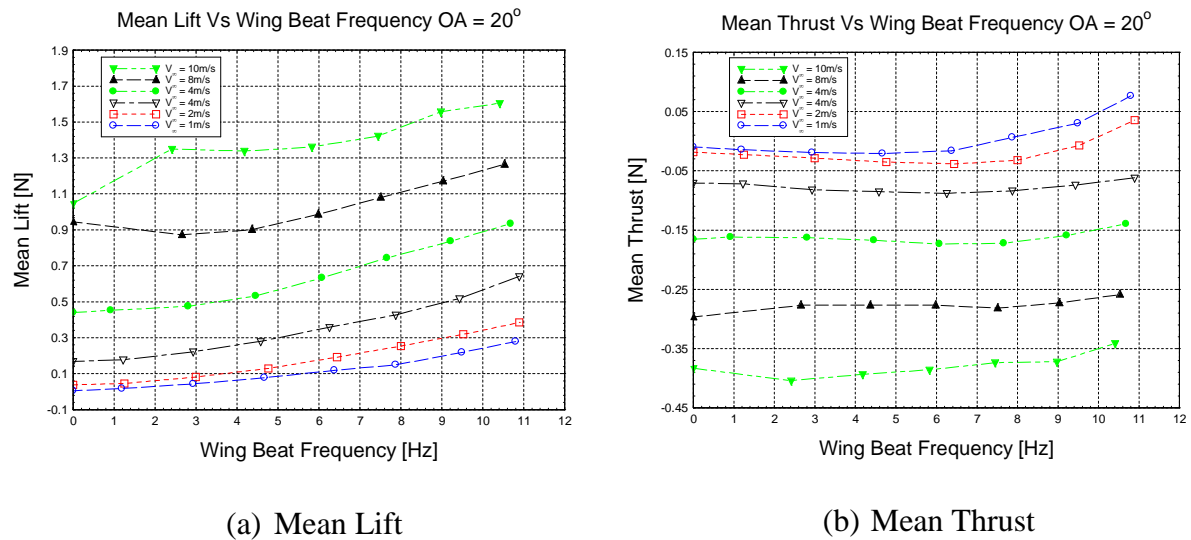
Figure 2.22. Time averaged Lift and Thrust values at OA = 20°

For the initial case, the mechanism was placed at an Angle of Attack of 0° to study the effects of level flight. During this case, it was observed that the system was found to generate sufficient amount of thrust. On the other hand, the lift values were found to be very low and do not display any specific pattern, this is because at level flight flapping wings are unable to generate lift forces and thrust is the only force which would be produced. On the other hand the thrust produced by the system was found to form a definite pattern. With the increase in the free stream velocity values, the thrust was found to show decreasing values though this was found to increase with increase in the wing beat frequency in each case. The negative values of thrust are understood to be in the drag region. Also the values of thrust which are observed in this case do not seem to be significantly higher than the lift values though it is higher by a small factor. At higher flow velocities, the wing performance was found to be balanced towards the drag region with lift being produced only at higher flapping frequencies. It can be concluded that the aerodynamic force generation in this particular

orientation angle is the lowest. As the orientation angle is varied by an increment of 5°, it can be observed that the lift values generated due to flapping flight have increased significantly with increase in flow velocity. Also with the increase in the orientation angle, the thrust values were also found to decrease with respect to the free stream velocity. However similar to previous results, the lift and thrust values which are being generated during the experiment were found to increase with increasing wing beat frequency. The lift values in these cases were found to be the maximum at highest free-stream velocities and for positive orientation angle, these lift values were found to increase with increase in orientation angle. As for the thrust being generated, as the orientation angle increases drag was found to be produced at higher free stream velocities and this trend was found to increase with an increasing orientation angle. This trend is always observed in the case of positive orientation angles. Another observation to be made would be that the motor of the Cybird mechanism was found to lack the ability to flap the wings at higher orientation angles when the wing beat frequency was the lowest. Such case where the motor does not generate enough lift was ignored and force measurement data was gathered at the next possible case where the wings are able to flap.

A different trend emerges with the use of negative orientation angles. In the negative region, the orientation angle of the wings were varied to -5° and -10°. It was found that the lift values generated by the wings were decreasing with increase in free-stream velocity. Another observation to be made is that the lift values were found to decrease with the increase in wing beat frequency especially at higher free stream velocities. On the other hand the thrust values were found to have a similar increasing trend as observed with the

orientation angle increases. Though in this case thrust production is severely limited except for some cases when the free stream velocity is low and a high wing beat frequency comes to the picture. It could also be noted that the thrust values were not found to change significantly during the course of tests conducted with negative angle of attack. However the lift values were also found not to vary in a similar downward trend with increase in wing beat frequency is spotted in both cases though a large change cannot be observed as the angle of attack in this direction is limited to only -10°.

(a) Lift Vs Orientation Angle   (b) Thrust Vs Orientation Angle
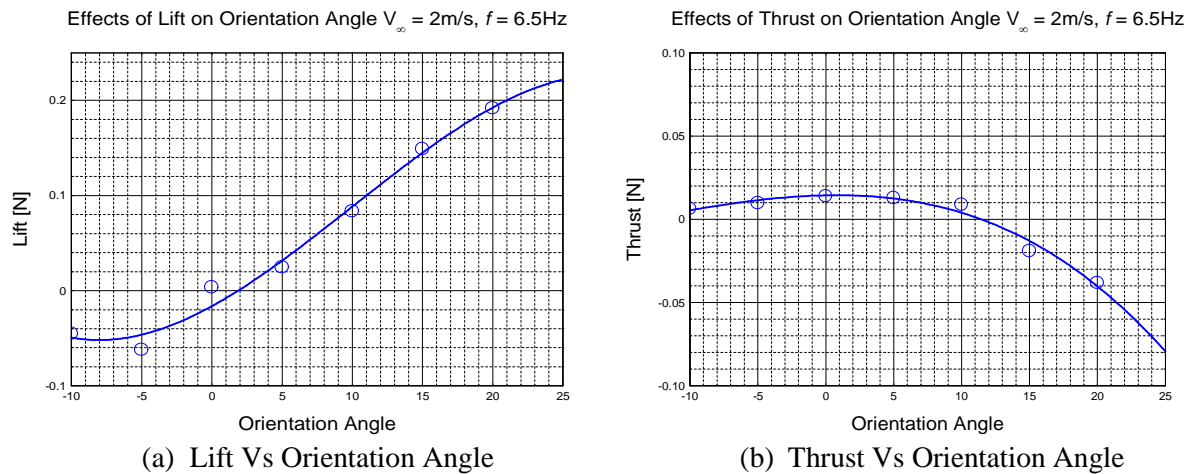
Figure 2.23. Lift and Thrust values at different Orientation Angles

To summarize the results obtained from the above cases, it was found that the thrust values decreases with increasing orientation angle. The lift values on the other hand were found to increase with increasing angle of attack. At negative orientation angles, the thrust values were found to increase slightly at first then was found to decrease at positive orientation angles.

2.2.3 Advance Ratio

Another factor which is to be taken into account for flapping flight is the aerodynamic regime in which the flapping wing flier operates. Aerodynamics of such instances are divided into two types namely the quasi steady regime and the unsteady regime. As an application to MAV design parameters, Ho et al. [23] have conducted studies on how these flow regimes could be predicted with the help of controllable parameters. This stark difference in the aerodynamic regimes at which different flapping flyers operate can be observed in the flight characteristics of smaller birds such as the humming bird compared to that of much larger birds such as eagles. Smaller birds tend to flap their wings at a much higher frequency in the order of several thousand beats per minute compared to bigger birds such as the eagle that have a much lower wing beat frequency and rely much more on soaring to stay airborne for much longer period of time. In these studies by Ho et al. [23] the unsteadiness was found to be related to the wingtip velocity generated by the flapping wing. It was found that higher the wing beat frequency; the unsteadiness of the flow also increases. To express unsteadiness in the flow, a non dimensional parameter was introduced by Ho et al. [23] called the advanced ratio which is indicated by the formula

$$J = \frac{Forward\ Flight\ Speed}{Wingtip\ Velocity} = \frac{V_\infty}{2\ b\ f\ \Phi}$$

Where V_∞ is the free-stream velocity b is the wingspan of the flapping wing, f is the wing beat frequency and Φ is the sweep angle of the wing. The advance ratio can also be interpreted as a comparison of the wing tip velocity with respect to the free-stream velocity. This parameter is a lot similar to the inverse of the reduced frequency which is generally used

while describing systems involving oscillating or flapping bodies. The reduced frequency k which can also be expressed by the equation

$$k = \frac{\omega\ c}{2\ |V_\infty|}$$

Where ω is the angular velocity generated by flapping wing, c is the chord length of the wing and V_∞ is the free-stream velocity to which the wing is subjected.

According to the previously mentioned study, when the value of advance ratio is greater than one (J > 1), the flow is considered to be quasi-steady. This is the case when the free-stream velocity is higher than the wing tip velocity generated by the flapping. The wing tip velocity is a function of the wing beat frequency as the other parameters are generally fixed for flapping mechanisms. In this case the wake region generated due to flapping is expected to be severely influenced by the free stream flow as the vortex structures would be severely damped by the free-stream flow at higher flow velocities. When the advance ratio is less than 1 (J < 1), the flow is considered to be unsteady. This is the case when the wing tip velocity is higher than the free-stream velocity. As the wing flaps with this advance ratio, the wake region generated would be very unsteady and the vortex structures formed would have a limited interference by the free-stream velocity. Insects generally tend to fly in the unsteady regime as their wing beat frequencies are much higher than compared to larger flying animals. Finally, when the advance ratio is equal to 1 (J = 1) a transition point is formed between the quasi steady and the unsteady regimes of flight. In this region, the wing tip velocity would be equal to that of the free-stream velocity. The vortex structures generated in this advance ratio would be studied in greater detail in a later chapter.

Another purpose of this study would be to observe the advantages of flapping flight on wings in comparison to similar conditions where the wing is subjected to soaring flight. To bring forth this advantage, the augmentation of lift and thrust generated due to flapping flight are calculated. The following formulae were used to calculate the thrust and lift augmentation generated by flapping flight.

$$\Delta L_{Flapping} = L_{Flapping} - L_{Soaring}$$

$$\Delta T_{Flapping} = T_{Flapping} - T_{Soaring}$$

In both the cases, the lift and thrust values generated due to flapping flight and the soaring flight are subtracted from each other thereby giving the resultant forces observed during flapping flight. The next step is to non-dimensionalise these two parameters by converting them into coefficients similar to lift and thrust coefficients. The lift augmentation and thrust augmentation coefficients are calculated by the two equations shown below.

$$\Delta C_L = \frac{\Delta L_{Flapping}}{\frac{1}{2}\rho_\infty V_\infty^2 S} = \frac{L_{Flapping} - L_{Soaring}}{\frac{1}{2}\rho_\infty V_\infty^2 S}$$

$$\Delta C_T = \frac{\Delta T_{Flapping}}{\frac{1}{2}\rho_\infty V_\infty^2 S} = \frac{T_{Flapping} - T_{Soaring}}{\frac{1}{2}\rho_\infty V_\infty^2 S}$$

In the above two equations, ΔL is the lift augmentation due to flapping ΔT is the thrust augmentation due to flapping, ρ_∞ is the density of the fluid and S is the wing plan form area. The non-dimensionalisation of these terms provides the basis for a comparative study of the forces being generated during flapping flight and the advantages of each case. Figures 2.24 – 2.37 shows the lift and thrust augmentation plotted against their respective advance ratios.
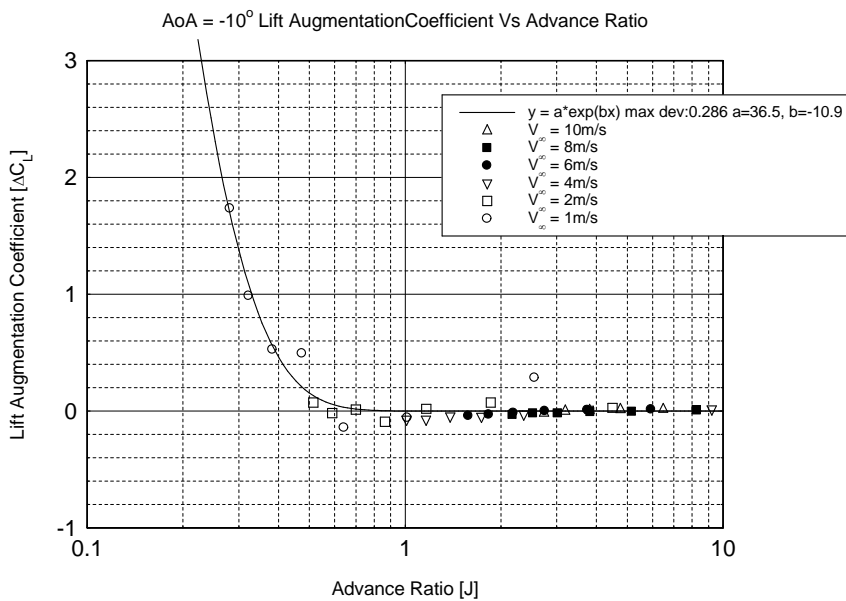
Figure 2.24. Lift Augmentation AoA = -10°
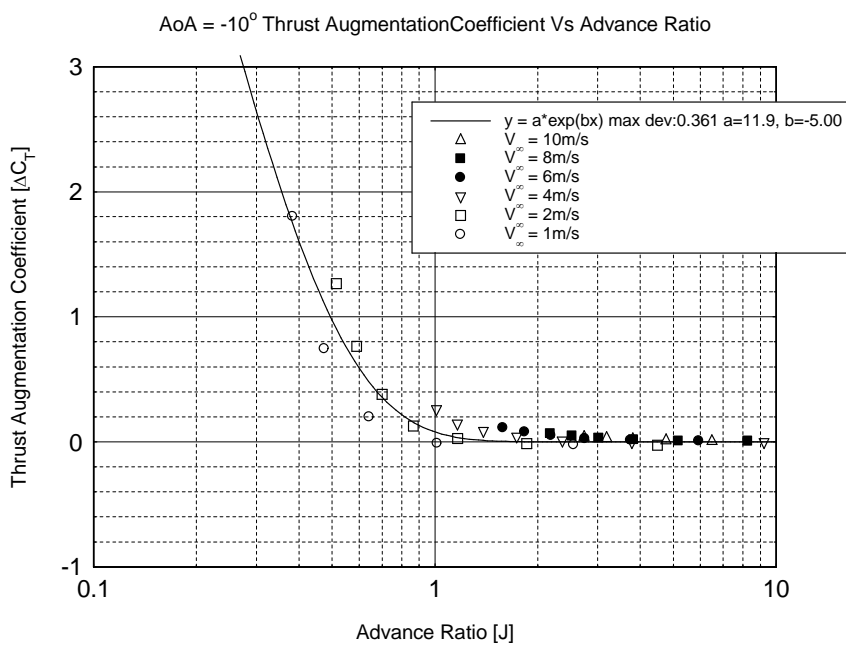
Figure 2.25. Thrust Augmentation AoA = -10°

AoA = -5° Lift AugmentationCoefficient Vs Advance Ratio
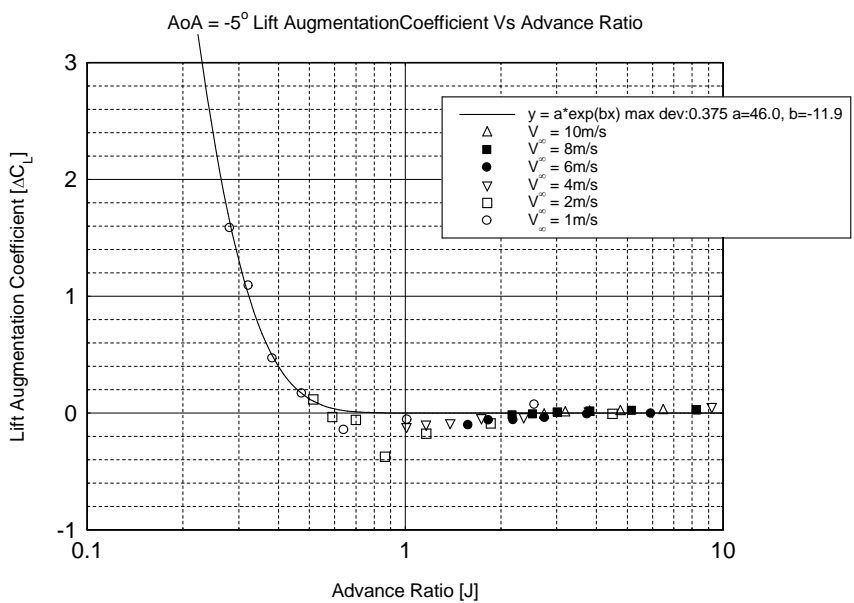
Figure 2.26. Lift Augmentation AoA = -5°

AoA = -5° Thrust AugmentationCoefficient Vs Advance Ratio
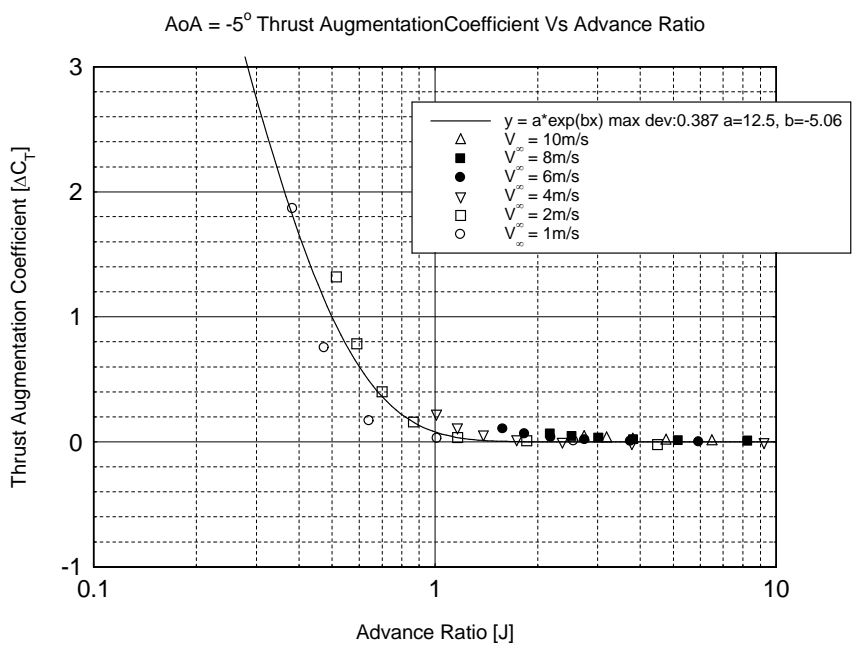
Figure 2.27. Thrust Augmentation AoA = -5°

AoA = 0° Lift AugmentationCoefficient Vs Advance Ratio
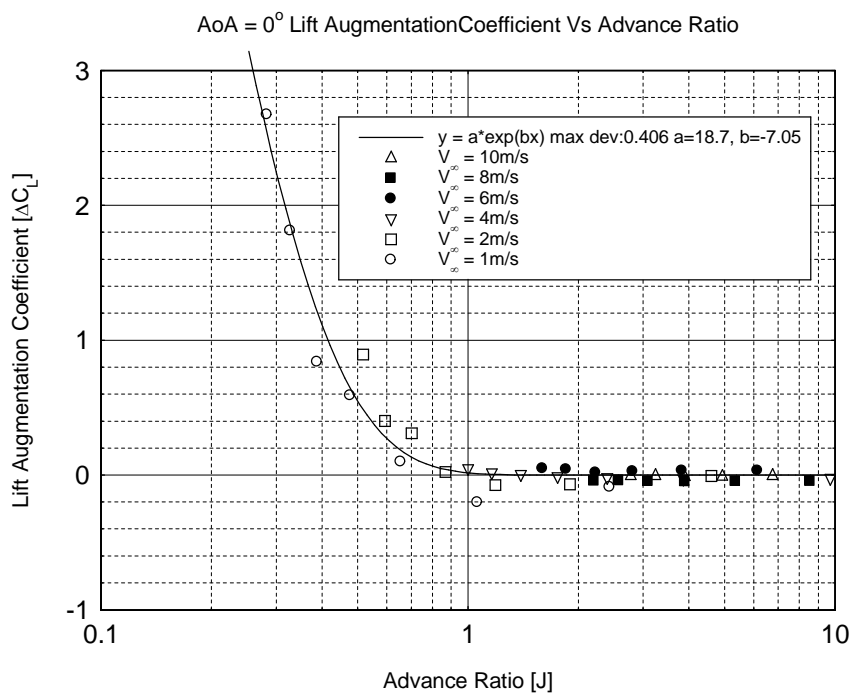
Figure 2.28. Lift Augmentation AoA = 0°

AoA = 0° Thrust AugmentationCoefficient Vs Advance Ratio
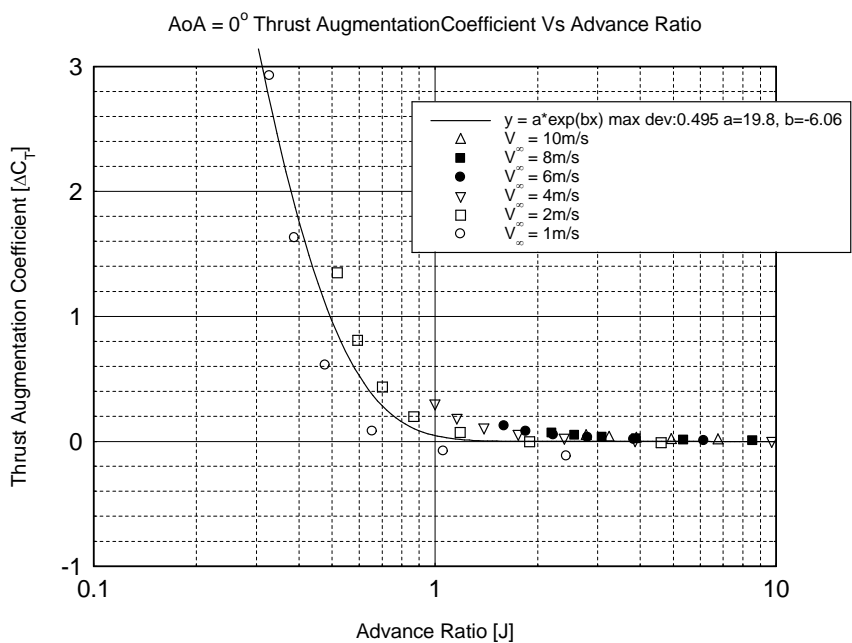
Figure 2.29. Thrust Augmentation AoA = 0°

AoA = 5° Lift AugmentationCoefficient Vs Advance Ratio
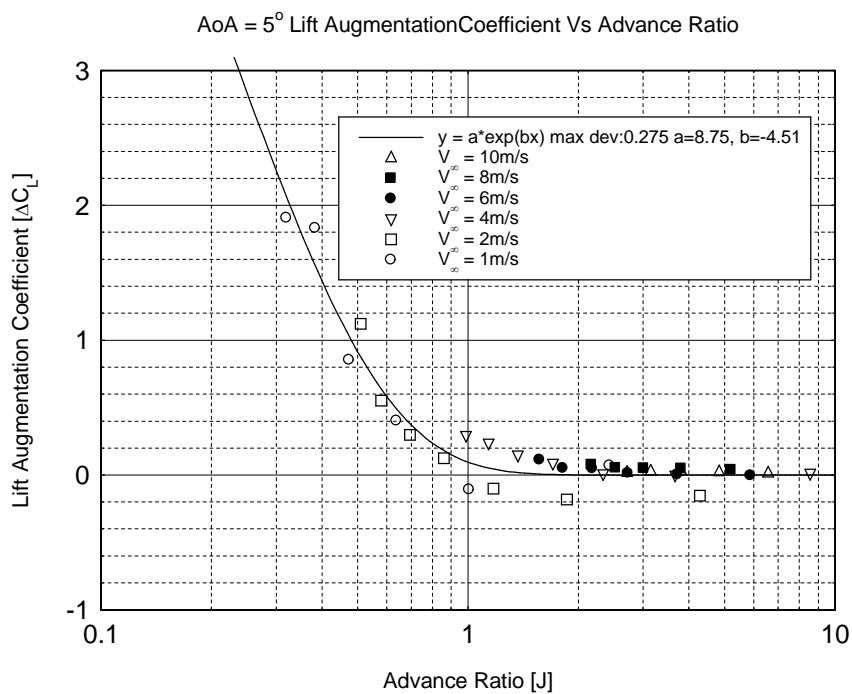
Figure 2.30. Lift Augmentation AoA = 5°

AoA = 5° Thrust AugmentationCoefficient Vs Advance Ratio
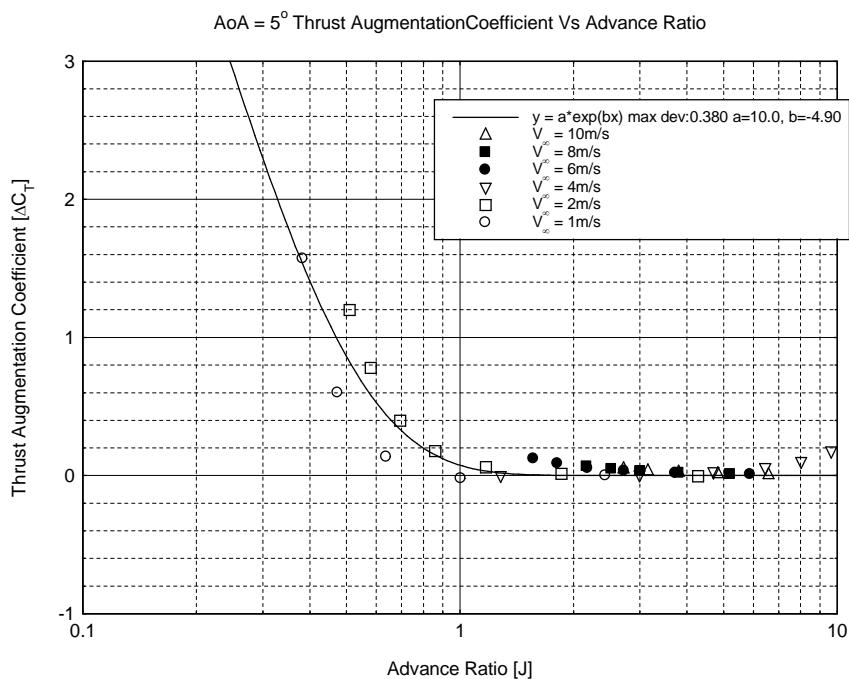
Figure 2.31. Thrust Augmentation AoA = 5°

AoA = 10° Lift AugmentationCoefficient Vs Advance Ratio
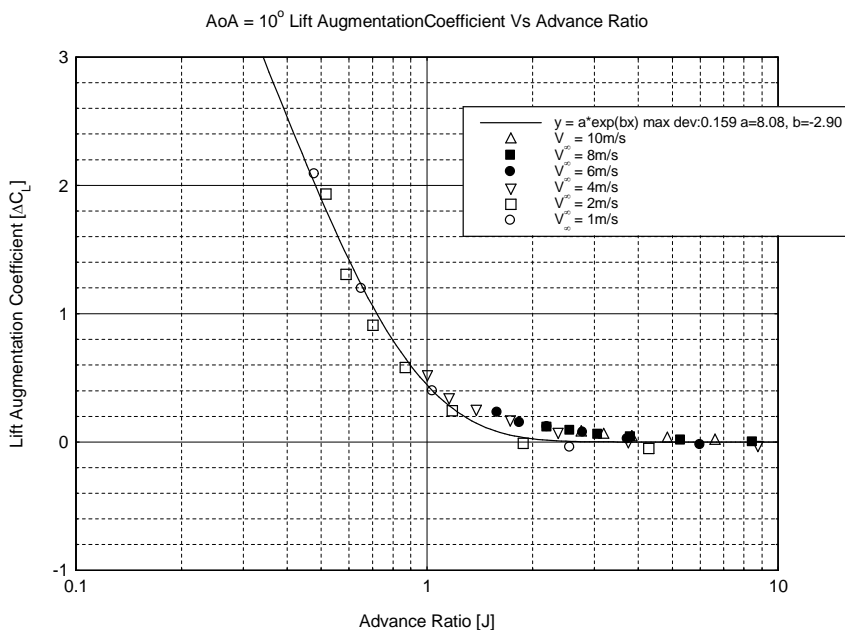
Figure 2.32. Lift Augmentation AoA = 10°

AoA = 10° Thrust AugmentationCoefficient Vs Advance Ratio
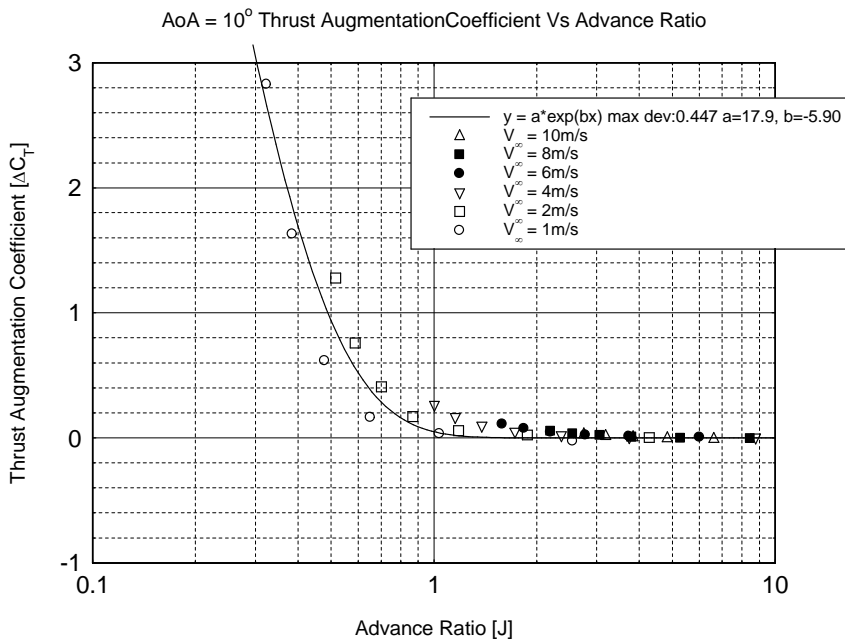
Figure 2.33. Thrust Augmentation AoA = 10°

AoA = 15° Lift AugmentationCoefficient Vs Advance Ratio
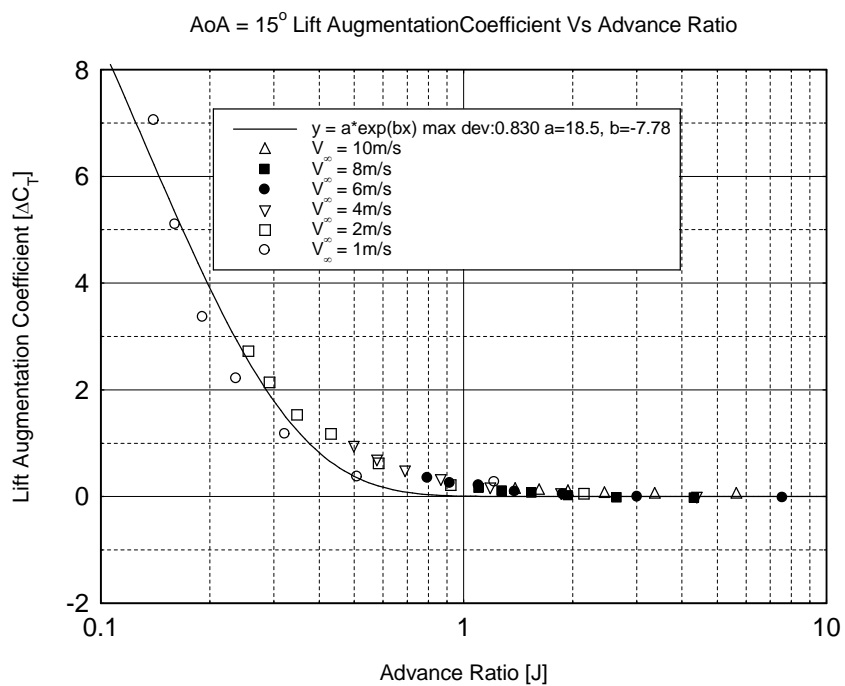
Figure 2.34. Lift Augmentation AoA = 15°

AoA = 15° Thrust AugmentationCoefficient Vs Advance Ratio
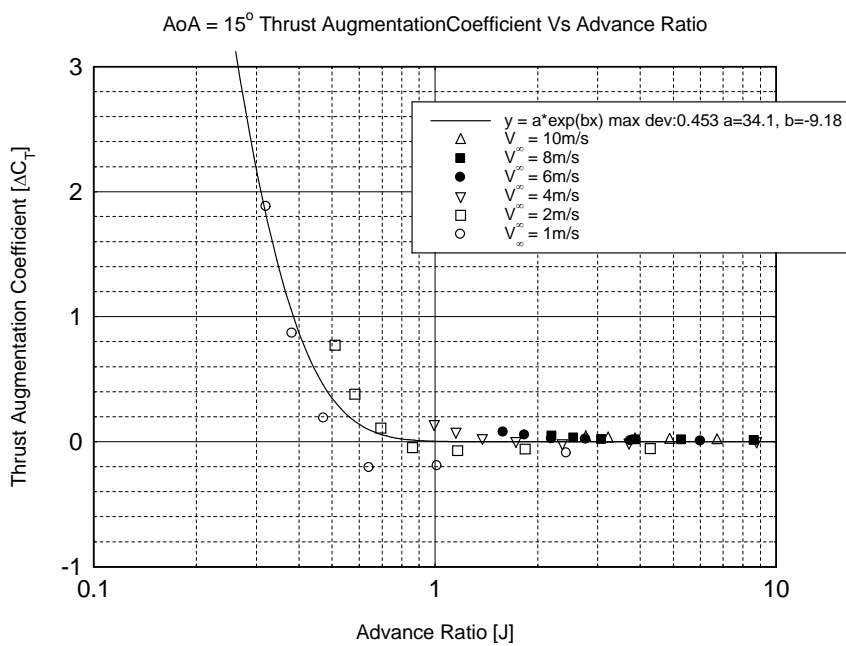
Figure 2.35. Thrust Augmentation AoA = 15°

AoA = 20° Lift AugmentationCoefficient Vs Advance Ratio
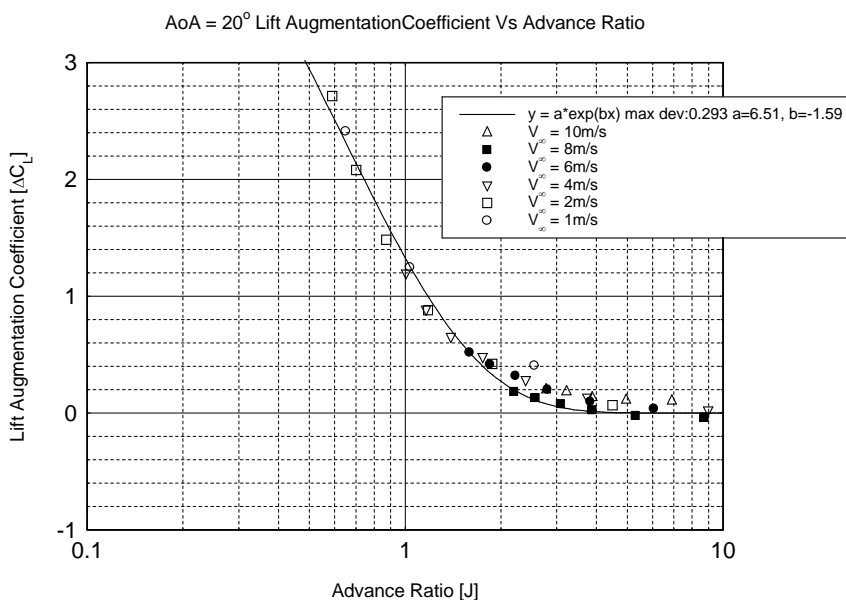
Figure 2.36. Lift Augmentation AoA = 20°

AoA = 20° Thrust AugmentationCoefficient Vs Advance Ratio
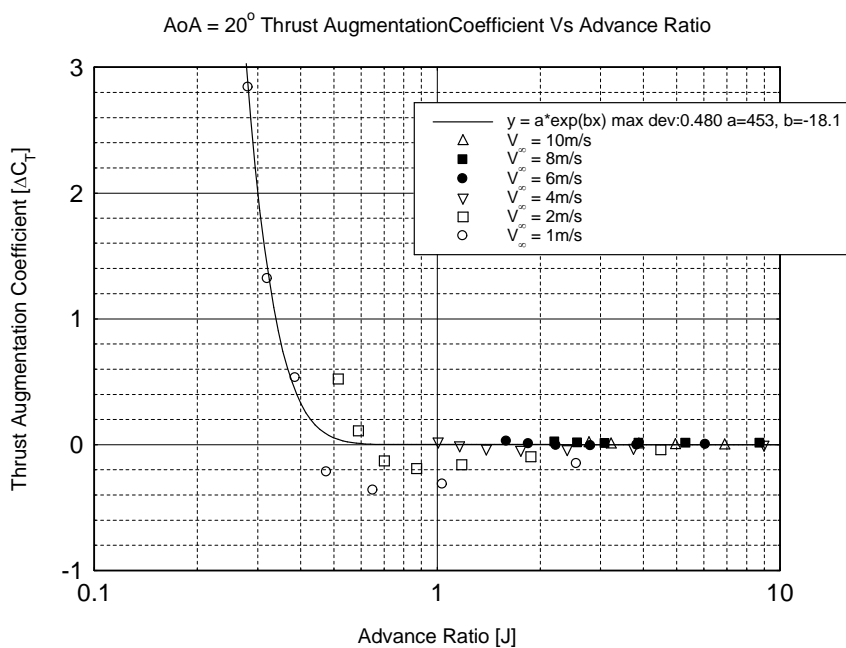
Figure 2.37. Thrust Augmentation AoA = 20°

From the above results, it can be observed that the results obtained from the experiments show an exponential decrease in lift and thrust augmentation values. As

mentioned in Ho et al. [23] the lift and thrust coefficient values are found decrease exponentially as the advance ratio increases as it is expected in low chord Reynolds number flows in the range Re< 10^4. This can be observed in each case throughout the results shown above. On the other hand it can also be observed that at lower advance ratios, the lift and thrust values observed are found to increase exponentially. When an exponential curve fit was placed on the results shown above, the values were found to agree with the trend fairly. From preliminary observations into these results, it can be concluded that due to the high aerodynamic forces being produced in the region where J<1 or in the unsteady flow regime. It can be concluded that higher flying in the unsteady regime would be more efficient for flapping flight as the lift and thrust values generated in this region is exponentially higher than soaring flight.

Upon closer inspection of the lift and thrust augmentation values shown above, it is found that at lower advance ratios, the augmented aerodynamic forces generated by the wings are much higher than compared to the ones generated at higher advance ratios. While observing the trend formed with increasing orientation angle, it can be concluded that as the orientation angle steadily increases from 0° with increments of 5° each, the thrust values are found to decrease gradually on the other hand the lift values being generated by the wings are increasing with the increase in angle of attack. When the angle of attack reaches 10° it was found that there has been a significant increase in lift produced by the wing which was found to be consistently increasing after this particular case, at the same time the thrust generation continues to gradually decrease. This trend continues as the angle of attack increases with the lift values increasing and the thrust values decreasing gradually. A similar trend is still

observed in results obtained from tests conducted at negative orientation angles. The thrust values were found to be the highest when the angle of attack is oriented in the negative region. It is also observed that the lift values are found to be lowest in this region. All these observations are noted at the lowest advance ratios at which the aerodynamic forces are found to be the maximum for that particular orientation angle. The comparison of the lift and thrust values being generated by flapping were done with reference to the plots in figures 2.12 and 2.13 where the soaring results of the wings were calculated. Another observation which can be made on the results is that the majority of the data points were found to lie within the region where the advance ratio is in the transition point between the unsteady and quasi-steady regime. This indicated that the region where the flapping wing mechanism would operate during flight. Similar results generated while the flexibility effects of flapping mechanisms were studied also indicate a concentration in data points in the region around where $J = 1$ these results would be discussed in a later chapter. This regime is more efficient as lower J values require higher flapping frequency which would require a larger amount of energy to be spent by the flapper. It is also observed in some of the cases in the lift and thrust augmentation graphs that certain values calculated do not follow the general exponential trend and in some cases, the values were found to lie in the negative region of the scales. These peculiar cases can be attributed to the measurement uncertainty of the force sensor as the regions where the oddities are found specially where the values fall over to the negative region were found be of very small magnitude and were present at low free stream velocities.

2.2.4 Efficiency Studies

Owing to the much smaller size of the micro air vehicles, another area which is of interest would be to study the efficiency of unmanned systems by which the endurance of such systems can be calculated and optimized. Early attempts to study the efficiency of thrust producing wings or oscillating airfoils was conducted by Anderson [6]. Gallivan and DeLaurier[24] has also performed studies on a similar manner by which the propulsive efficiency of flapping mechanism during wind tunnel testing was calculated. The studies by Gallivan and DeLaurier were specifically directed towards developing flapping wing MAV. While Gallivan and DeLaurier adopted these studies to compare the effectiveness of different types of wings during flapping flight and to find the effects of wing flexibility and their influence on the propulsive efficiency of the flapping mechanism.

For determining the propulsive efficiency of the flapping wing, the readings of the current flowing through the circuit during the experiment were measured with the help of a multi meter. During the experiment, the current flowing through the circuit was found to vary within a specific range. This fluctuation is specially noticed at higher orientation angles and can be explained by the motor drawing more power to overcome the aerodynamic forces acting on the wings. On finding the average value of the current being consumed by the system, the power required to drive the motor will be calculated by the formula.

$Power = V\,I$

Where P is the electrical power consumed by the system. V is the voltage input which is applied into the system. In the case of the current experiment, the voltage is varied through

the power source. I is the input current reading which is measured with the help of a multi meter connected in parallel to the circuit. The propulsive efficiency of the flapping wing is calculated using the equation

$$\eta = \frac{T\,U}{Power} \times 100$$

Where T is the thrust produced by the flapping mechanism and U is the free-stream velocity in the wind tunnel test section.
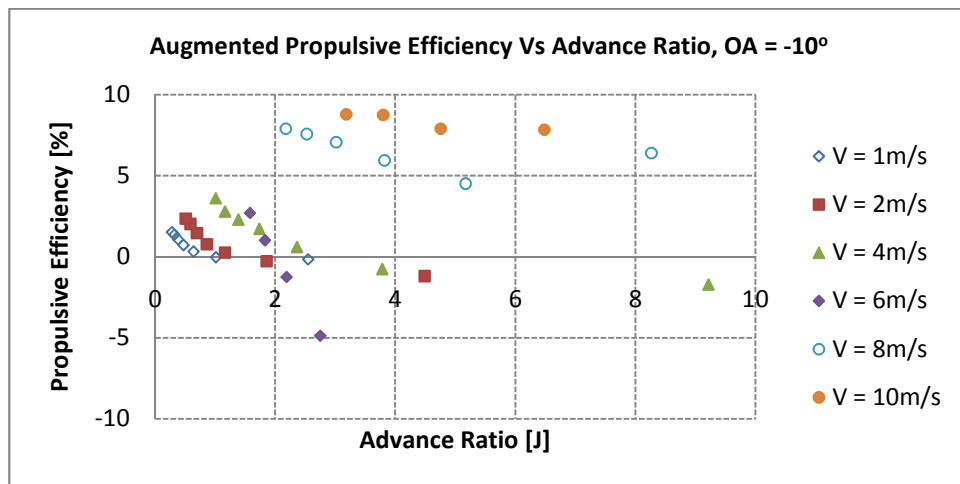
Figure 2.38. Propulsive Efficiency Vs Advance Ratio OA = -10°
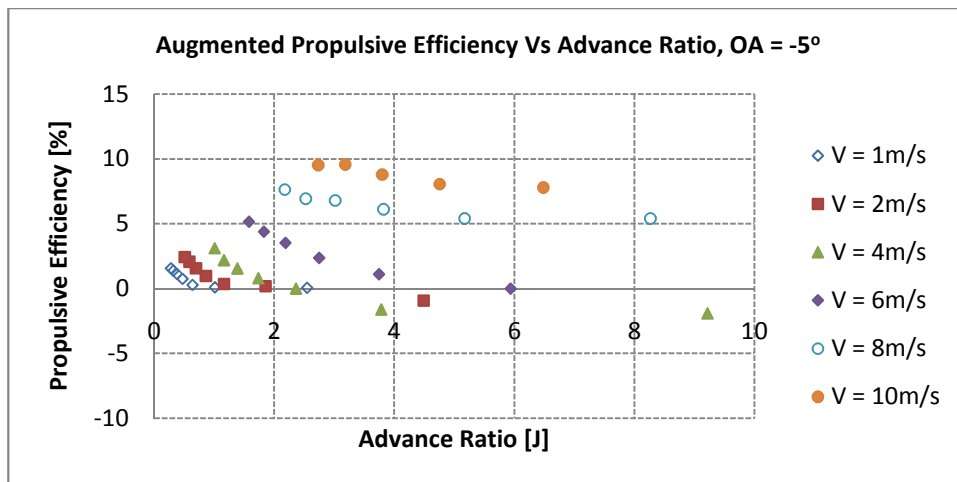
Figure 2.39. Propulsive Efficiency Vs Advance Ratio OA = -5°
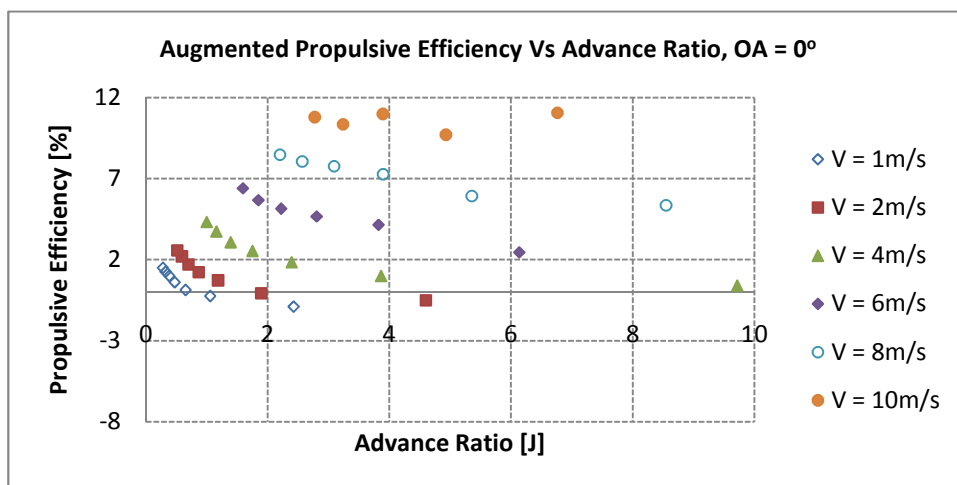
Figure 2.40. Propulsive Efficiency Vs Advance Ratio OA = 0°
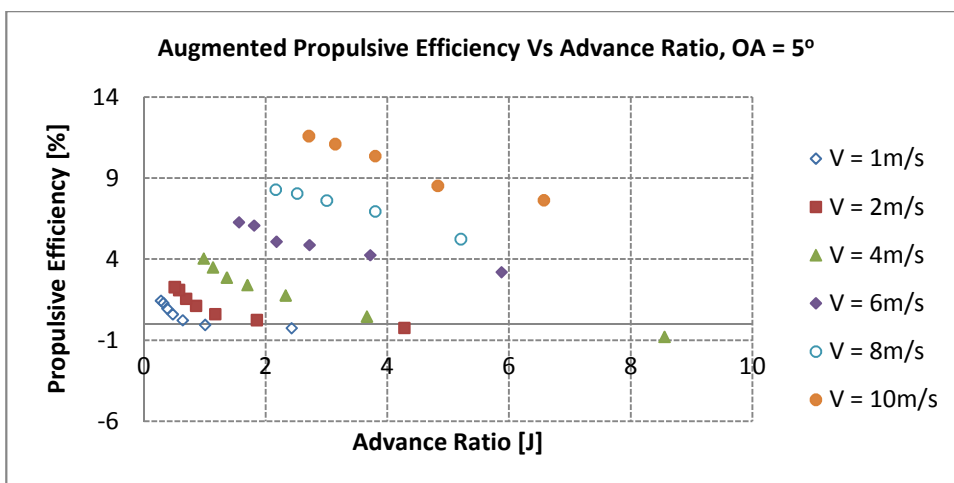
Figure 2.41. Propulsive Efficiency Vs Advance Ratio OA = 5°
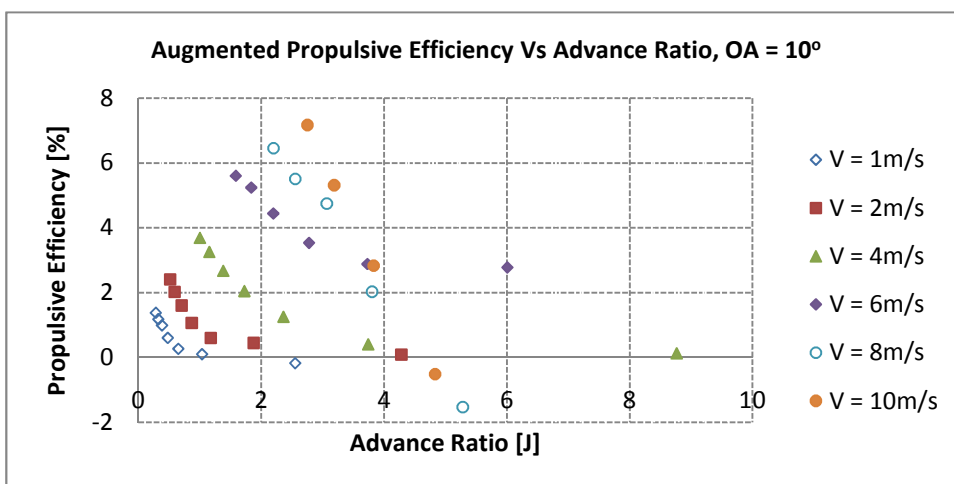
Figure 2.42. Propulsive Efficiency Vs Advance Ratio OA = 10°
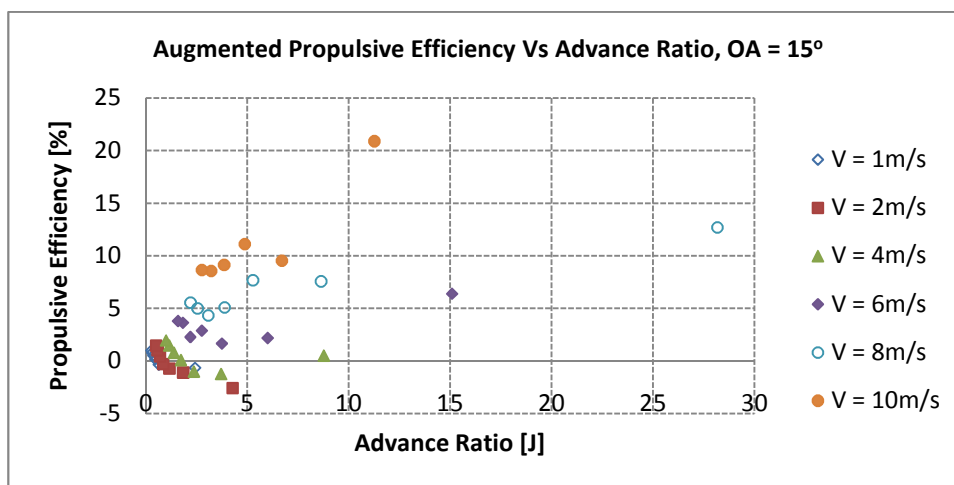
Figure 2.43. Propulsive Efficiency Vs Advance Ratio OA = 15°
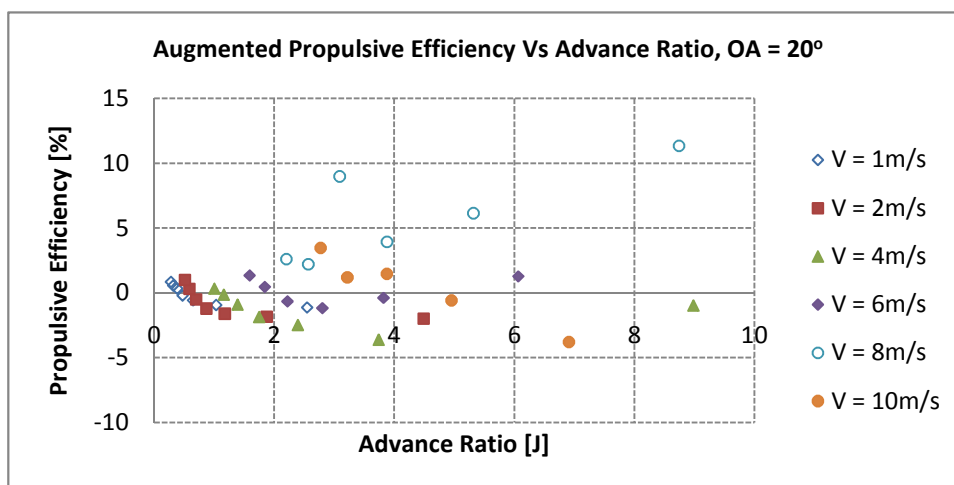
Figure 2.44. Propulsive Efficiency Vs Advance Ratio OA = 20°

The propulsive efficiencies obtained from the calculations are shown in figures 2.38 – 2.44 where the efficiencies are compared with respect to the advance ratios in which they operate. The results are plotted in a graph where the advance ratio is in the x-axis and the efficiency is portrayed as a function of the advance ratio. Some of the results lie within the negative axis of the efficiency scale and were deliberately removed from the graphs as they

are the drag produced by the flapping mechanism. In comparison with the work conducted by Gallivan, the drive efficiency of the flapping mechanism was ignored as the current results present a qualitative look at the effects of propulsive efficiency at varying orientance angles.

The experimental data indicates that the wings are able to produce a higher propulsive efficiency at higher free-stream velocities. This trend is continued in all orientation angles at which the experiments were conducted. The efficiency values were found to increase in each case with increase in the free stream velocity. In all the cases, the higher amount of propulsive efficiency was found in cases where the advance ratio is in the transition zone (J = 1) or in the early stages of the quasi steady state. The effects of orientation angle on the propulsive efficiency of the flapping wings is minimal for orientation angles ranging from -10° to 10° where the propulsive efficiency follows the same trend of increase with increasing freestream velocity. The efficiency values however are found to decrease by a very small factor till an orientation angle of 10°. However the least amount of efficiency values obtained is when the orientation angle is equal to 20°. This can be explained by the fact that high orientation angles and flow velocities would apply a significant amount of aerodynamic force on the surface of the wings. This would require the wings to consume a large amount of power in order to keep the wings flapping at the same time producing insufficient amount of thrust thereby decreasing the propulsive efficiency of the system. The current data indicates very low efficiency values being generated by the wing during flapping flight this large decrease in the propulsive efficiency value can be attributed ignoring the gear efficiency of the flapping mechanism. The gear efficiency can be ignored as the current study is a qualitative analysis of the propulsive efficiency as a function of the advance ratio of the

flapping wing. If the gear efficiency and the efficiency of the motor were to be considered in the calculations, a higher value of efficiency can be obtained.

2.2.5. Phase Analysis of Flapping Flight

For a better understanding of the flapping motion of wings, a deeper analysis of the force generated by the flapping wing can be obtained by observing the time series of the data gathered during the force measurements. The JR3 force measurement module was operated at a data acquisition frequency of 1kHz during the tests which lasted for a period of 30 seconds in each case.
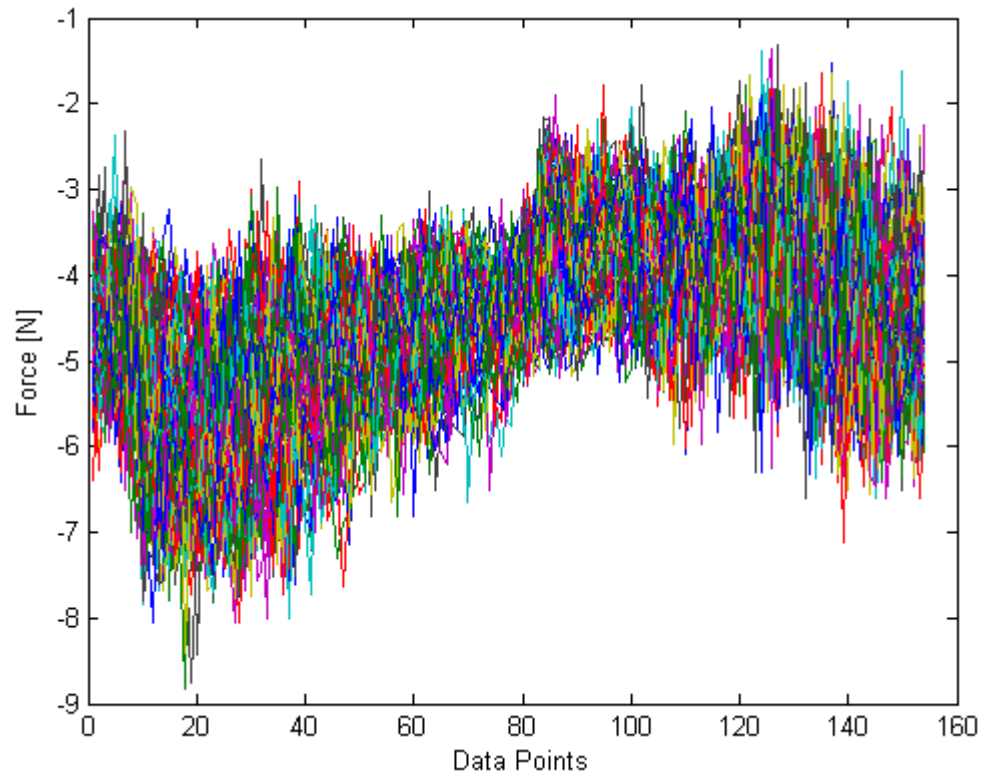
Figure 2.44. First one hundred waves gathered during lift measurements at OA = 10, $V_\infty = 2m/s$

The raw data from which the average force generated consists of a total of 30,000 data points. These data points appears in the form of waves especially in the case of force measurements conducted on flapping wings due to the variation of the forces from the flapping motion of the wings. Figure 2.44 shows the first hundred waves patterns which were formed due to flapping motion of the wings. The repetitive nature of the forces generated due to flapping wings can be analyzed by superimposing individual waves on top of each other which would reveal a pattern emerging. Figure 2.44 shows the superimposed image of the first one hundred waves gathered at an orientation angle of 10° with a free stream velocity of 2m/s. The image shows a clear pattern emerging from the time series of the force measurements conducted at that particular case.

To understand the aerodynamic force generation taking place during flapping motion, a phase averaged wave pattern of lift is generated from the time series force measurement. A similar approach into understanding the phase averaged lift and thrust generation of flapping wings were taken by Ho et. al. [23]. To generate a phase averaged lift profile, the superimposed wave patterns are all averaged into a single wave. An average value of this wave is determined and is considered as a baseline value to normalize the wave pattern which was formed. Figure 2.45 shows the normalized wave patterns formed at different flow velocities ranging from V = 1m/s to V = 10m/s at a constant wing beat frequency. This would indicate an increase in advance ratio in each case. The phase averaged wave pattern formed at each of the flow velocities are shown in figure 2.45.

Phase Averaged Lift Vs Phase Angle
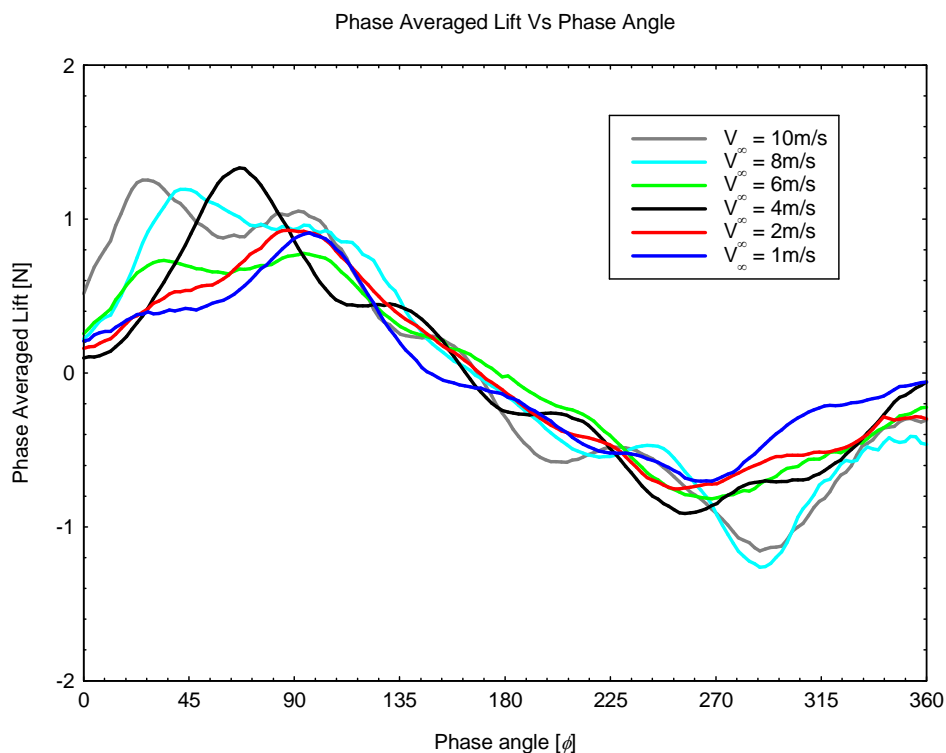
Figure 2.45. Phase averaged lift distribution during flapping motion at different free-stream velocities at OA = 10$^{\text{o}}$

The individual phase averaged lift profiles shown in figure 2.45 are calculated at different free stream velocities. All the waves exhibit a similar pattern which is indicative of the profile of the flapping wing for the current experiment. The force measurements obtained in this case shows an increase in the lift values with increasing free stream velocity. This is not obvious in the graph shown above as the oscillatory motion of the wave does not indicate any sudden increase in its amplitude however the average value of the wave pattern formed would indicate an increase in lift with increasing flow free stream velocity. Another point to be focused is the unsymmetrical nature of the wave structure. The crest of the wave is found to generate a higher amount of thrust than the trough. This is indicative of the unsymmetrical

flapping motion carried out by the wing as the Cybird flapping mechanism flaps with a larger angle in the upward direction than in the downward direction. This form of unsymmetrical flapping of the wings also causes the wings to produce a lift profile which is not similar to that of a sinusoidal wave.

CHAPTER 3. EFFECTS OF WING FLEXIBILITY ON BIO INSPIRED MEMBRANE WINGS

The importance of the flexibility parameter of membrane wings have been discussed thoroughly in section 2.4. It was concluded application of such a parameter in flapping wing micro air vehicles can increase the performance of such a system. Experiments were conducted to understand the effects of flexibility on flapping wings at University of Florida's Research and Engineering Education Facility (UF-REEF) near Air Force Research Laboratory at Eglin Air Force Base, FL [22]. These experiments were conducted to compare the aerodynamic performance of three different wings of varying levels of flexibility and thereby conclude an optimum level of wing flexibility which could enhance the performance of the MAV. The Nylon wing which is available with the Cybird model, a modified flexible wing made of a latex membrane and a rigid wing which is made by attaching a wooden plate over the surface of the Nylon wing. The three wings were subjected to similar test conditions and the resulting data obtained are discussed below.
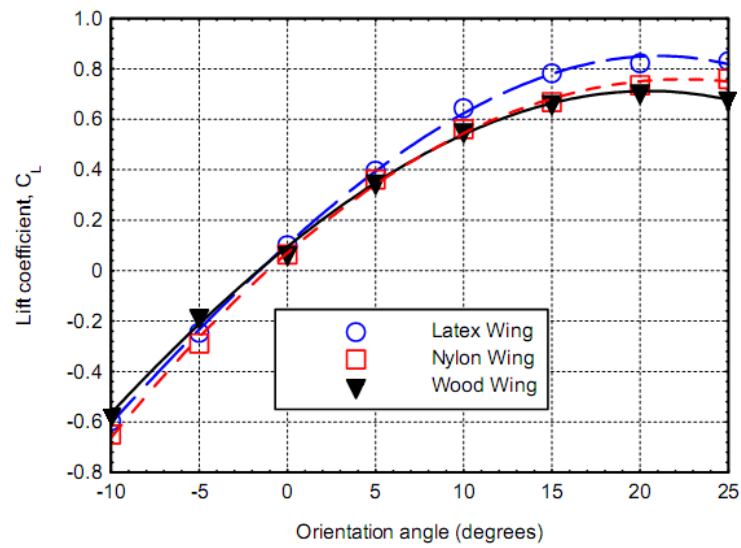
(a) Lift Coefficient
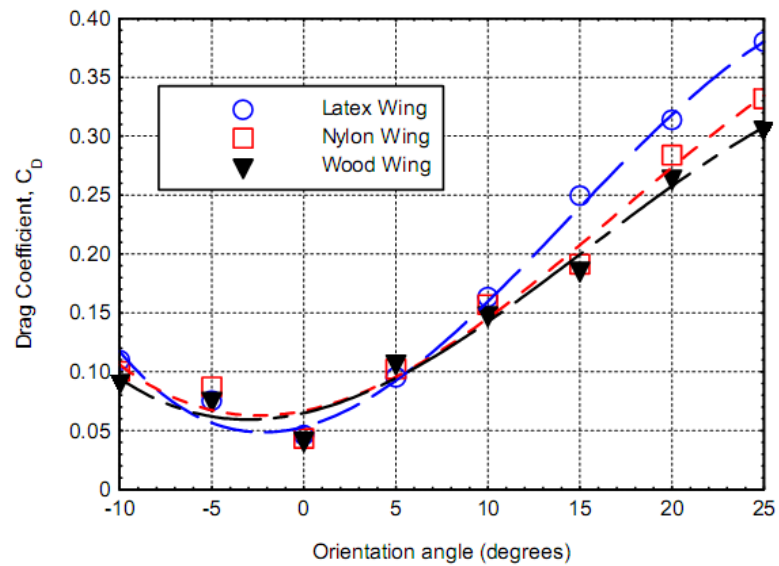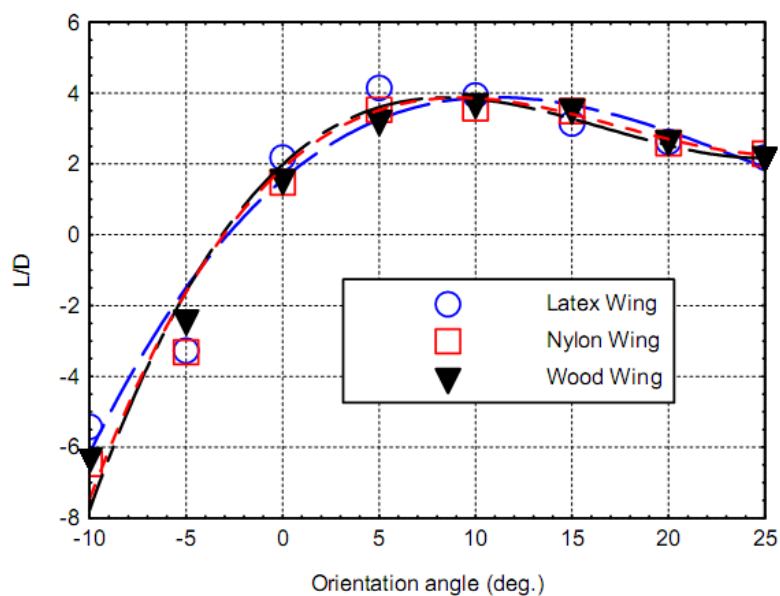
(b) Drag Coefficient

(c) Lift to Drag Ratio

Figure 3.1. Aerodynamic performance of wing of different flexibility at $V_\infty = 2m/s$

Figure 3.1 shows the soaring tests conducted on the three wings and the resultant lift and drag coefficients obtained during the experiments at different orientation angles of the wing and a relatively low flow velocity of 2m/s. On analyzing the data obtained from the soaring tests, the following conclusions were reached. At lower flow velocities, the level of deformation of the membrane wings was found to be almost nonexistent with and the results obtained at these velocities are almost similar for all the three wings. This is an indication that flexibility of the wing does not have any effect at lower flow velocities in the case of stationary wings. In these tests the lift coefficient of the latex wing is slightly higher than the Nylon wing due to a higher degree of flexibility of the membrane in the latex wing. However due to the increased flexibility of the latex wing, the trailing edge of the wing tends to flutter thereby causing a larger drag coefficient. The fluttering of the trailing edge of the membrane

is found to increase with an increasing orientation angle of the wing. Soaring at lower flight speeds will thereby give a deteriorated aerodynamic performance of the wings.

With an increase in the flow velocity, the effects of membrane flexibility become more apparent with the chord-wise profile of the membrane wing changes due to difference in forces acting on the upper and lower surface of the wing. With this increase in velocity, the trailing edge of the flexible wings will experience an increased deflection in the trailing edge which would cause the effective angle of attack of these wings to reduce. This reduction in the effective angle of attack would cause the wings to stall much later than its rigid wing counterpart. Figure 3.2 shows the results obtained from the aerodynamic testing of the membrane wings at a free stream velocity of 8m/s.

From the results obtained at these flow parameters, it was understood that the rigid wing shows a higher drag coefficient than the Nylon and latex wings. The rigid wing however exhibits lower drag coefficient values at negative orientation angles than the latex wing.

(a) Lift Coefficient

(b) Drag Coefficient

(c) Lift to Drag Ratio
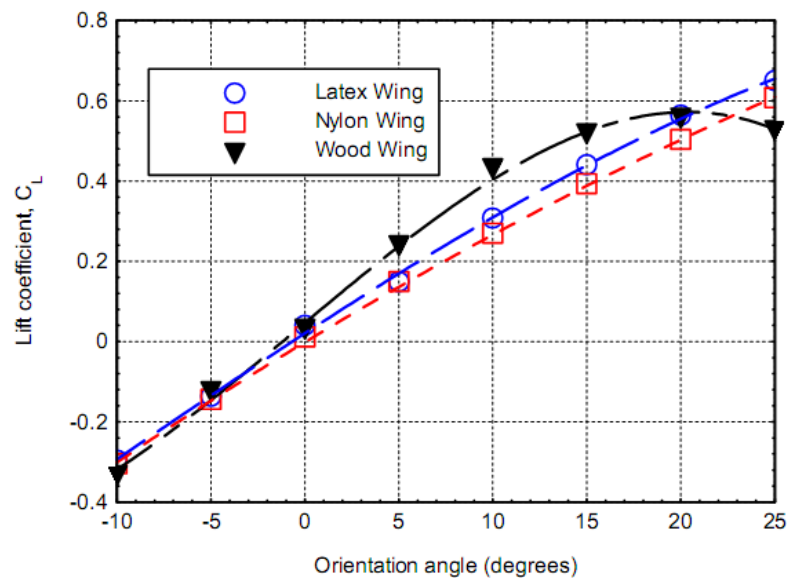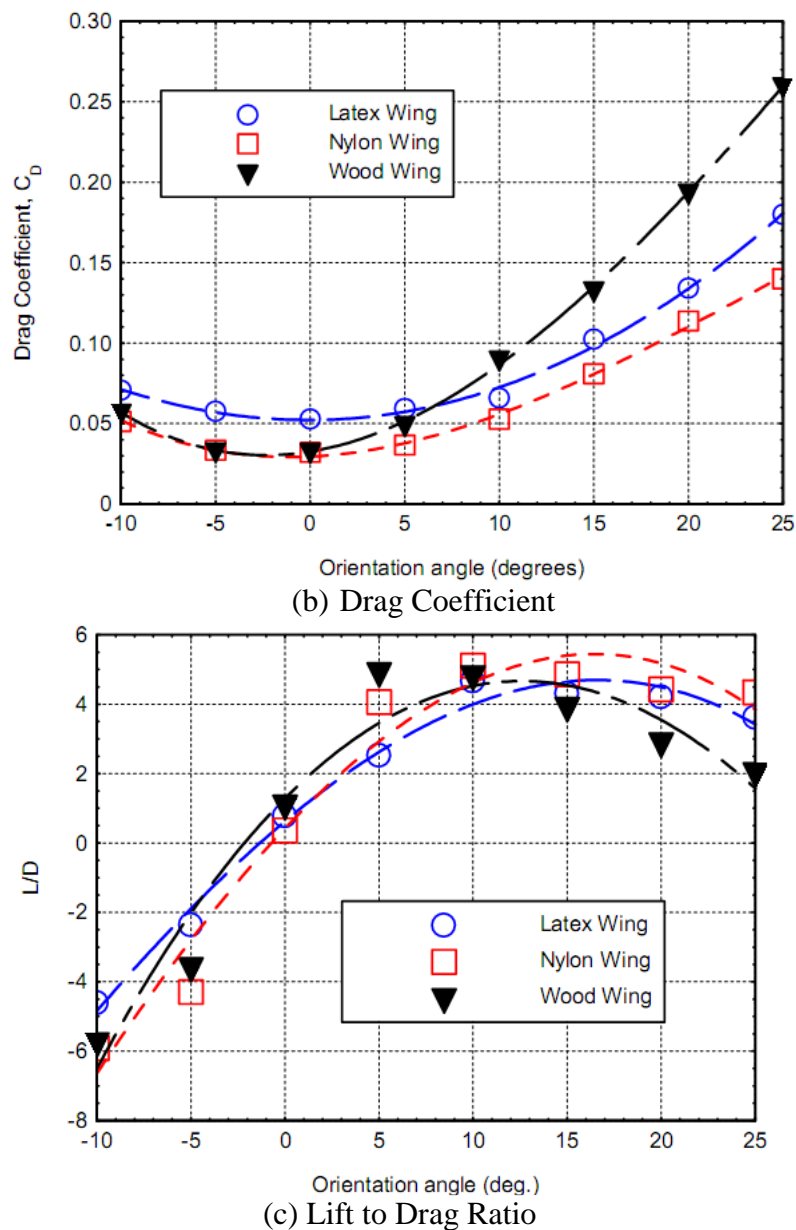
Figure 3.2. Aerodynamic Performance of wings of varying flexibility at $V_\infty = 8$m/s

The drag produced by the rigid wing at negative orientation angles is similar to that of the Nylon wing. In terms of the lift coefficient values, the latex and the Nylon wings have shown an increased lift coefficient values with increasing orientation angle and is found to increase way beyond an orientation angle of 25° without any indication of stall this can be

attributed to the flexibility of the wing which causes the effective angle of attack of the wing surface to vary. Due to the lack of such a capability, the rigid wing stalls at an orientation angle of 20°. On observing the lift to drag ratio graphs, it can be seen that the Nylon wing has a slightly higher lift to drag ratio than compared to other wings at higher orientation angles.

The next round of tests conducted on the wings to understand the effects of varying flapping frequency of the wings at different flow velocities at a constant orientation angle.

(a) Mean Lift   (b) Mean Thrust
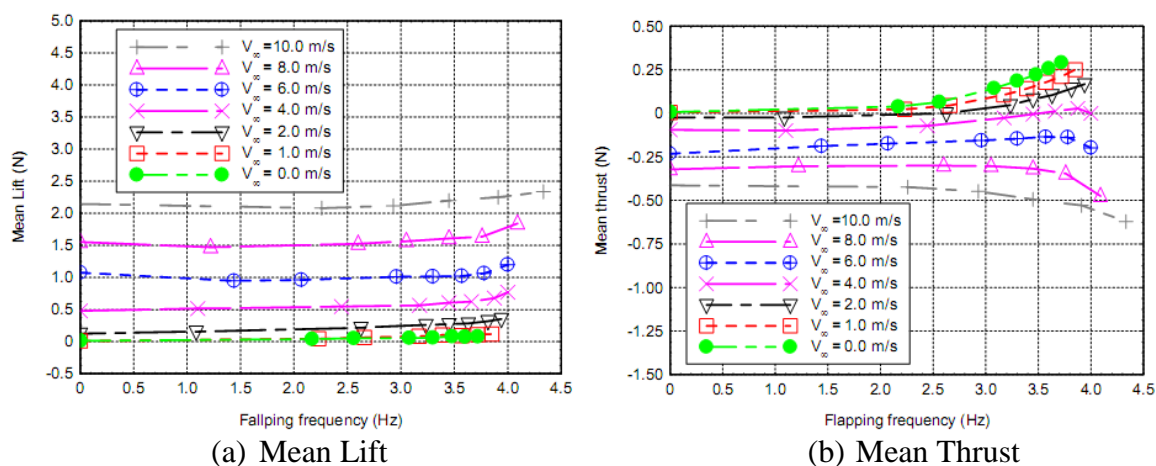
Figure 3.3. Time Averaged Lift and Thrust Values of Rigid Wing at OA = 10°

(c) Mean Lift   (d) Mean Thrust
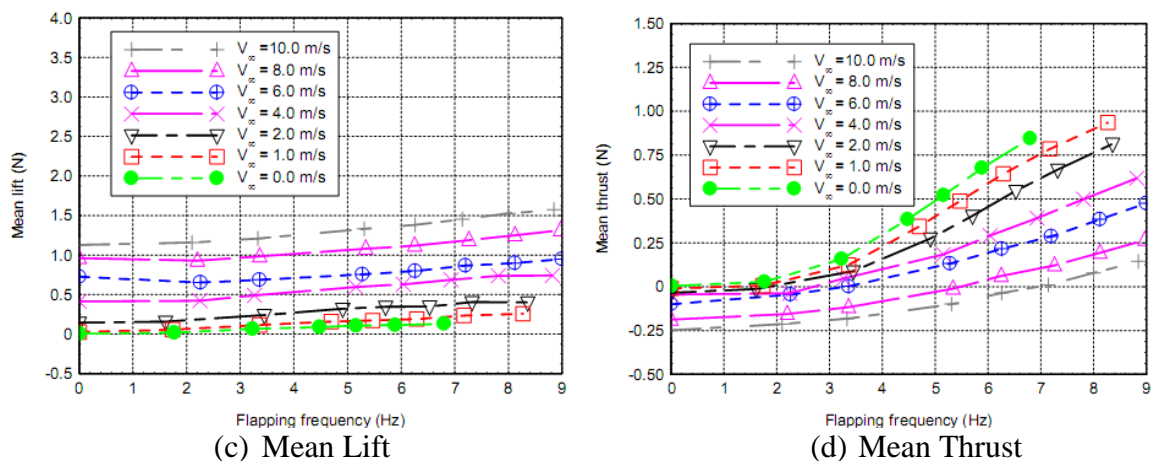
Figure 3.4. Time Averaged Lift and Thrust Values of Flexible Nylon Wing at OA = 10°

(a) Mean Lift (b) Mean Thrust
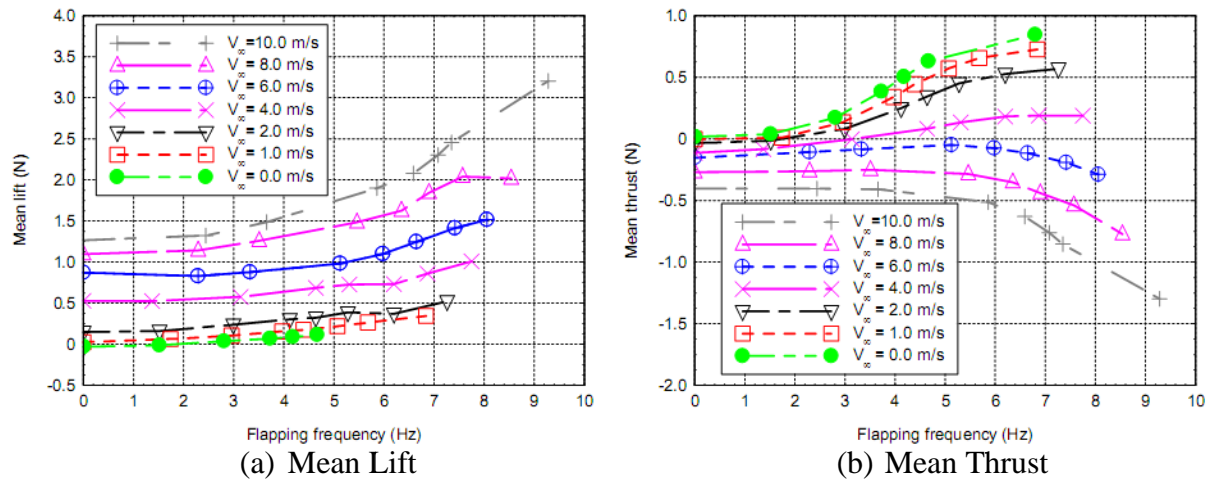
Figure 3.5. Time Averaged Lift and Thrust Values for Flexible Latex Wing at OA = 10°

Figure 3.6. High Speed Image of Flexibility of a Latex Wing During Hovering Tests

During the experiments conducted at varying flapping frequencies it was found that the thrust generated by the wings decrease with an increasing flow velocity. Thereby it is observed in all the cases that the aerodynamic performance observed during forward flight decreases with increasing free-stream velocity. This could explain the reason why smaller birds which fly at relatively lower flight velocities tend to have a higher wing beat frequency

as they make effective use of their wings for propulsion. On the other hand larger birds like eagles and seagulls have the tendency to flap their wings at a much lower wing beat frequency thereby using them in a fashion similar to that of fixed wing and having a much higher component of soaring flight in their flight envelope. On comparing the performance of each of these wings, the rigid wing was found to have the best thrust generation performance followed by the latex and the Nylon wings. Figure 3.6 shows the flexibility displayed by a latex wing while in flapping motion during a hovering test where $V_\infty = 0$m/s. The overall change in the wing profile is to be noted and a substantial wrinkling on the surface of the membrane is also noted expecially in the trailing edge region.
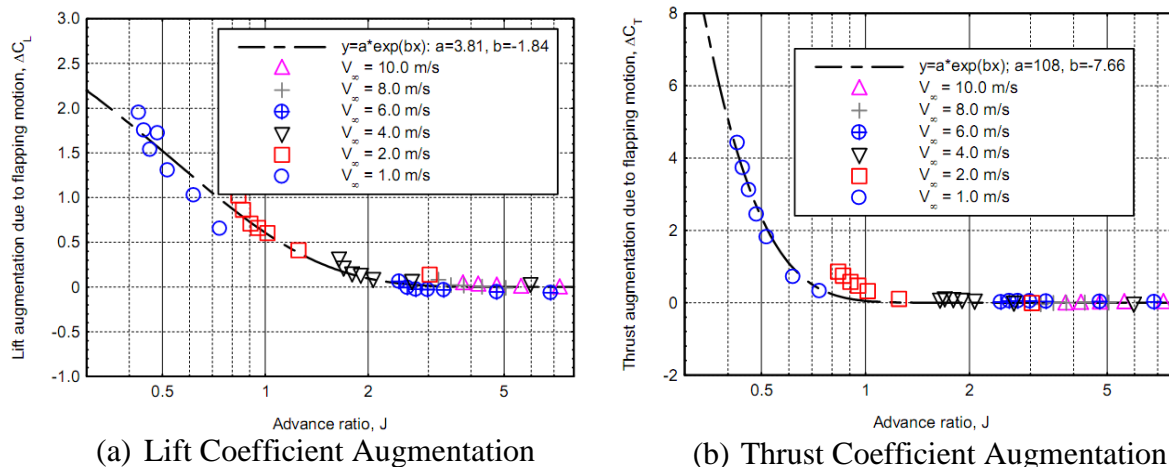
(a) Lift Coefficient Augmentation   (b) Thrust Coefficient Augmentation
Figure 3.7. Lift and Thrust Augmentation of Rigid Wing at OA = 10°

(a) Lift Coefficient Augmentation   (b) Thrust Coefficient Augmentation
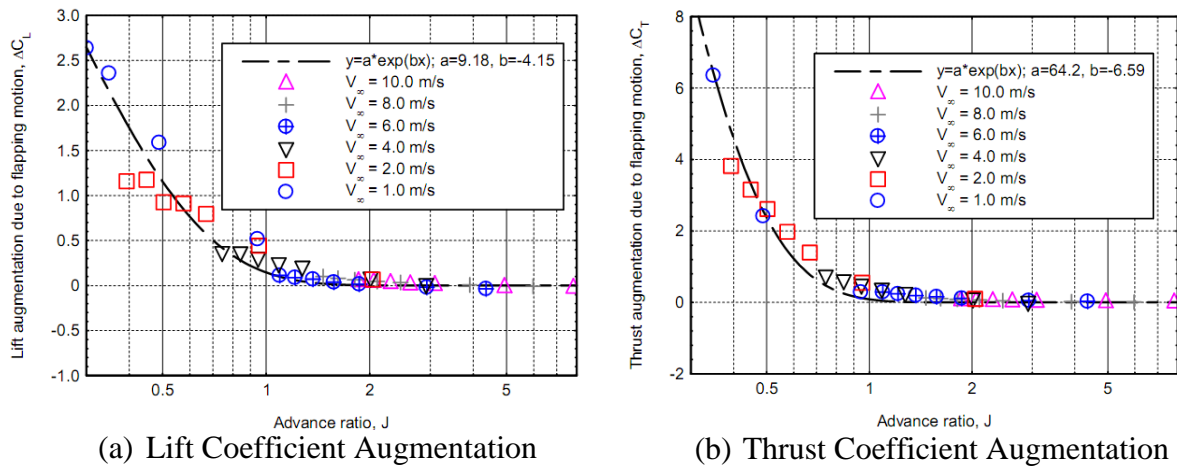
Figure 3.8. Lift and Thrust Augmentation of Nylon Wing at OA = 10°

(a) Lift Coefficient Augmentation   (b) Thrust Coefficient Augmentation
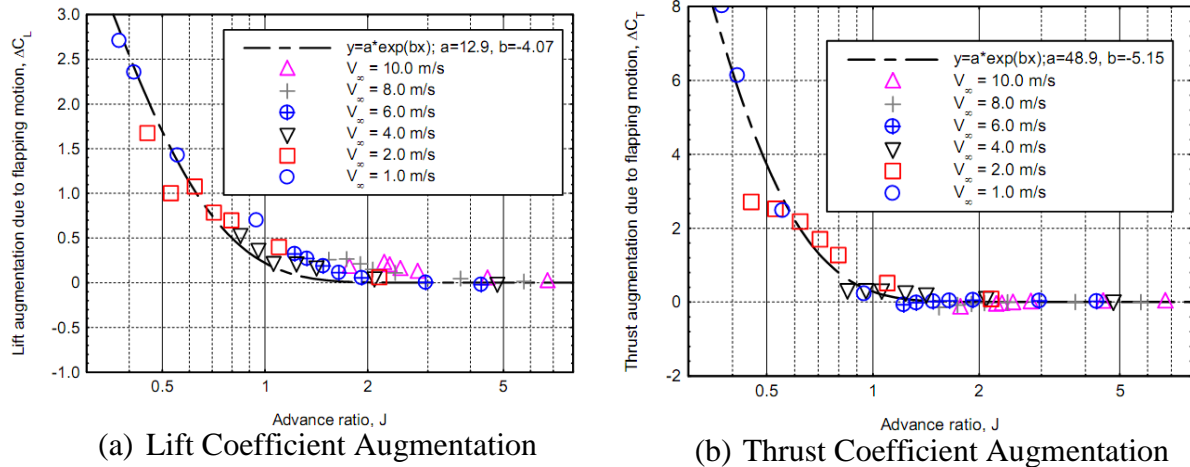
Figure 3.9. Lift and Thrust Augmentation of Latex Wing at OA = 10°

Figures 3.7 – 3.9 shows the lift and thrust augmentation results of the three wings in relation to the advance ratios at which they operate. All the cases show that the maximum amount of thrust and lift values are generated when the vehicle operates in the quasi steady. Thereby unsteady aerodynamics of the wing generates a higher amount of thrust and lift than compared to quasi steady case. Each of the wings displayed an exponential decrease in augmented lift and thrust values with the results showing a curve fit which agrees with an exponential function.

On comparing the performance of the three wings shown in figure 3.10, it was found

that the latex wing has the best thrust augmentation while the rigid wing and the Nylon wing displayed similar thrust augmentation characteristics. In terms of lift augmentation the rigid wing showed a much higher performance by generating lift even at the quasi steady regime and also in the lowest amount of advance ratio while the Nylon wing followed the trend with lift generation focused more on the unsteady regime then followed by the latex wing.

(a) Lift Coefficient Augmentation

(b) Thrust Coefficient Augmentation
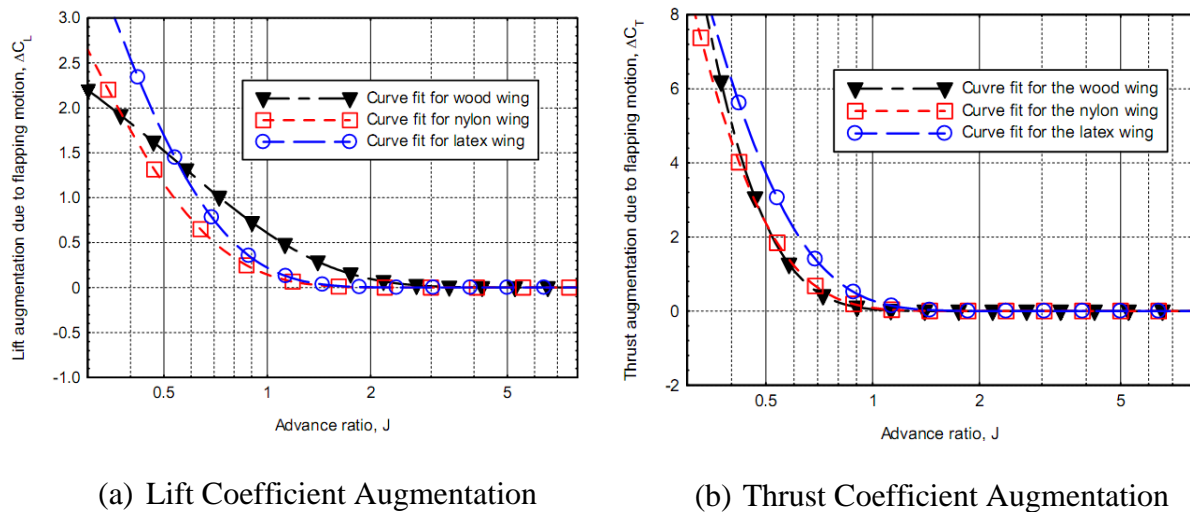
Figure 3.10. Comparison of Exponential Curve Fit of Lift and Thrust Augmentation Coefficient of the three tested wings at OA = 10°

(a) Lift Augment Coefficient at V_{∞} = 2m/s

(b) Thrust Augmentation Coefficient at V_{∞} = 2m/s

(c) Lift Augment Coefficient at V_∞ = 4m/s

(d) Thrust Augmentation Coefficient at V_∞ = 4m/s

(e) Lift Augment Coefficient at V_∞ = 8m/s

(f) Thrust Augmentation Coefficient at V_∞ = 8m/s
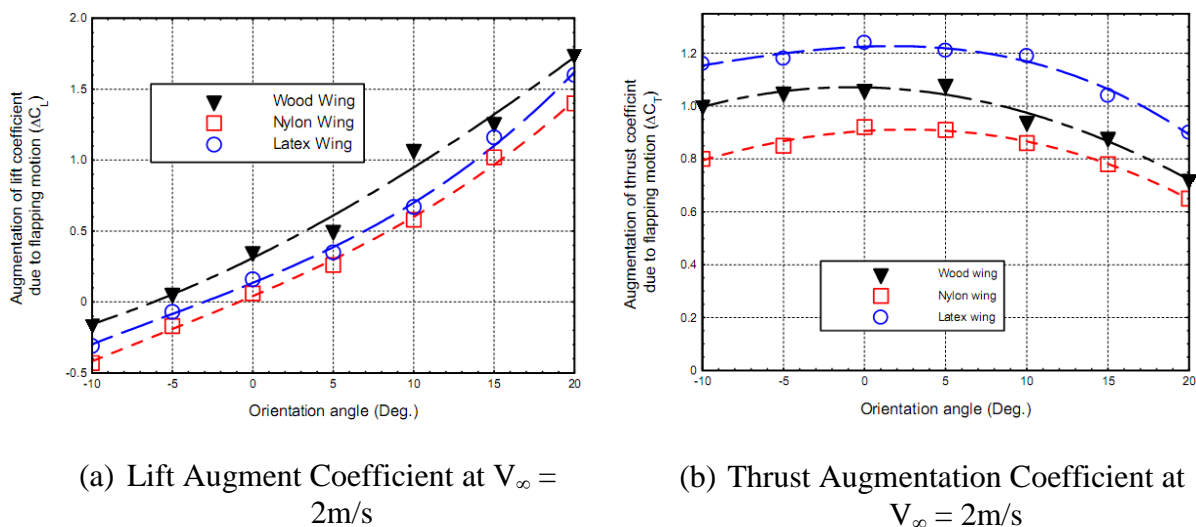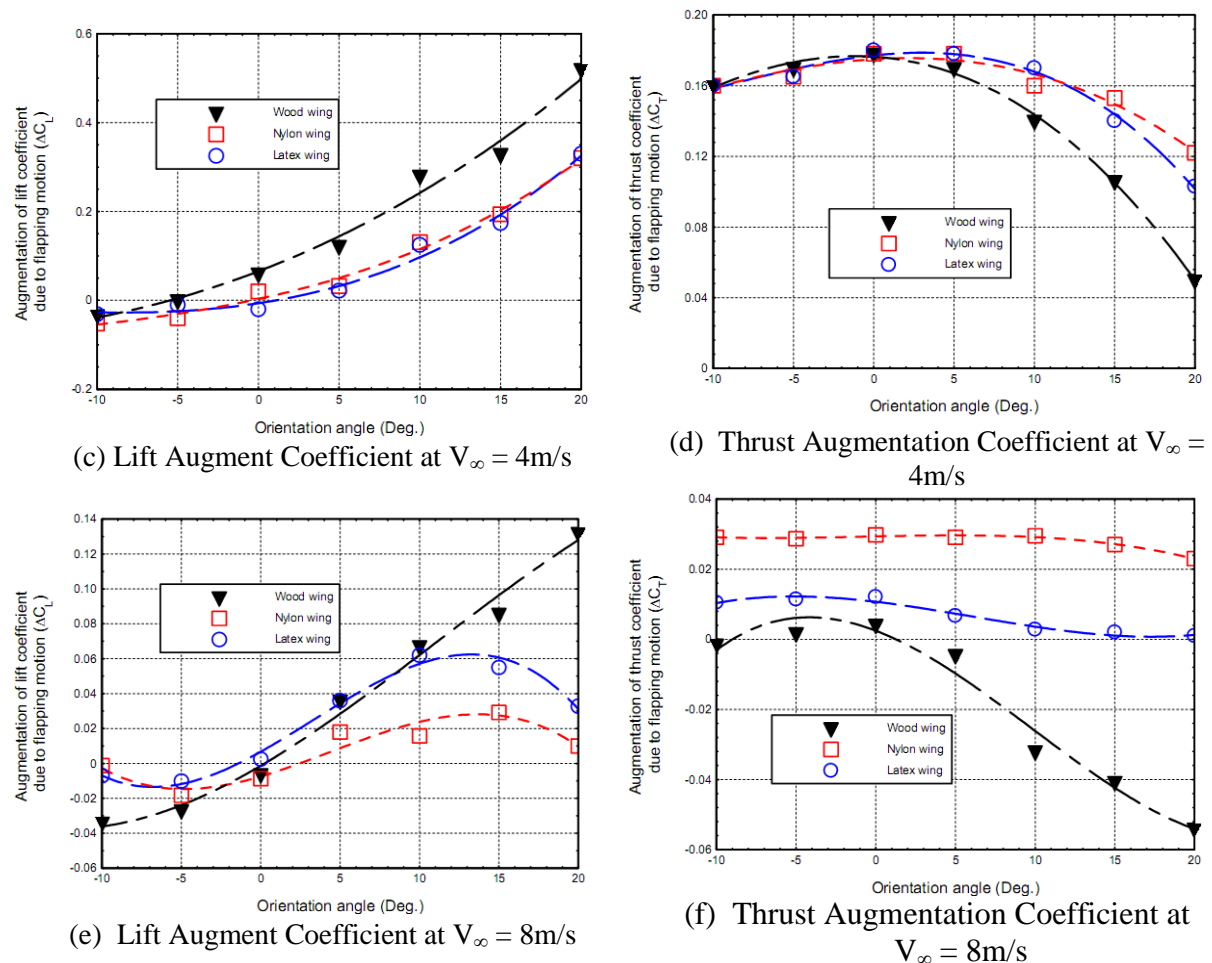
Figure 3.11. Effect of Change in Orientation Angle During a Constant Wing Beat Frequency (f = 4Hz)

The next level of comparative study includes understanding the effects of varying the orientation angle at different free stream velocities during a constant wing beat frequency. The data gathered from the experiments is shown in figure 3.11. It was observed that the lift augmentation of all three wings increases up to 6m/s. At free stream velocities above 6m/s the values of lift augmentation were found to peak then decrease. An abnormal performance was exhibited by the rigid wing where the lift augmentation coefficient was found to consistently increase in all cases from the lowest to the highest of free stream velocities. This leads to the conclusion that the rigid wing exhibits the best lift generation performance

consistently among all the three wings. The flexible wings involved in these tests exhibited the same kind of performance. With regard to the lift augmentation displayed by the wings, the Nylon wing exhibited the least amount of thrust coefficient at lower flow velocities followed by the rigid wing and the latex wing. However as the velocity increases we see an increase in thrust generated by the Nylon wing as it reaches the highest amount of thrust generated during flapping flight among all the three wings with the least amount of thrust being generated by the rigid wing at higher flow velocities. From all the cases observed above, the maximum amount of thrust generated by all the wings are when the orientation angle is 0°. A subsequent decrease in thrust and an increase in lift are observed in all the above mentioned cases with increasing orientation angle.

On observing all the above results shown, the following conclusions can reached. A higher amount of thrust is always observed in the case where the OA = 0°. The latex wing is found to generate the best values of thrust compared to all three cases. However the Nylon wing was found to produce the maximum amount of thrust in the quasi steady regime. The rigid wings in the experiment were found to generate a high amount of augmented thrust during relatively higher values of forward velocities. Despite this added advantage of the wooden wing, it was found to generate a high level of induced drag during flapping motion which prevents it from being an efficient answer to membrane flexibility with regard to flapping flight. From all the above results, it is once again very clearly observed that flapping flight is much more efficient within the unsteady regime.

CHAPTER 4. BIO INSPIRED TANDEM WING NANO AIR VEHICLES

4.1 Introduction

With progress in the areas of micro mechanics, semi conductor technology and miniaturization of other systems and sensors commonly used in defense and remote sensing applications, the next step in the application of unmanned systems is definitely inclined towards substantial progress in Nano Air Vehicles or NAVs. In a technology forecast conducted by the Center for Strategy and Technology [25] a survey was conducted on the potential applications and the feasibility of developing such systems for future applications and predicts the operational deployment of NAVs in the near future. The survey also predicts the use of NAVs as swarms rather than individual units to improve their efficiency thereby introducing new challenges in cluster application of autonomous robots. These systems would be integrated into a wider network of other airborne assets thereby significantly improving intelligence gathering and war fighting ability.

According to current DARPA specifications, a nano air vehicle is defined "as airborne vehicle no larger than 7.5 cm in length, width, or height, capable of performing a useful military mission at an affordable cost and gross takeoff weight (GTOW) of less than or equal to 10 grams" [26]. Another issue which is being addressed in the memo is the ability of such systems to withstand gusts of wind within small confined spaces. Endurance is also a high priority with the current requirements of 20 minutes in flight time and a command and control radius of up to 1 kilometer, the system also comes with an additional requirement for hovering while carrying a payload. The initial contract for the development of such a system was awarded to Aero Vironment with their concept NAV called Nano SCOUT (Sensor

Covert Observer in Urban Terrain). Future requirements would include an operating range much larger than the current specifications and also the ability to remain within a mission area for extended periods of time. This would require the NAV to recharge its onboard power systems using solar or chemical means. Certain concepts include the use of such nano air vehicles as precision guided munitions where by a high energy density explosive or a nerve agent could be used to neutralize enemy personnel or unexploded munitions. With a working model of such a system, the practical applications are limitless with the possibility of some systems being multi-role on similar lines with combat aircraft which are capable of carrying a variety of mission specific payload. Many bio inspired methods are being considered as a means to develop such technology. Insects are the best possible candidates for such a study as they are the most efficient systems which naturally fly at extremely low Reynolds numbers in their length scales. Many researchers have used insect anatomy as a means to study how nano air vehicles would perform as they represent the most efficient flyers due to years of evolution.

Various approaches have been attempted on developing such systems with working models being produced by AeroVironment and TU Delft. As part of the DARPA contract to produce a nano air vehicle, AeroVironment has developed a flapping wing nano air vehicle which is also capable of hovering flight. Another working model is the Delfly Micro which is developed by a research team from TU Delft. Flight test videos of the NAV show the Delfly carrying an onboard camera recording images and being controlled via remote control.
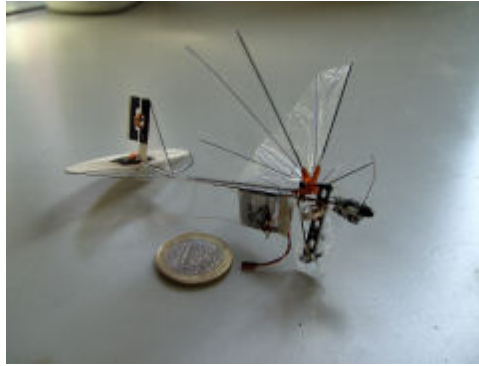
Figure 4.1. Delfly Micro [27]

Both these working models are designed based on mechanical actuators such as motors, gears and cranks. Other methods have also been developed which involve the use of piezoelectric actuators rather than mechanical systems to produce flapping motion. These actuators have the capability to impart a much higher wing beat frequency than compared to their mechanical counterparts. The maximum wing beat frequency observed in mechanical systems is close to 25 Hz while using piezoelectric actuators can cause the wing beat frequency to reach up to 100Hz making it similar to the wing beat frequency of insects. With recent advancements in high energy density piezoelectric materials, it is capable to produce actuators which can impart higher wing amplitude and still maintain a very high frequency.

Another promising work being carried out in the area of insect based nano air vehicles is the Harvard Micro Robotics Laboratory's Microfly program which uses piezoelectric actuators to power an NAV. This particular program has shown much progress in the field of micro mechanics and piezoelectric actuators by which an insect sized nano air vehicle is designed. Though it is in the initial stages of research, using the initial design a

secondary system was created with a tandem wing configuration similar to that of a dragonfly.
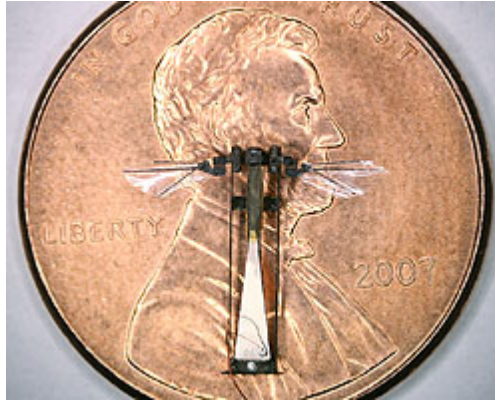
Figure 4.2. 10gram Microfly [28]
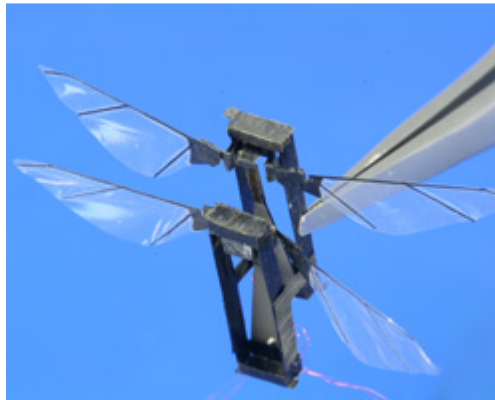
Figure 4.3. Four-winged Microrobotic Dragonfly [28]

Though these vehicles are capable of flight, there are no onboard means of control or a payload. Further work would include incorporating these onboard systems and making a working model of an insect size nano air vehicle.

Several other researchers have worked on propulsion techniques involving the use of piezoelectric actuators for applications in the design of micro air vehicles. Some of them have studied the possible application of piezoelectric actuators in flapping wings with

multiple degrees of motion. Work done by Chung et al [29] involved the use of piezoelectric materials to flap the wing in different phases. This involved the use of two different piezoelectric actuators which are attached to a flexible membrane fan. With different phase differences between the two piezoelectric patches, a twisting motion to the flexible membrane was achieved which could thereby be used in practical applications by providing an improved control over the vehicle. The study however provided an insight into the issues which were later faced during the experimental phase of the study. Every piezoelectric material has its own unique physical properties as they are manufactured individually. This would cause each actuator to have its own individual resonant frequency within a close range of its design frequency. Another factor which is to be considered with regard to the uniqueness of each piezoelectric actuator is that they have to be controlled individually in order to obtain a specific phase difference, this would mean that two actuators connected to the same power source does not guarantee similar amplitudes or phase angles.

Other research involving the use of piezoelectric fans include that of Bidakhvidi [30] where an extensive investigation was conducted on both computational and experimental realms to study the possible use applications of these fans in micro air vehicle propulsion. The propulsion concept in this study involves the use of piezoelectric fans in a pusher propeller configuration. Another working model designed by a group includes the use of a light weight piezo-composite actuator (LIPCA) connected to a hinge mechanism which amplifies the motion of the actuator to flap the wings [31]. The manufacturing of a LIPCA would involve the use of multiple layers of carbon/epoxy and glass/epoxy layers and the actuator will give a maximum bending motion at its resonant frequency. The LIPCA allows

the vehicle to flap at a natural frequency of 9Hz with a flapping angle of 80° the wings designed for this working model also rotates by an angle of 55° thereby making the flapping motion quiet similar to that of insect flight by incorporating both plunging and pitching motion.

Though many different approaches have been taken to produce a working model of an insect inspired nano air vehicle have been made the design which is most accurately mimics insect flight is that of the Harvard Microrobotics Laboratory which was mentioned earlier. The mechanism is powered with the help of a 10mm bi-morph PZT based high energy density piezoelectric bending actuator [32]. The manufacturing process for the central structure of the NAV was performed with the help of a process called Smart Composite Microstructure (SCM) [33] by which laser a micromachining process was used to create accurate micro scale structures on composites. Linkages and actuators for the mechanism were made by sandwiching the polymers between sheets of rigid composite materials where the gaps in the sheets act as flexures. These methods have allowed the manufacture of precision micro scale components which are far efficient than conventional manufacturing process which have many shortcomings when applied in micro scales. Studies on insect physiology have shown that insects use mechanical advantage to amplify their wing amplitudes and also have a wing beat frequency equal to the natural frequency of the aeromechanical system. Using these principles the significantly smaller amplitude of the piezoelectric actuator was increased significantly [34]. The wings of the NAV is made of carbon fiber reinforced composite beams covered with a polyester membrane, the attachment on the wing has a capability to rotate the wing along its axis with the help of intertial forces

acting on the wing itself. The added rotation to the wing along with plunging motion of the wings allows the wing to mimic insect flight to a much higher degree when compared to other systems which have only one degree of freedom.

4.2 Piezoelectric Effect

Piezoelectric materials are essentially crystals which possess piezoelectric properties by which they are able to generate small amounts of electricity when mechanical stress is applied on these materials. Figure 4.4 shows an illustration of the basic phenomenon that takes place during piezoelectric effect. These materials include crystals and certain ceramics including bone [35].

To understand this phenomenon better, the concept of dipole has to be bought into the picture; a molecule has a polarization by which the opposite ends of a molecule would have opposite charges which are connected through an imaginary line called the polar axis. Poly-crystals are materials where the polar axes of their molecules are oriented in different direction and a Mono-crystal is a material which has all its polar axes oriented in a single direction.

Piezoelectric materials can be created by heating a poly-crystal with a strong electric field. The heat allows the molecules to move freely and the electric field aligns the dipoles of all the molecules in a single direction thereby causing the material to have a single polar axis throughout. When the treated material is compressed or expanded, the same polarity as the direction in which the body is deformed appears between the electrodes to which it is connected. The same effect can be observed conversely when a similar voltage is applied on

a piezoelectric material, a deformation can be observed due to the applied voltage. Also when the circuit to which a piezoelectric material is connected to an AC signal, the material would vibrate with the same frequency as the input signal [36]. This phenomenon would be the primary application for piezoelectric materials by which it could be applied in fans which are used to cool confined spaces and also for the use of piezoelectric materials as an actuator.
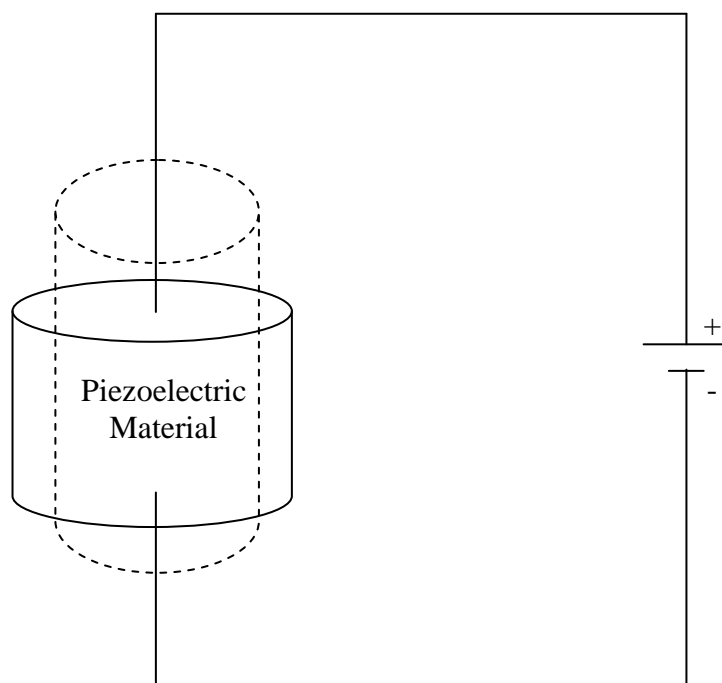

Figure 4.4. Piezoelectric Effect
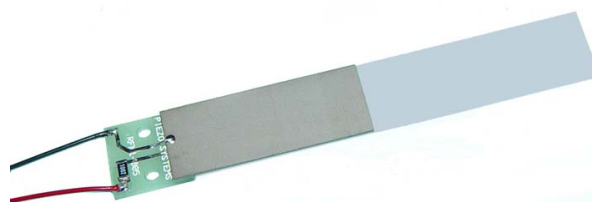
Figure 4.5. Piezoelectric Fan Blade [37]

Apart from being a highly efficient in comparison to similar mechanical systems, piezoelectric materials are also chemically inert, exhibit a high level of hardness and stiffness and are not affected by humidity or other atmospheric influences. Piezoelectric materials being applied for these applications are made of Lead Zirconate Titanate (PZT) ceramics which can be custom made for specific purposes [37]. To mimic the flapping motion of an insect wing, a commercially available piezoelectric fan has been used. These fans are generally used to cool electronic devices such as laptop computers, DVD players and some concepts include the application of piezoelectric fans for cooling mobile phones. The flapping motion of the fan is generated by a Bimorph actuator which is capable of producing flapping frequencies of up to 60HZ. In a bimorph actuator, two thin ceramic plates are stacked together and applied opposite electric fields. The stacked piezoelectric plates when exposed to opposite polarity causes the plates to deflect laterally. A plastic film is attached on to the piezoelectric patch, the deflection caused by the stacked piezoelectric plates are amplified by the lower plastic film thereby causing it to flap in the pattern of the AC signal given to the circuit [30].

4.3 Insect Flight

The fundamental principles of insect flight are quiet similar to that of bird flight. However insects operate at a much lower Reynolds number by which the viscosity effects acting on them are much higher compared to birds. A review of insect flight aerodynamics by Sane [38] shows an in-depth study into insect flight aerodynamics. The presence of a leading edge vortex on an insect wing allows the insect to hover and maneuver effectively. This observation shows that the leading edge vortices play a very important part in flapping flight.

Lift is generated by the wing once again by an induced downwash produced by the flapping of the wings. The difference in the direction of the flow causes a downward component which would result in the formation of lift which is generated by the wing. To get a much better understanding of lift generation, the concept of Kutta condition should also be brought into picture. As an airfoil experiences steady flow over its surface at a particular angle of attack, nature adopts a value of circulation (Γ) by which the fluid smoothly leaves at the trailing edge of the airfoil this phenomenon is known as the Kutta condition [39]. Additionally, Kutta condition ensures that when an airfoil is placed at an angle of attack it imparts a downward momentum to the flow.

The Kutta condition maintained by the wing imparts the momentum into the flow as the wing translates through the flow resulting in a substantial increase in the lift generated by the wings. The vortex sheets generated by oscillating wings can also be explained by the Kutta condition as the vorticity introduced into an inviscid flow by through the application of Kutta condition should be accompanied with an equal and opposite vortex. Flow visualization studies conducted in this chapter would corroborate this phenomenon as the results will show similar to that of a von Karman Vortex street shedding from the trailing edge of the wing during plunging motion.

4.4 Dragonfly flight

Dragonflies are considered to be one of the most agile and maneuverable insects known to man with an estimated top speed ranging between 30km/h to 60km/h depending on the species of the dragonfly [40]. They have also shown the ability to fly both forwards and backwards with effect use of their tandem wings. In terms of maneuverability, dragonflies

have shown that they are capable of making 90° turns in fewer than three wing beats [41]. This extreme maneuver is done by pivoting along the vertical axis without the actual body of the dragonfly rolling along its longitudinal axis. Owing to the size of the different species of dragonfly, the wing beat frequency also varies within a broad range. For example the average wing beat frequency of a dragonfly is 27Hz while the natural frequency of the wings is in the order of 170Hz [42]. With these capabilities, dragonflies are considered to be a very likely candidate on which a future bio inspired nano air vehicle designs could be based on. If a system which can mimic the aerodynamic characteristics shown by these insects, it would prove to be a formidable advantage over other conventional fixed wing miniature scale uninhabited air vehicles in terms of speed, agility and maneuverability.

Dragonfly wings have also proven to be a source of great curiosity amongst both biologists and engineers. They possess unique properties by which they exhibit high aerodynamic performance at lower Reynolds numbers. Experimental investigations into dragonfly wings such as the one by Murphy and Hu [43] have shown that the corrugated airfoil made from the cross sectional profile of a dragonfly wing displays a higher lift and delayed airfoil stall during low Reynolds number applications (Re < 100,000). The aerodynamics performance of the corrugated airfoil was found to display no effect to the varying Reynolds number. Flow visualization studies with the help of digital particle image velocimetry (DPIV) have shown that protruding corrugation corners if the wing profile act as boundary layer trips thereby allowing the boundary layer to remain attached to the surface of the airfoil. This delays the flow separation over the airfoil surface thereby allowing it to operate at higher angles of attack.

Other studies on dragonfly wing morphology include that of Tsuyuki et al. [44] which include flow visualization studies conducted on live insects to understand their wing performance. Observations made from the wing profiles of insects in this study shows that dragonfly and gadfly wings have a large V – shaped groove near the leading edge of the wing. Another observation made during this study is the large undulation in the center region of the wing which was found to significantly increase the lift generated by the wing. The flow visualization studies also indicate the presence of interaction between the fore-wing and hind wing during flapping motion of a dragonfly.

A much more in-depth look into the effects of fore-wing and hind wings in dragonfly flight has been shown with the help of computational studies by Wang and Sun [45] and also by Huang and Sun [46]. These studies have mentioned work by Sun and Lan [47] where a CFD analysis was conducted from 3D wing and original wing kinematic data from dragonflies. The results show the vertical coefficients of fore-wing and hind-wing are twice as large as quasi steady values and the mean vertical forces generated by the wings could be used to balance the weight of the dragonfly.

The computational studies by Huang and Sun [46] have shown that fore-wing-hind-wing interaction is strongly influenced by the forward flight speed of the insect and also the phase difference between the wings during flight. From the force data obtained from these studies show that the fore-wing shows only small signs of influence by the hind-wing on the other hand the hind-wing is heavily influenced by the motion of the fore-wing especially in the case where the phase difference between the wings is negative. A negative phase difference would mean that the fore-wing has a lead during flapping motion over the hind-

wing of the dragonfly. Due to the interaction between the fore-wing and the hind-wing, the aerodynamic force generated by the hind-wing is lower than that of the fore-wing. The decrease in forces is produced when the fore-wing causes the effective angle of attack of the hind-wing to decrease. A difference in the forces generated by the wings would cause a drop in the resultant aerodynamic forces generated by the wings in the case where the wings are flapping in a negative phase difference. As the wings flap with a positive phase difference, the mean total thrust of the fore-wing and hind-wing are slightly influenced by the interaction between the wings. In conclusion it was found that having a negative phase difference would lead significant loss in aerodynamic performance of a tandem wing configuration. This explains why dragonflies use only a positive phase difference between them during flight which involves the hind wing leads during flapping motion than the forewing.

4.5 Wing motion in Dragonflies

Insects have unique motion of their wings during flight which could vary depending on the necessary aerodynamic parameters which are required during flight. Especially in the case of a dragonfly a variety of flapping profiles are generated by the wing during flight. The most common pattern followed by birds and insects alike is the "Clap and Fling" motion. This particular wing motion was first proposed by Weis-Fogh [48] as a means to explain the lift generation of the *Encarsia formosa* wasp.
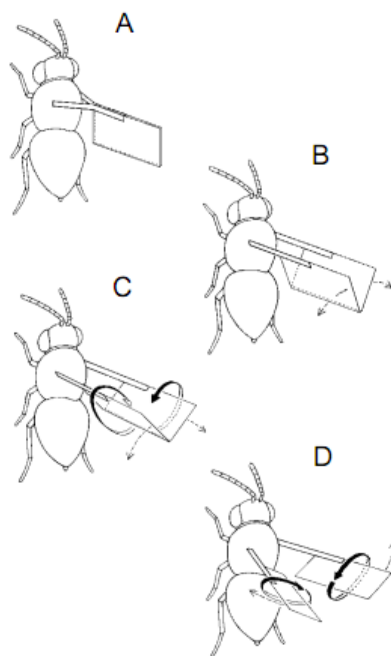
Figure 4.6. Clap and Fling motion exhibited by *Encarsia formosa* [48]

This motion would include the initial phase of the wings touching each other dorsally during pronation or the highest point in the wing amplitude during flapping motion which is known as the "Clap". Figure 4.6 shows an illustration of the clap and fling mechanism by Weis-Fogh. After the clapping motion of the wing the individual wings roll along their axis as the leading edges of both wings separate from each other with the trailing edge still remaining stationary making this motion look similar to that of a book being flung open hence the name "Fling". Though first observed in insects, this particular wing motion is very common among birds. The attached circulation on both the wings allows them to generate a large amount of lift. The interesting fact is that most insects do not make use of clap and fling motion despite its advantages.

Another type of flapping motion observed in tandem wing insects is that of in-phase and out of phase flapping. The motion of the tandem wings are classified as "in-phase" when both pairs of wings are oscillating with a phase difference of $\phi = 0^o$. This would mean that the two sets of wings would move up and down in a sinusoidal pattern together. The other pattern adopted by the wings during flapping motion is that of "out-of-phase" or "anti-phase" motion. During this flapping motion, the wings would have a phase difference of $\phi = 180^o$ which would mean that the wing would oscillate in opposite directions or when one wing strokes in the downward direction, the other wing would move in the upward direction and vice versa. Alexander [41] has studied the phase difference relationships exhibited by dragonflies at different instances during un-tethered flight. Using a high speed movie camera, Alexander was able to observe that dragonflies flapped their wings primarily out-of-phase and the in-phase flapping motion was observed to take place only at certain instances. The extended use of out-of-phase flapping by the wing could be explained both as being aerodynamically more efficient and also the basic physiology of the dragonfly would prompt its wings to flap out-of-phase. The transition between the different phases occurs in as little as 5-6 beats. In-phase flapping of the wings has found to provide a large amount of normal force for instances such as takeoff or quick yaw turns. However in-phase flight theoretically would decrease the lift generated by the wings as the hind-wing would have a reduced effective angle of attack thereby reducing the mean lift generated by the wing. Due to this reason, the in-phase flight is used only to generate large impulses of forces which would last only for a few wing beats. However when a time averaged value of the forces generated by in-phase flapping is considered, it would show a lower value as the wing interaction can be detrimental to the force produced by the wing. Another explanation for the use of fore-wing –

hind-wing phase difference would be the effective removal of 'swirl' over the tandem wings [49].

4.6 Experimental Setup

The aerodynamic tests conducted on the tandem wing were carried out at the undergraduate wind tunnel at Iowa State University's Wind Simulation and Testing Laboratory. A closed circuit wind tunnel is used for this experiment by which the airflow through the test section is not introduced from ambient air but it recycled throughout the experiment as the air within the test section is recycled during the experiment. Particle Image Velocimetry experiments in such wind tunnels are particular easier as the flow is consistently seeded with smoke particles throughout the experiment. A Corona Integrated Technologies Inc. Colt 4 smoke generator was used to seed the flow with smoke particles which would act as a tracer for visualizing the flow through the test section. The smoke generator burns a petrochemical with insufficient supply of oxygen thereby generating smoke particles of up 5µm in diameter. The wind tunnel has a test section of 1ft x 1ft in dimension and has the capability of reaching a top speed of 67m/s.

The set of tandem wings used in the experiment are two 115VAC, 60Hz piezoelectric fans made by Piezo Systems Inc. as shown in Figure 4.5. Each of the fans have a chord length of 12.7mm (0.5"). Two of these fans were screwed on to a Plexiglas disk which also allows the fans to move closer or further apart from each other so that the interaction due to wing spacing could be studied. The structure to which the wings are affixed to also allows the geometric angle of attack of the wings to be varied with respect to the free stream flow. Figure 4.7 shows a photograph of the tandem wing configuration of the piezoelectric fans

which is being tested in the current experiment and also structure to which it is used to mount the fans in tandem configuration. For the current experiment the distance between the two fans is kept at 0.5C which would be 6.35mm (0.25"). This distance is maintained throughout the current set of experiments.

Apart from the two piezoelectric fans, the experimental setup consists of a function generator which generates a sinusoidal wave pattern which is similar to the insect wing flapping motion. The output wave pattern generated by the function generator is not enough to produce a significant amount of amplitude in the fans. To increase the amplitude of the fans, the output signal from the function generator is fed into an amplifier where the signal is amplified by a factor of 1000. The amplified power from the function generator is then supplied into the fans. The phase difference between the fans is generated by changing the connection between the fans from series to parallel. When the fans are connected in series to each other, they exhibit a phase difference of 0°. On the other hand when the circuit is connected parallel to each other with opposite terminals connecting one of the fans, they were found to exhibit a phase difference of 180°.
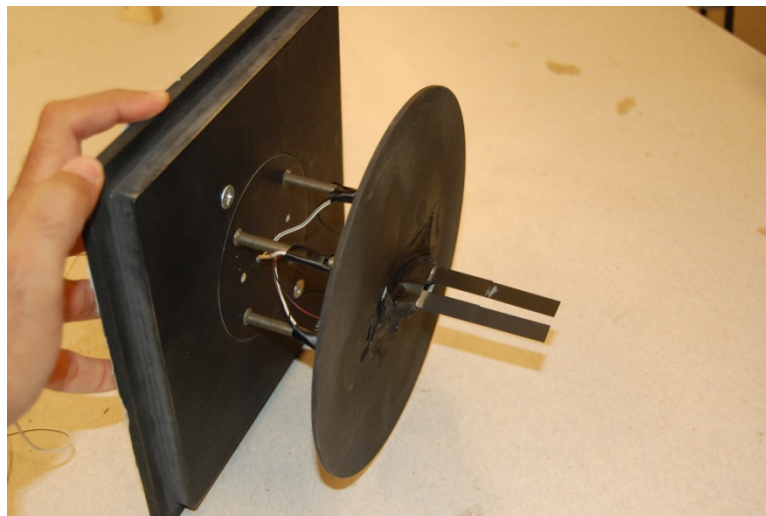
Figure 4.7. Piezoelectric Fans in tandem wing configuration

Figure 4.8. WiST Laboratory Undergraduate Wind Tunnel
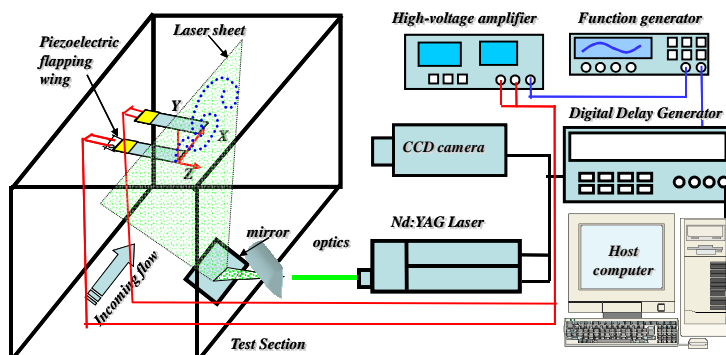
Figure 4.9. Experimental setup
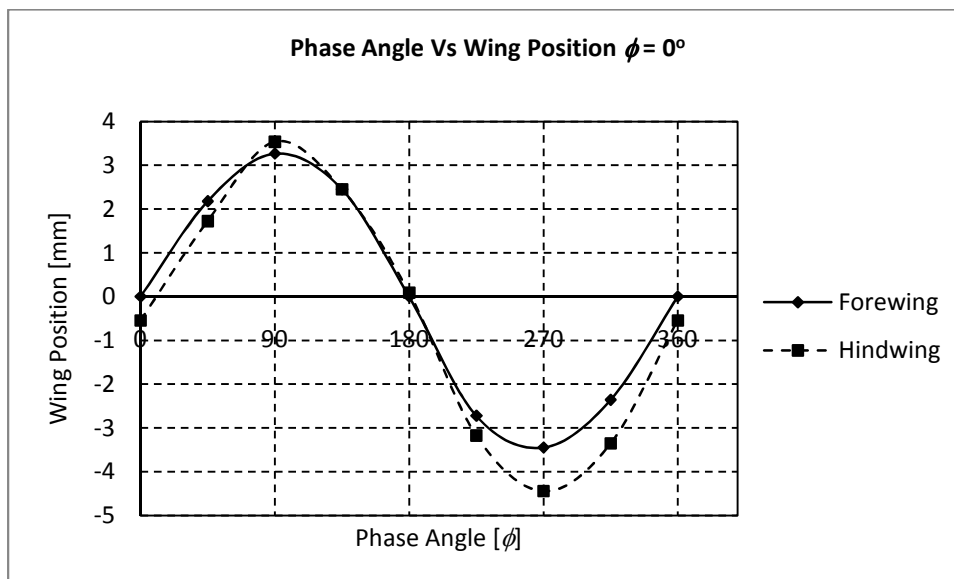
(a) In-phase Flapping
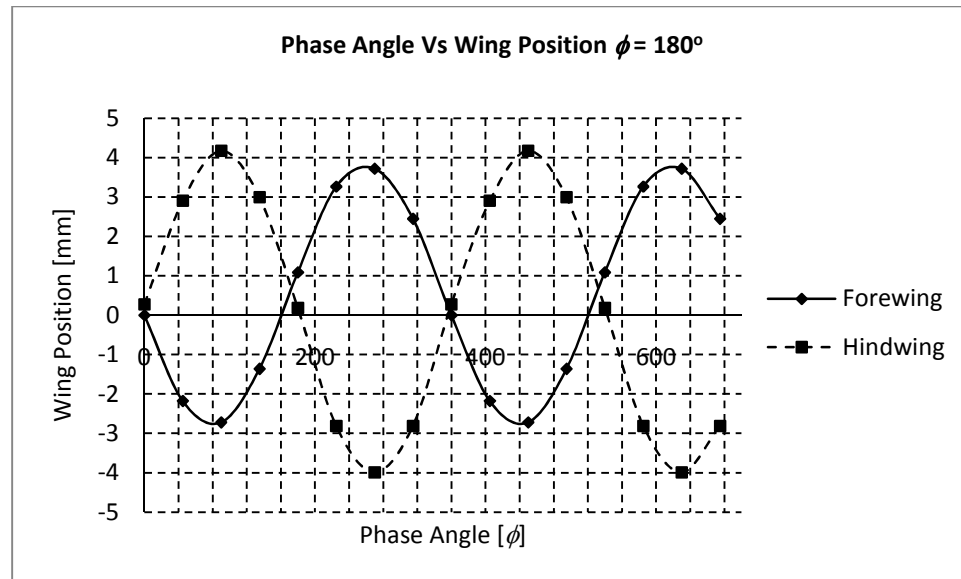
(b) Anti-phase Flapping

Figure 4.10. Wing positions at different phase angles for in-phase and anti-phase flapping

Another output from the function generator is connected to the triggering mechanism in the delay generator. By this function, the delay generator can trigger the image acquisition by the camera in the PIV system thereby allowing the user to specifically gather the images of the flow structure at a particular phase angle of the wing where the image would be "phase locked". In each of the cases, the fore-wing is considered as the baseline for the phase angle of the wing. The flow particles are illuminated with the help of a NewWave Gemini 200 Nd:Yag laser with a wavelength of 532 nm for this particular experiment. The image acquisition was carried out by a Cooke 12 bit 1376 x 1040 pixel Pixelfly CCD camera. Using the phase lock method, a total of eight phase angles were used in the experiment. The resulting wing positions at the individual phases for both in-phase and anti-phase flapping are shown in Figure 4.10. The results show that both the wings display a sinusoidal wave pattern in both in-phase and anti-phase cases. A slight difference in amplitude between the wings are

observed during the experiment, however this would amount only to a difference of about half a millimeter between the fore-wing and the hind-wing amplitudes. This small difference in amplitude can be ignored for the experiment and is attributed to the unique nature of the piezoelectric patches which makes them exhibit different performance characteristics though they are present in the same circuit.
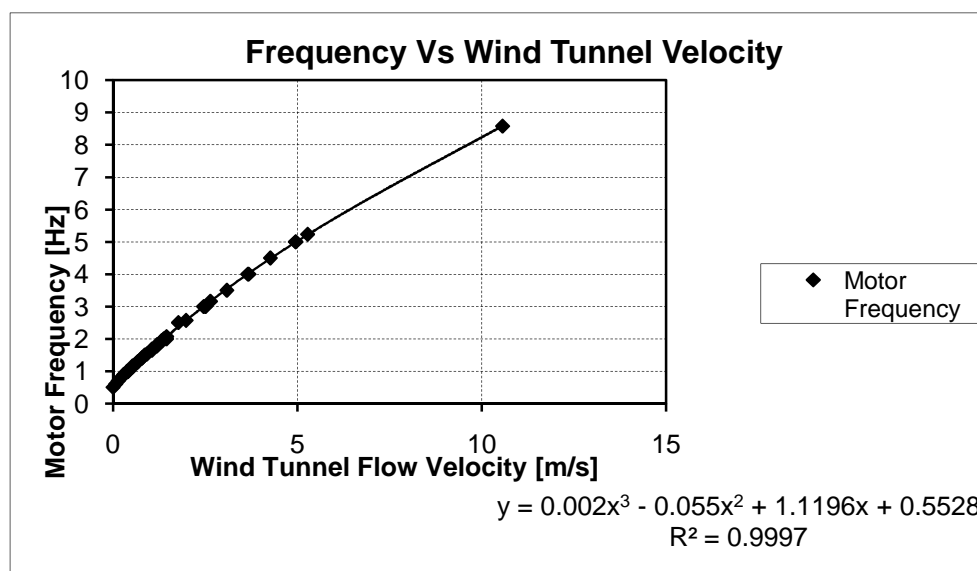

Figure 4.11.Wind Tunnel Calibration for Undergraduate Wind Tunnel

Flow velocities at different wind tunnel frequencies were calculated with the help of data gathered from Clemons [50]. The average flow velocities at the test section of the wind tunnel were obtained through PIV measurements at different motor frequencies. Owing to the requirements of having a low flow velocities to study nano air vehicle flight, Particle Image Velocimetry was used due to its high level of accuracy and non intrusive behavior compared to other flow measurement techniques such as hotwire anemometry or pressure measurements using a pitot-static probe. The data gathered from this experiment is plotted in figure 4.11 which shows the relation between the motor frequency of the wind tunnel and the

flow velocity in the test section. The relationship between the wind tunnel flow velocity and the corresponding motor frequency is shown by the third order polynomial equation which is obtained by a curve fit. Experimental results also show that the graph plotted above is accurate to a high degree.

4.7 Tandem Wing Aerodynamic Testing

The current set of experiments was carried out in the wind tunnel with a flow velocity of 0.8 m/s. The wing beat frequency of the wings was changed to 65Hz thereby causing both the wings to flap with amplitude of 6.44mm. The amplitude value was obtained by using the sequence of images obtained from the PIV data. The velocity used during the experiment when calculated against the wing tip velocity of the flapping wings would yield an advance ratio (J) equal to 0.955. Though the design frequencies of the piezoelectric wings are fixed at 60Hz, but higher amplitude was observed at an increased frequency of 65Hz.

With the current parameters, PIV experiments were conducted in both phase averaged and time averaged conditions. For the phase averaged condition, data was gathered from different phases of the wings with the help of the triggering mechanism described in the previous section. A total of eight different phase angles were used as cases for gathering data during the experiment with each case having an increment of 45° in the phase angle of the fore-wing. In the phase averaged condition, a total of 166 images were gathered for each of the cases. Finally the entire sequence of phase averaged cases is turned into an animation. For these experiments the fore-wing (ϕ_{FW}) was taken as a reference value for the phase angle in all cases. The phase averaged cases are repeated for varying geometric angles of attack of 0° and 10° for both in-phase and anti-phase conditions. For time averaged cases, the

triggering mechanism of the experimental setup is shut off and the real time video of the flapping wings is recorded. The purpose of having two different cases for this experiment is due to the high flapping frequency of the piezoelectric fans. The Pixelfly camera which is used in this experiment has a maximum image acquisition frequency of 11 Hz. Due to this large difference between both the frequencies; the phase averaged case is executed so that the wake pattern of the entire flapping sequence can be captured over a period of time. The turbulent kinetic energy measurements were also obtained from each of the cases and a time averaged result of these readings are also shown in the results below. The phase averaged results for the wake sequence and the time averaged velocity profile for AoA = 0° is shown for both in-phase and out of phase measurements in figures 4.12 – 4.16.

(a) AoA = 0, $\phi_{FW} = 0^o$ (b) AoA = 0, $\phi_{FW} = 45^o$

(c) AoA = 0, $\phi_{\text{FW}} = 90^{\text{o}}$

(d) AoA = 0, $\phi_{\text{FW}} = 135^{\text{o}}$

(e) AoA = 0, $\phi_{\text{FW}} = 180^{\text{o}}$
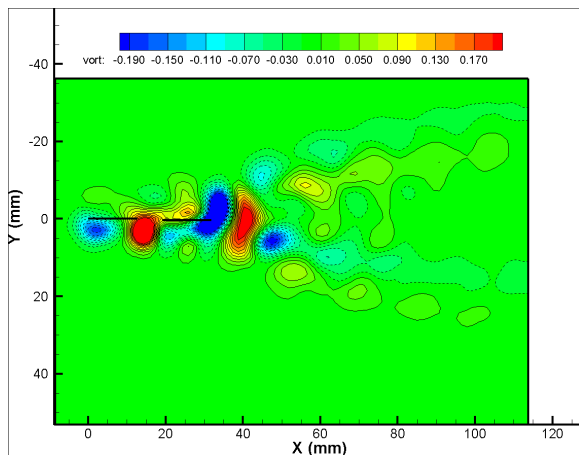
(f) AoA = 0, $\phi_{\text{FW}} = 225^{\text{o}}$
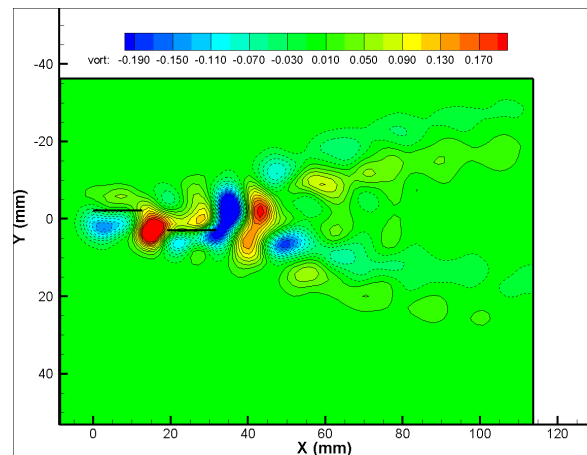
(g) AoA = 0, $\phi_{\text{FW}} = 270^{\text{o}}$
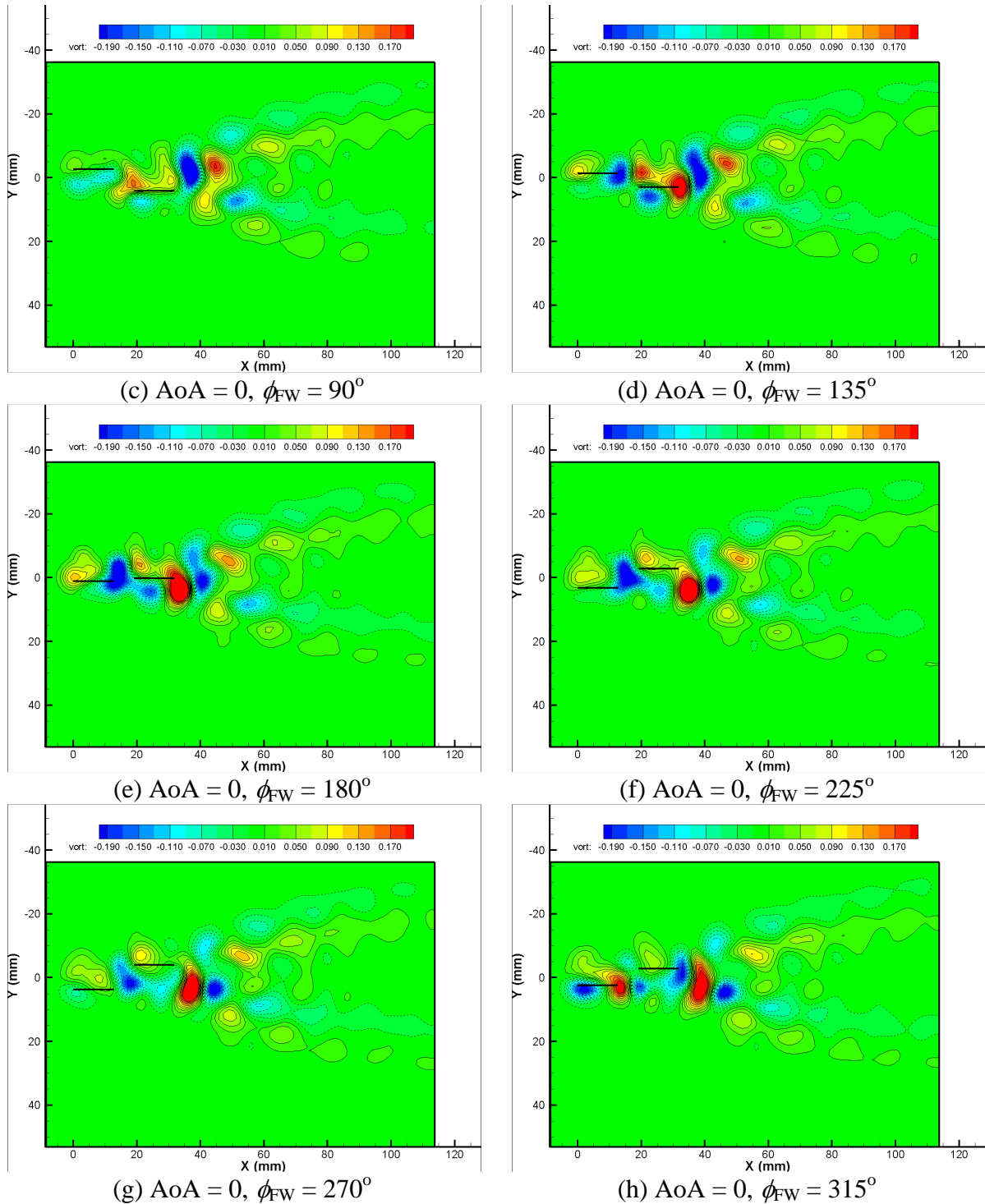
(h) AoA = 0, $\phi_{\text{FW}} = 315^{\text{o}}$

Figure 4.12. Phase Averaged results for AoA = 0°, $\phi = 180^{\text{o}}$ different fore-wing phase angles
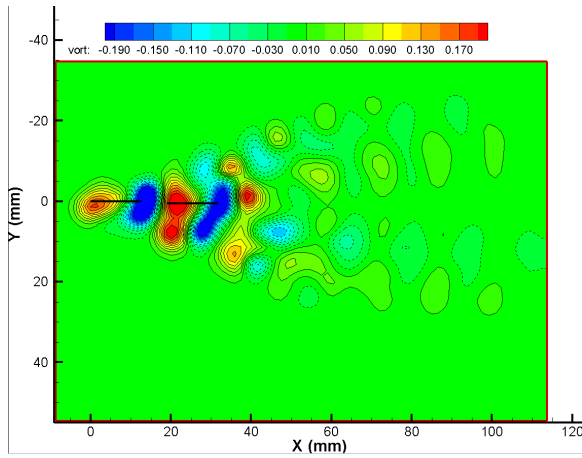
(a) AoA = 0, $\phi_{FW} = 0^o$
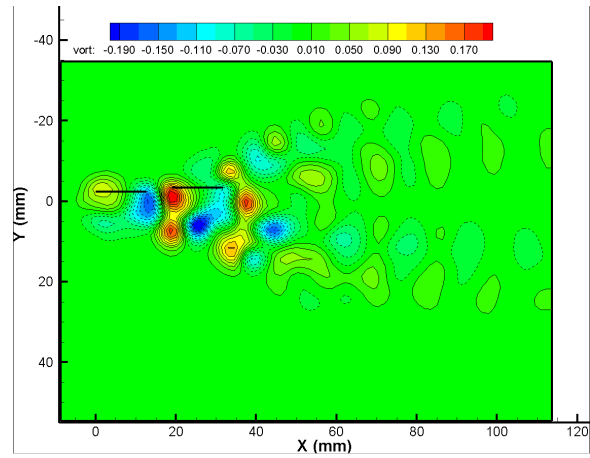
(b) AoA = 0, $\phi_{FW} = 45^o$
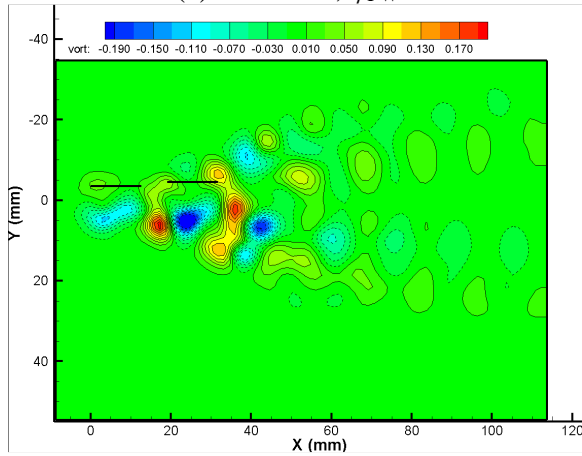
(c) AoA = 0, $\phi_{FW} = 90^o$
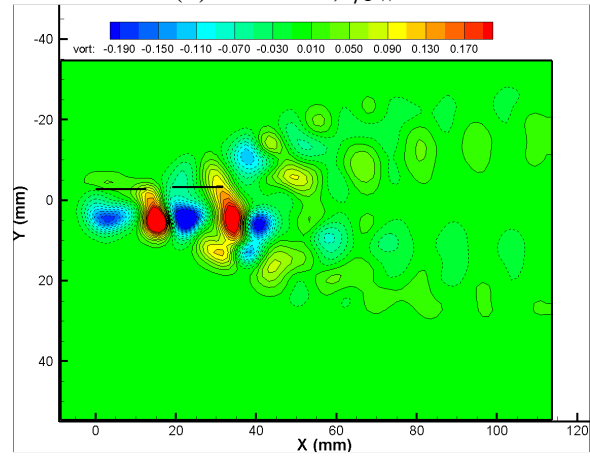
(d) AoA = 0, $\phi_{FW} = 135^o$
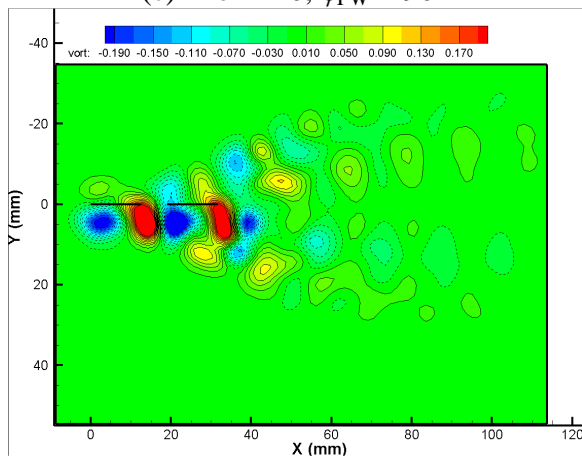
(e) AoA = 0, $\phi_{FW} = 180^o$
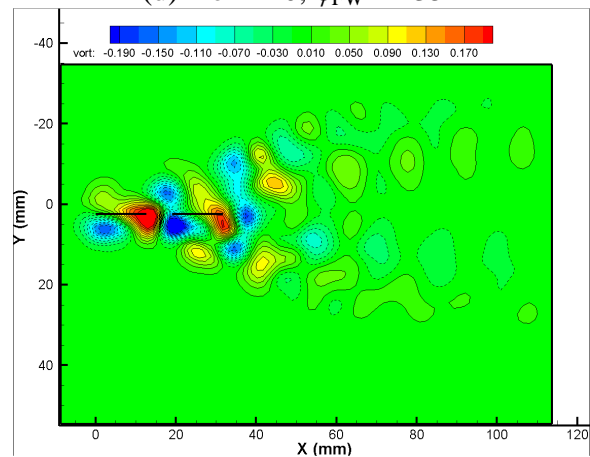
(f) AoA = 0, $\phi_{FW} = 225^o$
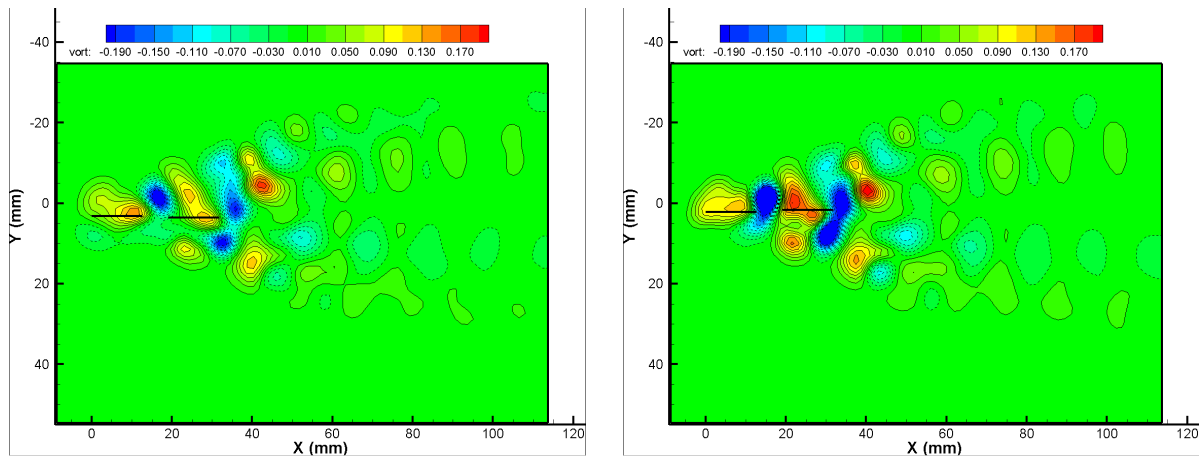
(g) AoA = 0, $\phi_{FW} = 270^o$

(h) AoA = 0, $\phi_{FW} = 315^o$

Figure 4.13. Phase averaged results for AoA = 0° $\phi = 0^o$ at different fore-wing phases
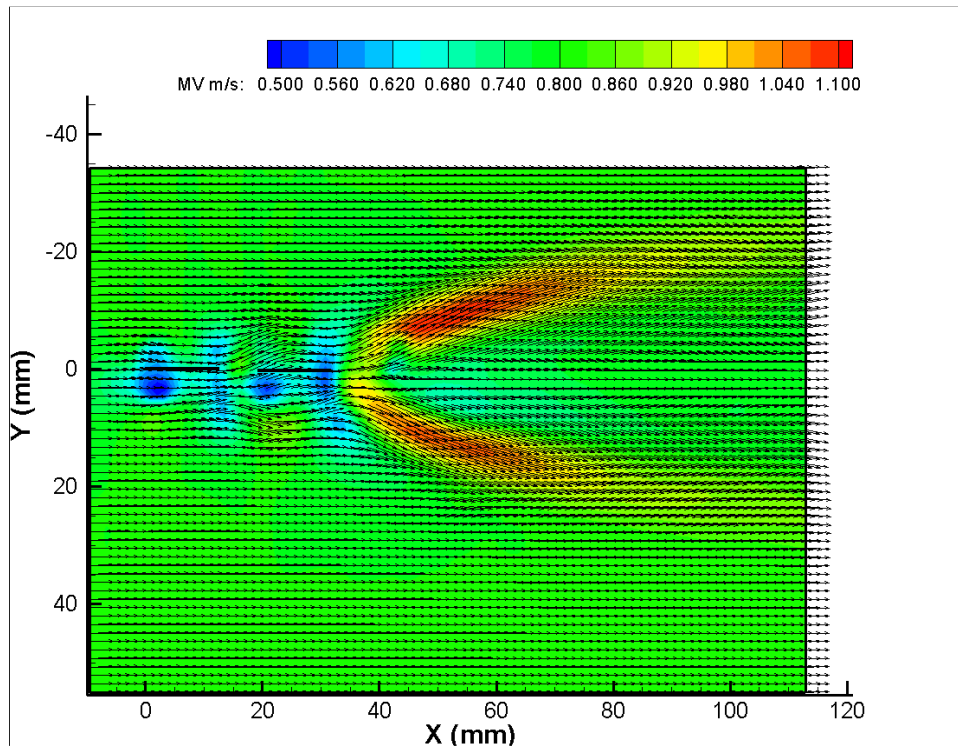
Figure 4.14. AoA = 0° $\phi = 180^o$ Time Averaged Mean Velocity
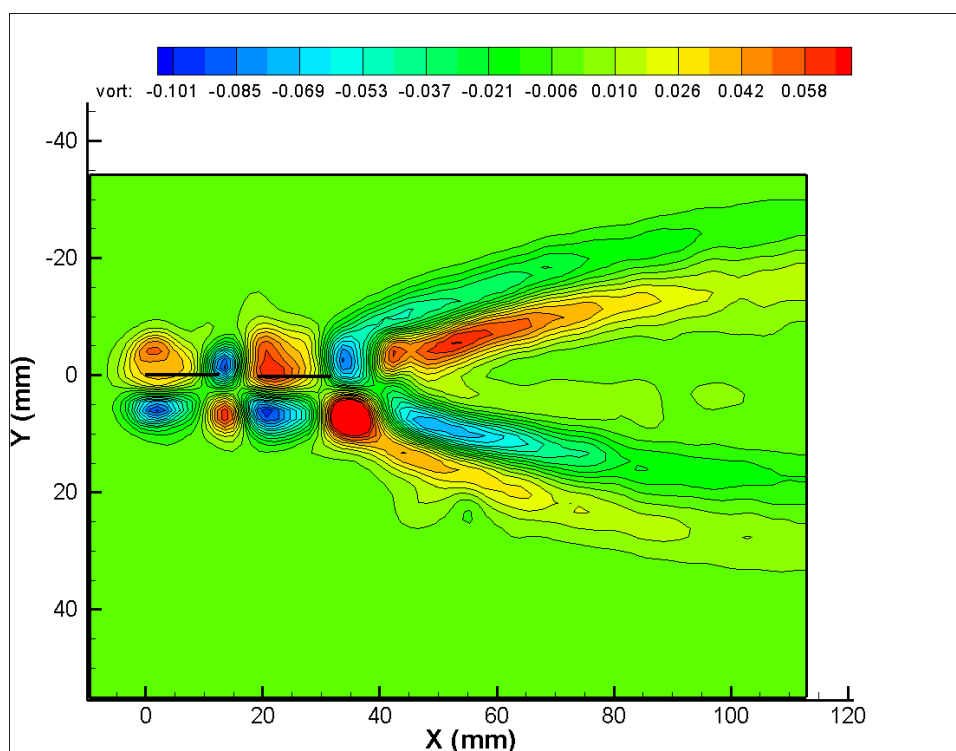
Figure 4.15. AoA = 0° ϕ = 180° Time Averaged Mean Vorticity
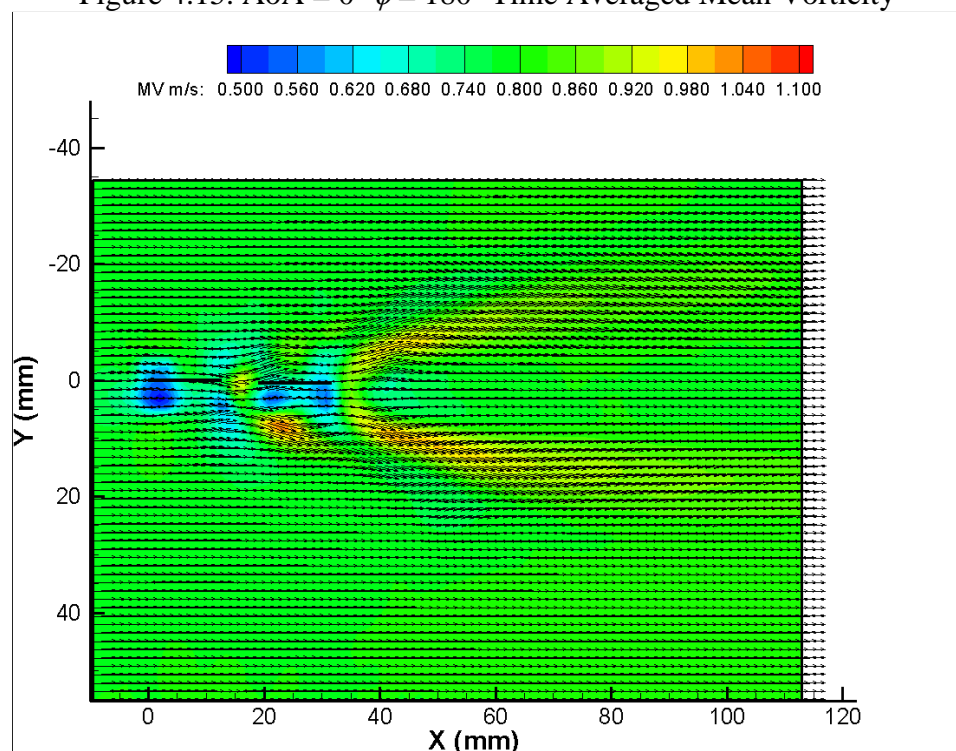
Figure 4.16. AoA = 0° ϕ = 0° Time Averaged Mean Velocity
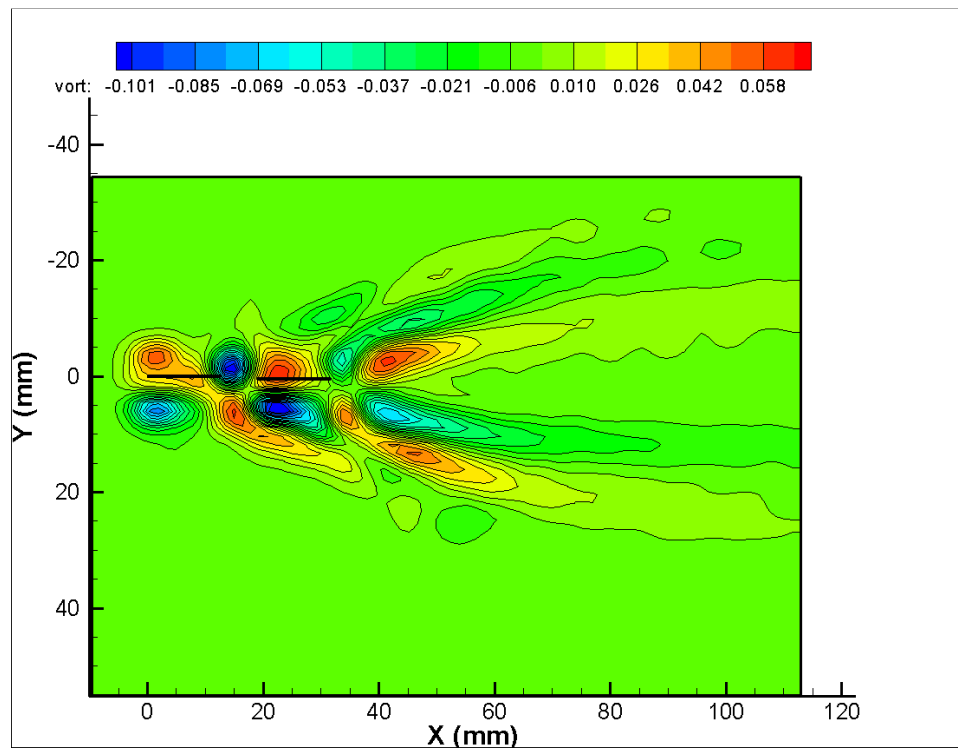
Figure 4.17. AoA = 0° $\phi = 0^o$ Time Averaged Mean Vorticity

The image sequences shown in figures 4.12 and 4.13 show vortex structures observed by Koochesfahani [5] where the presence of a dual vortex structure can be observed in the upper and lower planes of the vortex sheets. When the AoA = 0 during anti-phase flapping, a prominent vortex of alternating magnitudes are formed between the fore-wing and the hind-wing. The size of this vortex decreases as the hind-wing interacts with it and the vortex is then shed into the free-stream. Immediately after the first vortex is detached the following vortex in the wake pattern splits the previous vortex into two parts. This causes the wake structure to have a double vortex configuration with alternating magnitudes. In the case of in-phase flapping at the same angle of attack, a prominent vortex pair is observed between the fore-wing and the hind-wing. The vortex produced by the fore-wing moves away from the

hind-wing due to the presence of this alternating vortex. The vortex produced by the hind-wing is again split into two parts. The resulting wake would show two alternating vortices being formed followed a smaller vortex which was formed by the forewing of the tandem wing configuration. Figures 4.14 and 4.16 shows the time averaged mean velocity profile produced due to both in-phase and anti-phase flapping of the tandem wings. At 0° angle of attack, the time averaged mean velocity profile shows the presence of two jets being generated by the flapping wings directed towards the upper and lower regions of the wake. These jets indicate the generation of thrust by the flapping wings in both phase differences. Figures 4.15 and 4.17 shows the time averaged vorticity pattern being formed in the wake region due to both in-phase and anti-phase flapping of the tandem wings. The patterns clearly indicate vortices of opposite magnitude being shed in the upper and lower planes of the wake. This dual vortex pairs are observed in both the upper and lower planes of the wake region.

(a) AoA $= 10^o$, $\phi_{FW} = 0^o$ (b) AoA $= 10^o$, $\phi_{FW} = 45^o$

(c) AoA = 10°, $\phi_{FW} = 90^{o}$

(d) AoA = 10°, $\phi_{FW} = 135^{o}$

(g) AoA = 10°, $\phi_{FW} = 180^{o}$

(h) AoA = 10°, $\phi_{FW} = 225^{o}$

(i) AoA = 10°, $\phi_{FW} = 270^{o}$

(j) AoA = 10°, $\phi_{FW} = 315^{o}$
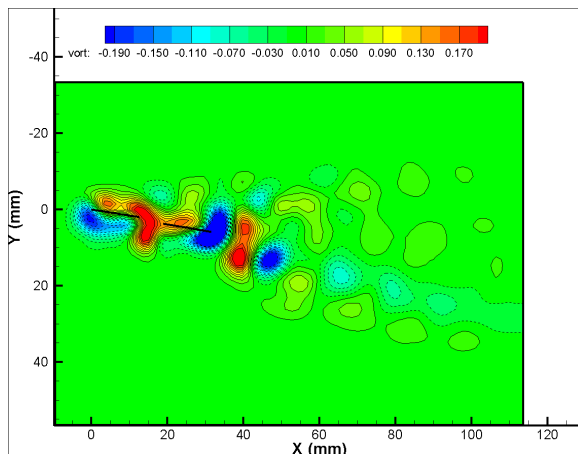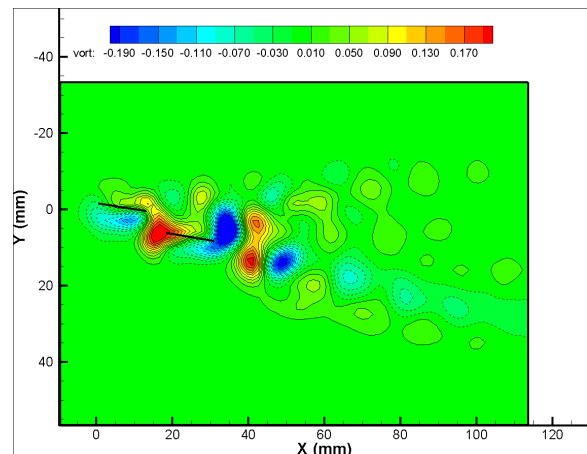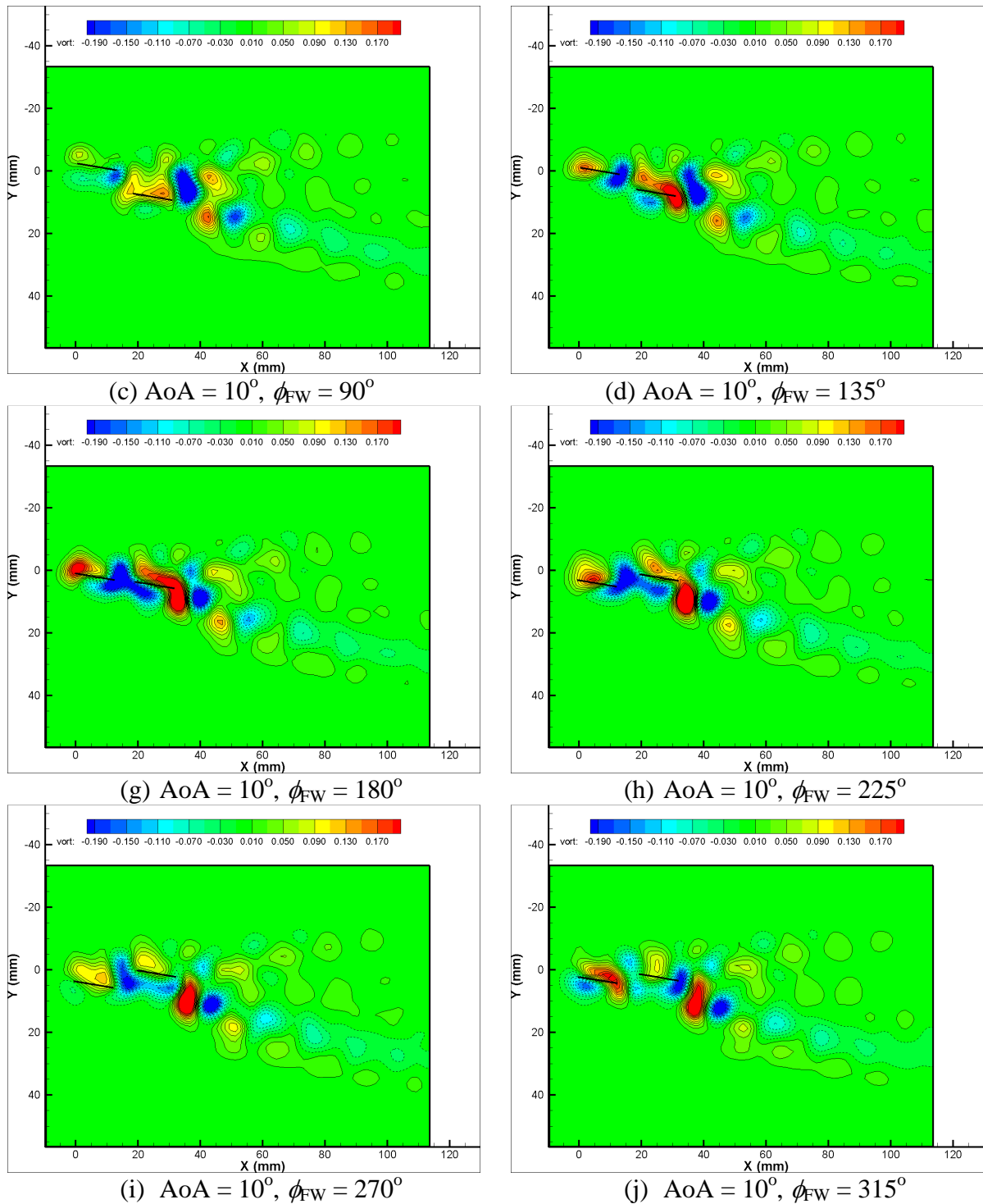
Figure 4.18. Phase Averaged Results for AoA = 10° $\phi = 180^{o}$ at Different Leading Edge Phase angles
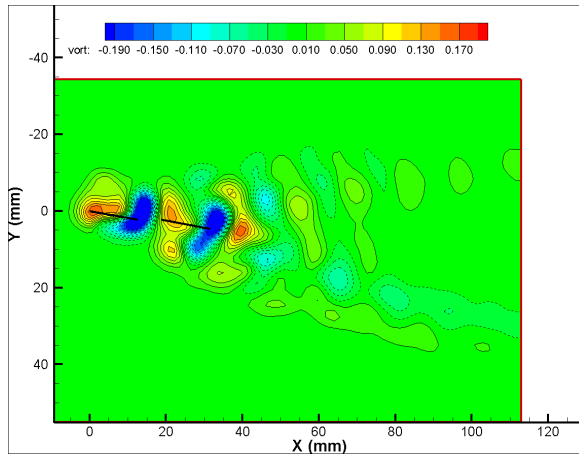
(a) AoA = 10°, $\phi_{FW} = 0°$
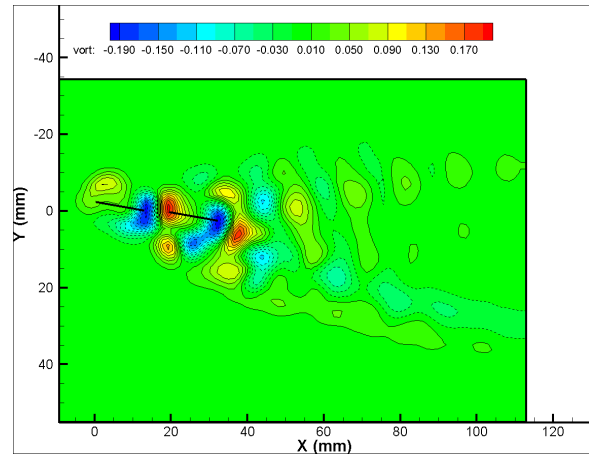
(b) AoA = 10°, $\phi_{FW} = 45°$
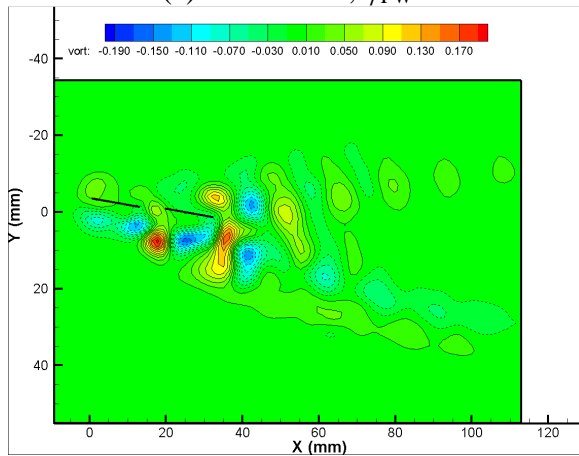
(c) AoA = 10°, $\phi_{FW} = 90°$
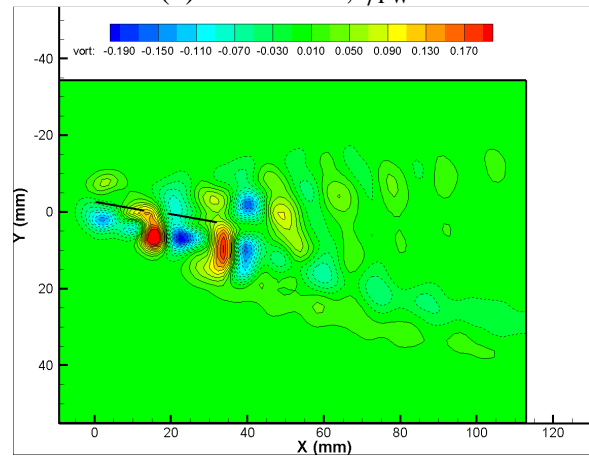
(d) AoA = 10°, $\phi_{FW} = 135°$
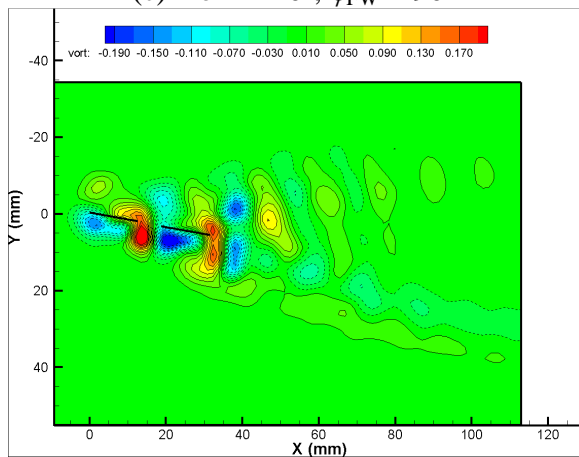
(e) AoA = 10°, $\phi_{FW} = 180°$

(f) AoA = 10°, $\phi_{FW} = 225°$

(g) AoA = 10°, ϕ_{FW} = 270° (h) AoA = 10°, ϕ_{FW} = 315°
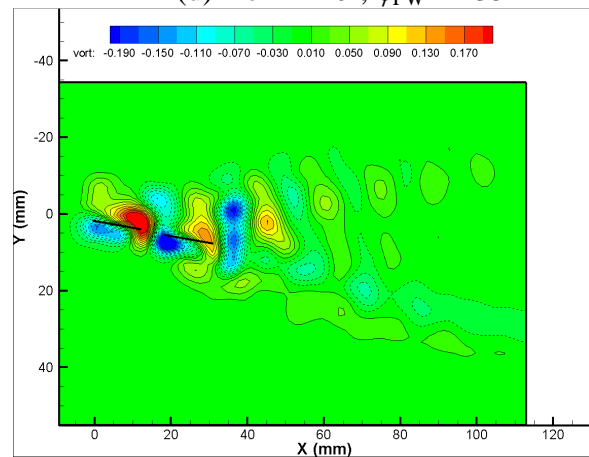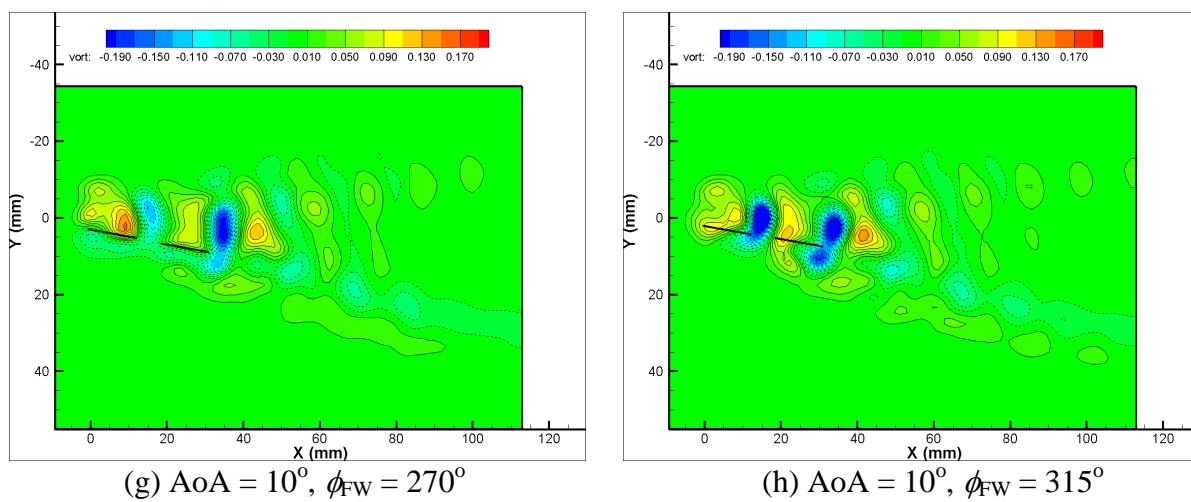
Figure 4.19. Phase Averaged Results for AoA = 10° ϕ = 0° at Different Leading Edge Phase angles
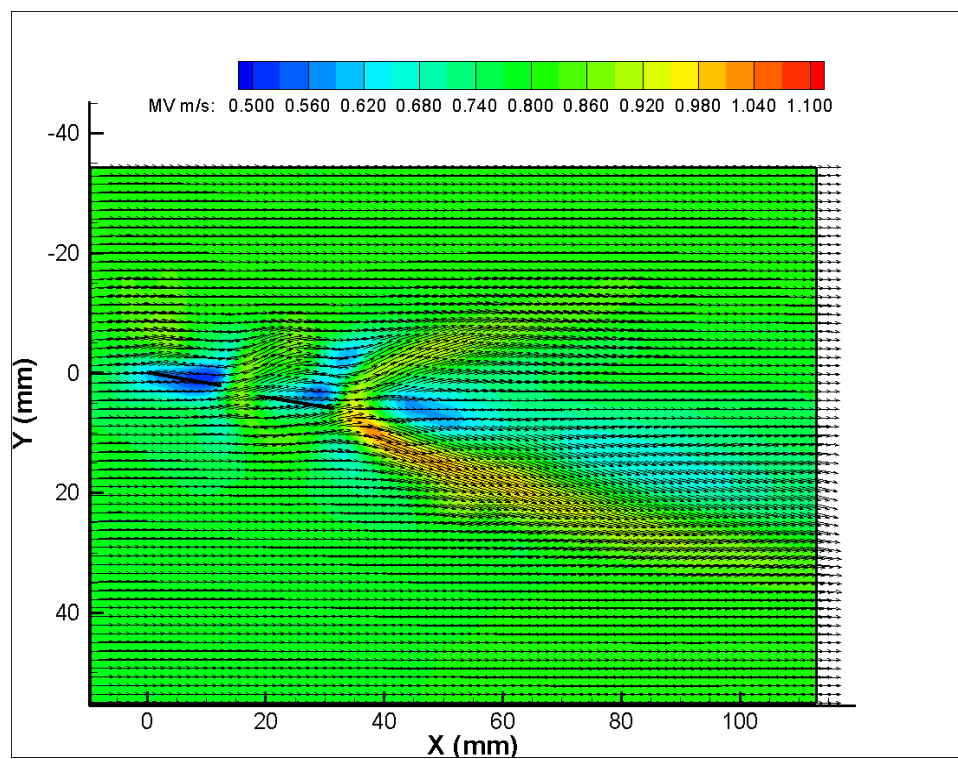
Figure 4.20. AoA = 10°, ϕ = 180° Time Averaged Mean Velocity
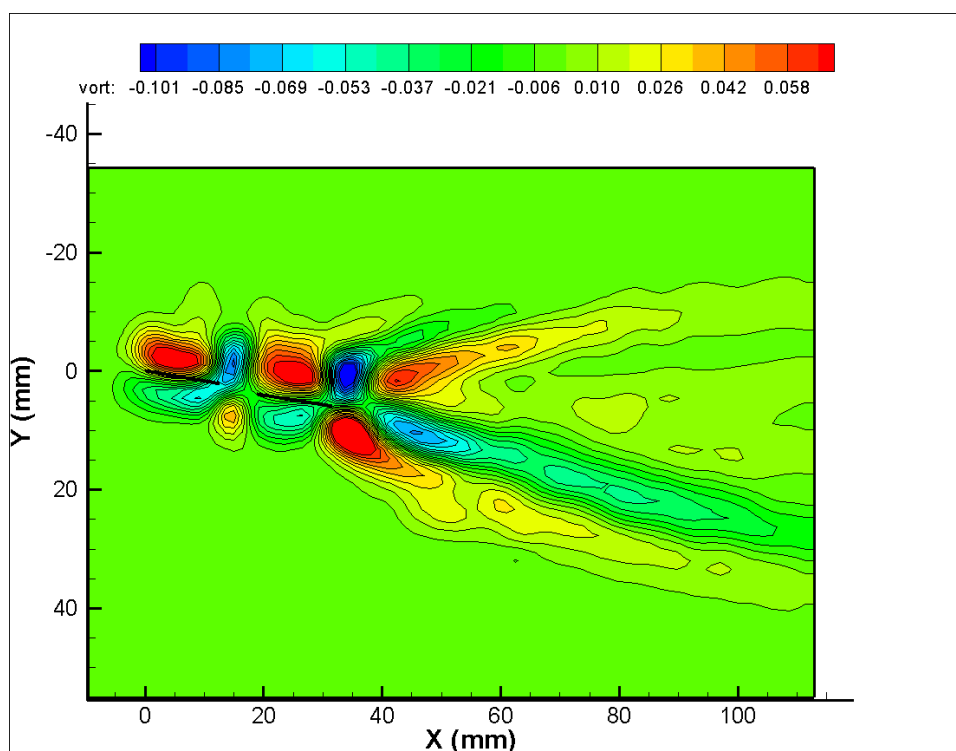
Figure 4.21. AoA = 10°, ϕ = 180° Time Averaged Vorticity
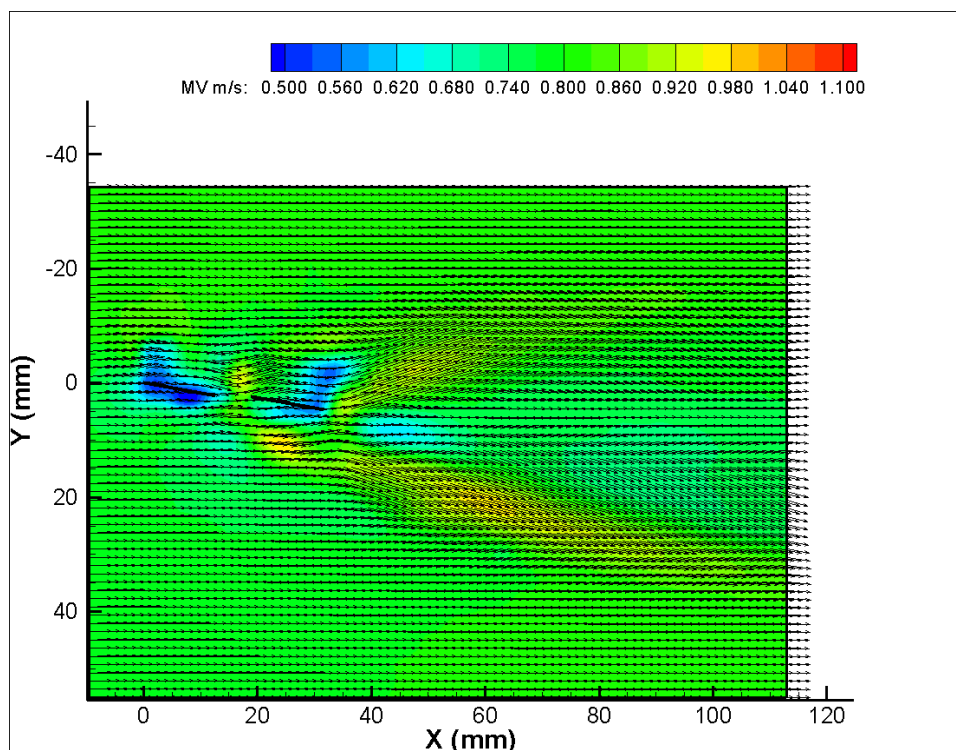
Figure 4.22. AoA = 10°, ϕ = 0° Time Averaged Mean Velocity
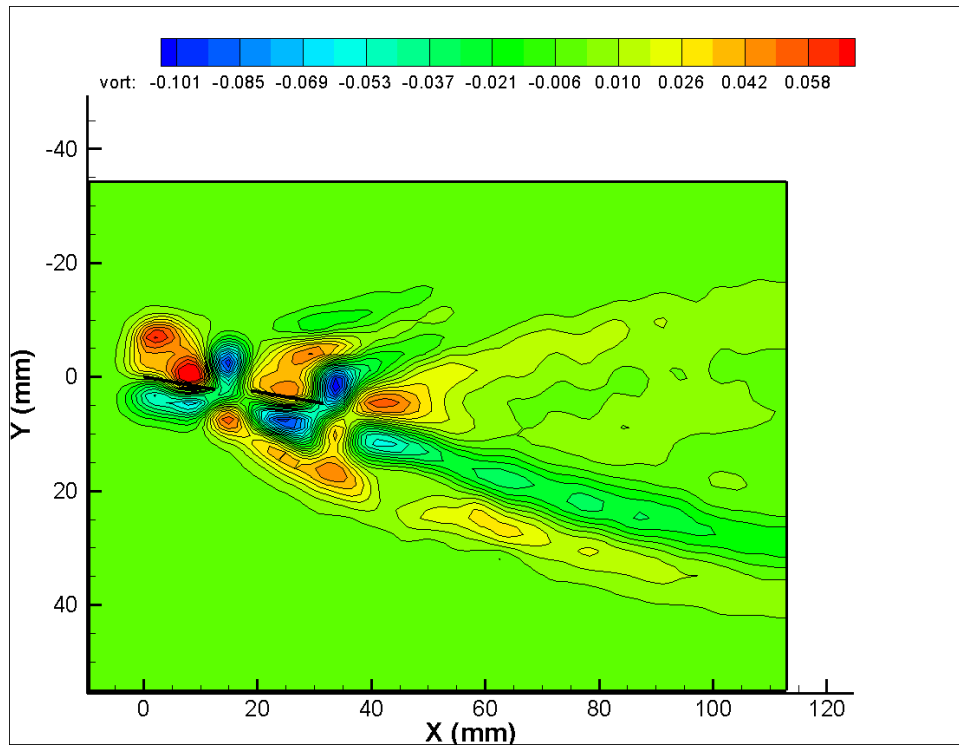
Figure 4.23. AoA = 10°, $\phi = 0°$ Time Averaged Vorticity

Figures 4.18 and 4.19 show the sequence of vortices being shed for both in-phase and anti-phase flapping motions at an angle of attack of 10°. The results in the anti-phase flapping motion indicates the presence of a prominent vortex being formed once again between the fore-wing and hind-wing similar to the case where AoA = 0°. In this case, the hind-wing sheds a vortex of a very large magnitude which is later split into two parts by the following vortex which is of an opposite orientation. The resulting wake pattern shows an alternating dual vortex pattern on both the upper and lower plane of the wake structure. The velocity vectors in the flow field indicate the formation of a jet pattern which is directed downward indicating the presence of a larger amount of lift than seen in the case where AoA = 0°. On the other hand a much more complex wake structure is observed during in-phase flapping of the wings. As observed earlier when AoA = 0°, a vortex pair of opposite magnitudes are spotted between the fore-wing and hind-wing. The vortex shed from the fore-wing moves

away from the hind-wing due to the presence of a vortex of opposite magnitude however this vortex later mixes with the resulting vortex structure formed by the hind-wing. The wake formed in this case is very complex and a definite pattern is not found. While observing the velocity vectors in this case, along with the jet which is directed in the downward direction of the flow field a higher magnitude velocity along the axis of the thrust generation is observed. This is indicative that the in-phase flapping would generate a higher amount of thrust than the anti-phase condition.

Figures 4.20 and 4.22 shows the time averaged mean velocity profiles of both in-phase and anti-phase flapping at AoA = 10°. In both the cases, the velocity jets are more prominent in the downward direction, indicative of a higher amount of lift being produced as the angle of attack of the wings increase. In the cases with an increased angle of attack, it can be noticed that the jet formed in the upper region of the wake is smaller in size then the lower region. In the case of in-phase flapping it is to be noticed that the jet in the upper region is of a larger size than that of the same jet in the anti-phase flapping condition. This would indicate that a higher amount of thrust is being produced by in-phase flapping than anti-phase flapping of the wings. Figures 4.21 and 4.23 show the time average vorticity in the wake region for in-phase and anti-phase flapping at AoA = 10°. The vorticity profile is directed downward and also shows the presence of dual vortex pairs of opposite magnitudes being shed in the wake region.

4.8 Velocity Profile Analysis

To have a deeper understanding of the wake structure, and its effects on the force generation by the tandem wings a velocity profile was generated at the wake region of the

flow field. Using the existing PIV measurement data that was gathered to understand the vortex structure of the airfoil, a velocity profile along the Y-axis of the flow field was obtained. A probing location along the flow field was selected at a distance of 100mm downstream from the leading edge of the fore-wing. The approximate location of the velocity profile can be classified as 7.87C where C is the chord length of the fan (C = 12.7mm). This location was chosen as a more stable velocity profile can be generated as the phasing between the two wings could cause large amounts of turbulence closer to the tandem wing configuration. As the flow moves much further downstream the effects of the wing interaction would have dissipated by a small level.

Once the velocity profile is gathered at this location the values are normalized with the free stream velocity. To determine the free stream velocity, the first column of velocity vectors from the PIV data is gathered and averaged. The magnitudes of the vectors are averaged and the resultant velocity value is concurrent to the predicted velocity from the calibration curve. The average velocity of first row of velocity vectors from the incoming flow is approximately equal to 0.8m/s. This velocity value is used to divide the subsequent velocity values in the array thereby generating the normalized velocity profile of the wing. The time averaged results obtained from the PIV measurements are used to calculate the normalized velocity profiles for each of the cases. Figure 4.24 shows the normalized velocity profile at AoA $= 0^o$ for both the anti phase and the in-phase flapping motion. The normalized velocity profile for AoA $= 10^o$ for both in-phase and anti phase flapping is shown in figure 4.24.
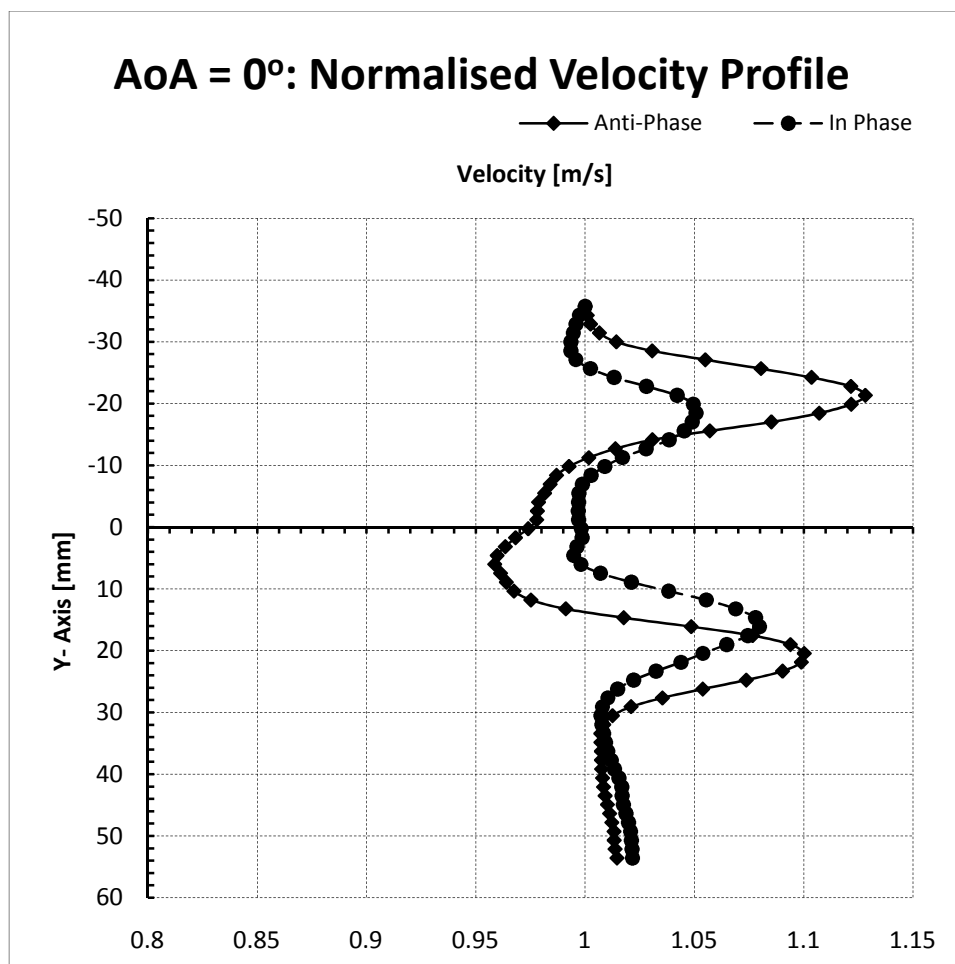
Figure 4.24. Normalized Velocity Profile for AoA = 0° for In-phase and Anti Phase Flapping Motion

The velocity profile shown above in figure 4.24 indicates the momentum surfeit as described in the reverse Karman Vortex Street or thrust generating vortex. However the wake structure is a lot more similar to that described by Koochesfahani [5]. The presence of a dual peak surfeit corresponds to the generation of a dual pair of vortices in each of rows of the vortex street. The wake structure shows a larger momentum surfeit being displayed by the anti-phase flapping phase difference than the in-phase condition. This is contrary to the observation from past studies that the in-phase flapping is used to generate a higher amount

of thrust by tandem wings. This analysis was observation was further confirmed when the thrust in the X – direction of the flow field was calculated with the help of the momentum flux in that particular direction. Using the principle of mass conservation, the following equation can be used to obtain the thrust produced in a 2 dimensional flow field.

$$T = \rho \int_{\infty}^{-\infty} u(y)(u(y) - U_\infty)\, dy$$

Figure 4.25 shows the normalized velocity profile of the flow field for both the in-phase and the anti phase condition for AoA = 10°. The preliminary flow profile shows a momentum deficit especially in the region which forms a jet which is directed in the downward direction. This indicates the presence of drag in the flow profile. This observation is quiet similar to the results obtained from the flapping wing micro air vehicle experiments and the comparative study of wing flexibility which indicates a decrease in thrust generated by the wing with increasing geometric angle of attack. Despite of the generation of drag by the tandem wings at higher angle of attack, the thrust generated by calculating the velocity profile of the flow field shows a lower amount of drag being generated by in-phase flapping in comparison to the anti-phase flapping. This could indicate that the in-phase flapping does provide a slight increase in the thrust generated by the wings at higher angles of attack.
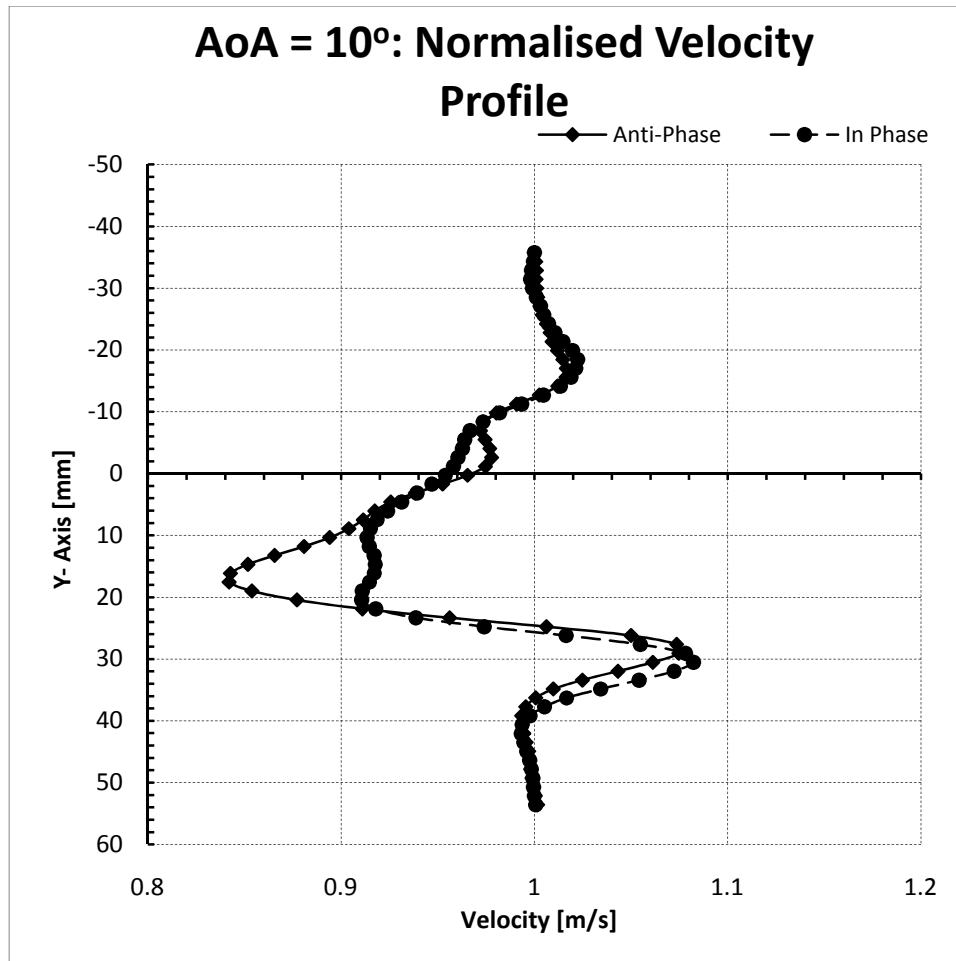
Figure 4.25. Normalized Velocity Profile for AoA = 10° for In-phase and Anti Phase Flapping Motion

In the case of dragonflies and other insects with tandem wings, the situation where an in-phase flapping is employed is cases such as take off and during extreme maneuvering. Either of these cases do not take place at zero angles of attack but they rather would include the wings to have a higher than usual geometric angle of attack. This could lead to a speculation on the effectiveness of in-phase flapping during level flight. However with an indication that the anti phase flapping generates a higher amount of thrust during level flight could explain why dragonflies would prefer using an anti phase flapping motion than in-

phase flapping in such conditions. However this observation is not conclusive as the span-wise velocity component of the flow during flapping flight is neglected while calculating the thrust values.
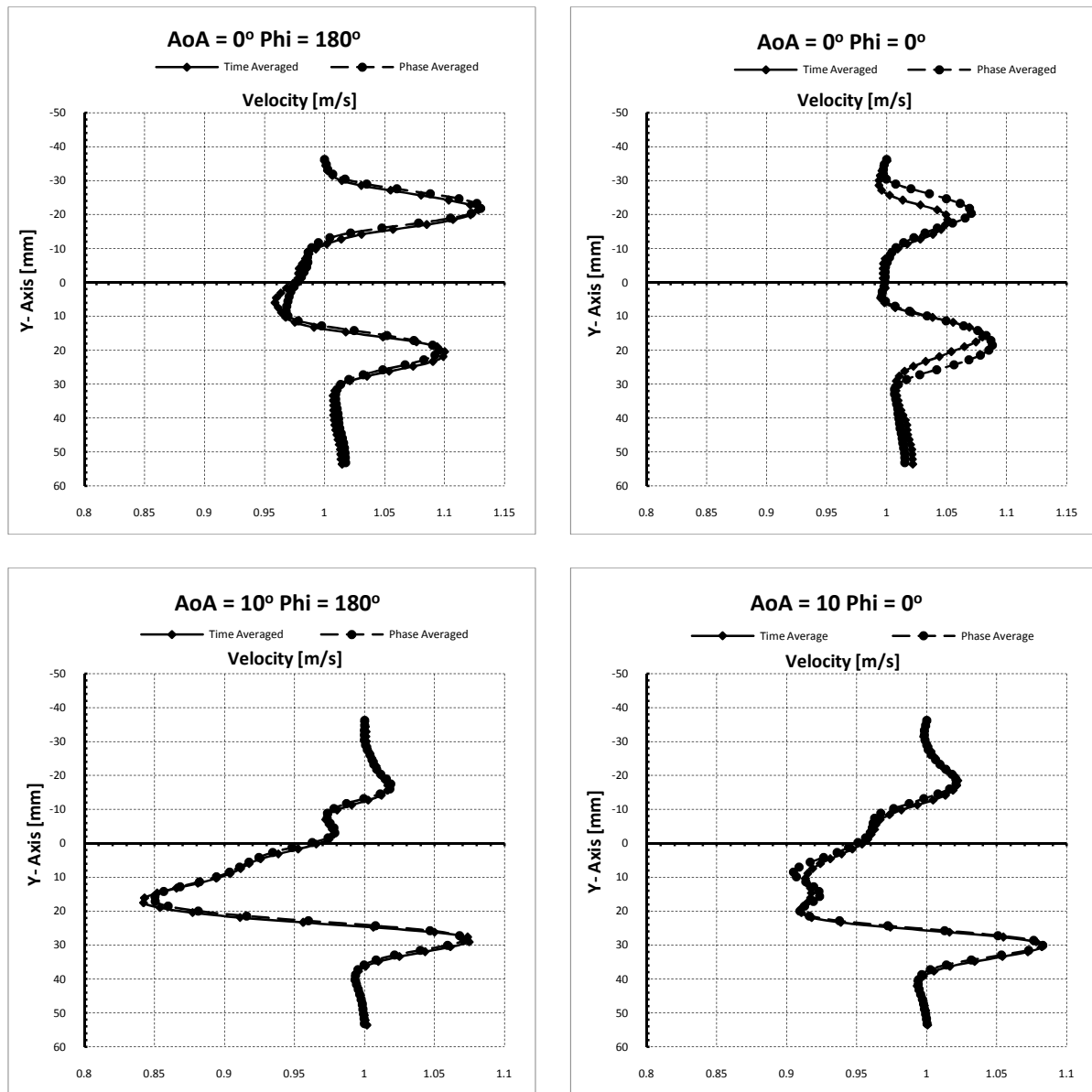
Figure 4.26. Comparison Between Phase Averaged and Time Averaged Results for All Cases

To avoid any discrepancy between the time averaged and the phase averaged results gathered for calculating the velocity profile of the flow field, the time and phase averaged results were compared. The eight phases generated during the flow measurements in the phase averaged case was once again averaged and was then plotted in the same manner as the time averaged results. Figure 4.26 shows the comparison between the time averaged and phase averaged results of the velocity profile. The velocity profile of most cases was found to match very closely with each other. The only anomaly was found while comparing the time averaged and phase averaged profiles of the zero degree angle of attack. Another observation made along with this anomaly is that the thrust generated in the phased average in-phase flapping is found to be slightly more than that of anti phase flapping. This observation is contradictory with the results obtained for the same case with the phase averaged data. However this particular set of data concurs with the assumption that in-phase flapping would increase the thrust generated by tandem wings.

These contradictions from the measurement data in the flow field could be attributed to the highly three dimensional nature of the vortex structures being formed in flapping flight. The additional component of wing tip vortex generation also interferes with the wake structure generated by the wings. Another factor to be taken into account is that the thrust equation which is used to calculate a qualitative value of the thrust being generated at different cases would be severely influenced by the three dimensional nature of the flow field. Unless out of plane measurements are made with the help of stereoscopic PIV measurements, a complete picture cannot be obtained on the wake structure generated by flapping of tandem wings at various phase differences.

CHAPTER 5. GENERAL CONCLUSIONS

The studies conducted in the flapping wing micro air vehicles have shown the following results. The augmented thrust and lift values in each case have shown that a higher amount of thrust and lift are generated when the vehicle would fly within the unsteady aerodynamic region. The qualitative efficiency studies also indicated that the flying at lower advance ratios exhibit a greater propulsive efficiency. When a comparative study was conducted on the effects of flexibility of the wings, it was found that the wing with moderate flexibility or the Nylon wing was found to have a higher performance in terms of aerodynamic characteristics. The latex and the rigid wings exhibited better characteristics in both lift and thrust individually though the combined performance in both lift and thrust generation showed that the Nylon wing performed better compared to the other two.

PIV measurements of the tandem wing configuration showed the vortex patterns which are formed with high amplitude to chord ratio – high frequency wings. The study also proved an interesting understanding into why a dual vortex pair is formed in the wake of the flapping wing is due to interference between the vortices being shed from the hind-wing. The velocity profile observations and the thrust calculation proved conflicting results. This is likely to be due to the highly three dimensional nature of the vortex structure formed due to flapping of wings as the PIV measurements taken in this case neglected the out of plane flow measurements.

CHAPTER 6. RECOMMENDATIONS FOR FUTURE WORK

The current experiments have given a greater understand into the performance of flapping wing micro air vehicles and the effects of flexibility of the membrane wing which can be used to enhance the overall aerodynamic performance of the vehicle and also the efficiency study allows us to decide specific flight parameters by which the battery life can be extended. However in the current study, the wing is only restricted to plunging motion. On the other hand, pitching motion along the axis of the wing is not considered in this study though it is a very important part of flapping flight. Future research into flapping wing flight would include the use of a model which would also have a pitching motion of the wing during flapping flight.

Nano air vehicle wings which have been used in these experiments are similar to flat plates. The next step in the study of flapping wing nano air vehicle wings would involve the design of a wing structure of a micro scale. The geometry of this wing would be based on an insect wing. Another issue which has come into light during the PIV measurements of the flow field is the presence of a large out-of-plane velocity component. The next step in the flow measurement would include gathering from Stereoscopic PIV (SPIV) measurements. This technique allows the measurement of out-of-plane velocity components which plays a key part in the aerodynamics of flapping flight. A further understanding on the aerodynamic forces being generated by the wings can also be obtained with the help of the out of plane velocity component.

BIBLIOGRAPHY

1. Spedding, G.R., Lissaman, P.B.S., "Technical Aspects of Microscale Flight Systems," Journal of Avian Biology, Vol. 29, 1998, pp. 458 – 468.

2. von Karman, T., Burgers, J.M., "General Aerodynamic Theory," Aerodynamic Theory: A General Review of Progress, edited by W.F. Durand, Vol. 2, Springer , Berlin, 1935.

3. Young, J., "Numerical Simulation of the Unsteady Aerodynamics of Flapping Airfoils", PhD Thesis, University of New South Wales.

4. Lai, J. C. S., Platzer, M. F., "Jet Characteristics of a Plunging Airfoil", AIAA Journal, Vol. 37, No.12, December 1999, pp 1529 – 1537.

5. Koochesfahani, M. M., "Vortical Patterns in the Wake of an Oscillating Airfoil", AIAA Journal, Vol. 27, No. 9, pp. 1200 – 1205.

6. Anderson, J. M., Streintlien, K., Barrett, D.S., Triantafyllou, M. S., "Oscillating Foils of High Propulsive Efficiency," Journal of Fluid Mechanics, Vol. 360, 1998, pp. 41-72.

7. Ellington, C. P., van den Berg, E., Willmott, A.P., Thomas, A. L.R., "Leading-edge vortices in insect flight," Nature, Vol. 384, 1996, pp. 19 – 26.

8. Viieru, D., Tang, J., Lian, L., Lui, H., Shyy, W., "Flapping and Flexible Wing Aerodynamics of Low Reynolds Number Flight Vehicles," 44th AIAA Aerospace Sciences Meeting and Exhibit, 2006.

9. Lu, Y., Shen, G. X., Su, W, H., "Flow Visualization of Dragonfly Hovering via an Electromechanical Model," AIAA Journal, Vol. 45, No.3, March 2007, pp. 615- 623.

10. Lu, Y., Shen, G. X., "Three-dimensional Flow Structures and Evolution of the Leading-edge Vortices in a Flapping Wing," The Journal of Experimental Biology, Vol. 221, 2008, pp. 1221 – 1230.

11. Yang, Z., Haan, F.L., Hu, H., and Ma, H., "An Experimental Investigation on the Flow Separation on a Low-Reynolds Number Airfoil", 45th AIAA Aerospace Sciences Meeting and Exhibit, Jan 8-11. 2007, Reno, Nevada.

12. Hu, H., Tamai, M., Murphy, J.T., "Flexible-Membrane Airfoils at Low Reynolds Numbers" Journal of Aircraft, Vol.45, No.5, September-October 2008.

13. Shyy, W., Ifju, P., Viieru, D., "Membrane Wing-Based Micro Air Vehicles", Applied Mechanics Reviews, Vol. 58, July 2005.

14. Anonymous, "Townstead's big-eared bat", Wikipedia, November 2009. [http://en.wikipedia.org/wiki/Corynorhinus_townsendii. Accessed 11/28/2009.]

15. Anonymous, "Northern Flying Squirrel", Wikipedia, November 2009. [http://en.wikipedia.org/wiki/Glaucomys_sabrinus. Accessed 11/28/2009.]

16. Hong, Y., Altman, A., "Streamwise Vorticity in Simple Mechanical Flapping

wings," Journal of Aircraft, Vol. 44, No. 5, 2007, pp. 1588 – 1597.

17. Kim, D., Kim, H., Han, J., Kwon, K., "Experimental Investigation on the Aerodynamic Characteristics of a Bio-mimetic Flapping Wing with Macro-fober Composites," Journal of Intelligent Material Systems and Structures,Vol. 00, 2007, pp. 1 – 10.

18. Anonymous, JR3 Incorporated.
[http://www.jr3.com. Accessed 11/28/2009.]

19. Anonymous, "Smaller Scale Wind Tunnels", Wind Simulation and Testing Laboratory.
[http://weea.aere.iastate.edu/facilities/smaller-scale-wind-tunnels.html. Accessed 11/28/2009.]

20. Anonymous, Scanivalve Corporation.
[http://www.scanivalve.com/home.htm. Accessed 11/28/2009.]

21. Anonymous, BK Precision.
[http://www.bkprecision.com. Accessed 10/9/2009.]

22. Hu, H., Gopa Kumar, A., Abate, G., Albertani, R., "An Experimental Study of Flexible Membrane Wings in Flapping Flight," 46th AIAA Aerospace Sciences Meeting and Exhibit, Orlando Florida, 2008.

23. Ho, S., Nassef, Hanny., Pornsinsirirak, N., Tai, Y., Ho, C., "Unsteady Aerodynamics and Flow Control for Flapping Wing Flyers", Progress in Aerospace Sciences, Vol. 39, 2003, pp 635-681.

24. Gallivan, P., DeLaurier ,J., "An Experimental Study of Flapping Membrane Wings," Canadian Aeronautical and Space Institute, Vol. 53, No. 2, June 2007.

25. Davis, W. A., "Nano Air Vehicles A Technology Forecase," Blue Horizons Paper, Center for Strategy and Technology, Air War College, April 2007.

26. Defense Advanced Research Projects Agency Fact Sheet, "DARPA Nano Air Vehicle Program," December 2008.

27. Anonymous, "DelFly Micro", Delfly.
[http://www.delfly.nl. 10/5/2009.]

28. Harvard Microrobotics Lab

29. Chung, H.C., Kummari, K.L., Croucher, S.J., Lawson, N.J., Guo, S., Huang, Z., "Coupled Piezoelectric Fans with Two Degree of Freedom Motion for the Application of Flapping Wing Micro Aerial Vehicles," Sensors and Actuators A, Vol. 147, 2008, pp. 607 – 612.

30. Bidakhvidi, M. A., "The Design of a Piezoelectric Fan System for the Flapping Wing Micro–Air–Vehicle application," Masters Thesis, Department of Mechanical Engineering, Vrije Universiteit Brussel, Brussels, Belgium, 2009.

31. Syaifuddin, M., Park, H.C., Goo, N. S., "Design and Evaluation of a LIPCA-actuated Flapping Device," Smart Materials and Structures, Vol. 15, 2006, pp. 1225 – 1230.

32. Wood, R. J., Steltz, E., Fearing, R. S., "Optimal Energy Density Piezoelectric Bending Actuators," Sensors and Actuators A, Vol. 199, 2005, pp. 476 – 488.

33. Wood, R.J., Avadhanula, S., Sahai, R., Steltz, E., Fearing, R.S., "Microrobot Design Using Fiber Reinforced Composites," Journal of Mechanical Design, Vol. 130, May 2008, pp. 052304-1 – 05230411.

34. Wood, R.J., "The First Takeoff of a Biologically Inspired At-Scale Robotic Insect", IEEE Transactions on Robotics, Vol. 24, No. 2, April 2008, pp. 341 – 347.

35. Anonymous, "Piezoelectricity", Wikipedia, October 2009.
[http://en.wikipedia.org/wiki/Piezoelectricity. Accessed 10-5-09.]

36. Anonymous, "The Piezoelectric Effect".
[http://www.aurelinr.com/electronique/piezo/piezo.pdf. October 2009.]

37. Anonymous "115VAC / 60Hz Piezoelectric Fan" Piezo Systems, Catalog #7B, page 12. 2007.
[http://www.piezo.com/prodfan1vac.html. Accessed 10-5-09.]

38. Sane, S.P., "The Aerodynamics of Insect Flight," The Journal of Experimental Biology, Vol. 206, 2003, pp. 4191 – 4208.

39. Anderson, J, D., "Fundamentals of Aerodynamics," The McGraw-Hill Companies Inc., New York, NY, 2001.

40. Mikula Web Solutions, Inc., "The Dragonfly WebSite – FAQ", The Dragonfly Website.
[http://dragonflywebsite.com/faq.htm. Accessed 7/23/2009.]

41. Alexander, D.E., "Unusual Phase Relationships Between the Forewing and Hindwings in Flying Dragonflies," Journal of Experimental Biology, Vol. 109, 1984, pp. 379 – 383.

42. Chen, J., Chen, J., Chou, Y., "On the Natural Frequencies and Mode Shapes of Dragonfly Wings," Journal of Sound and Vibration, Vol. 313, 2008, pp. 643 – 654.

43. Murphy, J., Hu, H., "An Experimental Investigation on a Bio-inspired Corrugated Airfoil," 47th AIAA Aerospace Sciences Meeting and Exhibit, Orlando, Florida, January. 5 – 8, 2009.

44. Tsuyuki, K., Sudo, S., Tani, J., "Morphology of Insect Wings and Airflows Produced by Flapping Insects," Journal of Intelligent Material Systems and Structures, Vol. 17, 2006, pp. 743 – 751.

45. Wang, J.K., Sun, M., "A Computational Study of the Aerodynamics and Forewing-Hindwing Interaction of a Model Dragonfly in Forward Flight," The Journal of Experimental Biology, Vol. 208, 2005, pp. 3785 – 3804.

46. Huang, H., Sun, M., "Dragonfly Forewing-Hindwing Interaction at Various Flight Speeds and Wing Phasing," AIAA Journal, Vol. 45, No. 2, February 2007, pp. 508 – 511.

47. Sun, M., Lan, S.L., "A Computational Study of the Aerodynamic Forces and Power Requirements of Dragonfly (Aeshna Juneca) Hovering," The Journal of Experimental Biology, Vol. 207, 2004, pp. 1887 – 1901.

48. Weis-Fogh, T., "Unusual Mechanisms for the Generation of Lift in Flying Animals," Scientific American, Vol. 233, 1975, pp. 80 – 87.

49. Usherwood, J.R., Lehmann, F., "Phasing of Dragonfly Wings Can Improve Aerodynamic Efficiency by Removing Swirl," J. R. Soc. *Interface*, Vol. 5, 2008, pp. 1303 – 1307.

50. Clemons, L.A., "An Experimental Study of the Vortex Structures in the Wake of a Piezoelectric Flapping Plate for Nano Air Vehicle Applications," Masters Thesis, Department of Aerospace Engineering, Iowa State University, Ames, IA, 2009.